# Optical properties of
# metal-hydrides:
# switchable mirrors

15th June 2004

**R. Griessen, I.A.M.E. Giebels, and B. Dam**

# Contents

# Chapter 1

# Review on switchable mirrors

## 1.1 Introduction

For decades the great majority of experiments on metal-hydrogen systems were carried without actually looking at the samples. In many cases there was no need of doing so (for example for all pressure-composition isotherm, electrical resistivity, specific heat, neutron and x-ray scattering measurements). In other cases optical measurements could only be carried out for certain hydrides. For example, Weaver *et al.* [169, 170] measured in detail the reflectivity of dihydrides of Sc, Y and La but could not extend their interesting measurements to the trihydrides of Y and La. This is unfortunate since the pioneering work of Libowitz *et al.* [99] on Ce-hydrides had demonstrated the existence of a metal-insulator transition between $CeH_2$ and $CeH_3$. In Y and La, however, hydrogenation from the dihydride to the trihydride leads irrevocably to the powdering of bulk samples.

It is only much later, in a search for new high-$T_c$ superconductors not based on copper-oxide, that the Amsterdam group [74] discovered in 1995 spectacular changes in the optical properties of metal-hydride films of yttrium and lanthanum near their metal-insulator transition: the dihydrides are excellent metals and shiny while the trihydrides are semiconductors and transparent in the visible part of the optical spectrum (see Fig. 1.1). The transition from a shiny to a transparent state is reversible and simply induced at room temperature by changing the surrounding hydrogen gas pressure or electrolytic cell potential. Not only $YH_x$ and $LaH_x$, but all the trivalent rare-earth hydrides and even some of their alloys exhibit switchable optical and electrical properties [56, 156]. In the transparent state they have characteristic colours: for example, $YH_3$ is yellowish, $LaH_3$ red, while some fully hydrogenated alloys containing magnesium are colourless.

One of the most surprising results of these early measurements was, however, that the films retained their structural integrity even though they expanded by typically 15 % during hydrogenation of the pure parent metal to the trihydride. This meant that for the first time physical properties, such as electrical resistivity, Hall effect, optical transmission, reflection and absorption, were amenable to experimental investigations. This led to the discovery of new phenomena in the electrical, optical and mechanical properties of these materials. Furthermore, the possibility to fine-tune their properties by alloying and the ease to change continuously their hydrogen content made them especially attractive for fundamental condensed matter physics. Soon after their discovery it became clear that switchable metal-hydride films would pose intriguing questions. So far the nature of their insulating state is not understood and completely different mechanisms for their metal-insulator transition have been proposed. They offer also interesting possibilities to investigate continuous metal-insulator (quantum) phase transitions. Moreover, they can be used to tune magnetic interactions in for example superlattices (see e.g. Refs. [70, 100] and references therein)

The purpose of this article is to review the essential properties of switchable mirror materials with special emphasis on their optical properties. So far three generations of hydrogen-based switchable mirrors have been discovered:

- The rare-earth switchable mirrors
- The colour neutral magnesium-rare-earth (Mg-RE) switchable mirrors and
- The magnesium-transition-metal (Mg-TM) switchable mirrors

Each of these generations has specific properties that are described separately in the next sections. The rare-earth switchable mirrors are historically important since they were the first to exhibit optical switching as a result of hydrogen absorption. Their transparent appearance in the fully loaded state posed a serious problem to theorists. In particular, the yellow appearance of $YH_3$ seemed to be in contradiction with state-of-the-art band structure calculations that predicted a metallic state for this material. The physics of rare-earth switchable mirrors is thus closely related to that of electron correlation and metal-insulator transitions.

The Mg-RE and the Mg-TM switchable mirrors exhibit both the three fundamental optical states of matter, i.e. shiny metallic, transparent and highly absorbing. The microscopic mechanisms responsible for their ‘black states is, however, different and needs to be discussed separately.

Furthermore, we show that alloys and multilayered samples can be used to fine tune all the essential properties of switchable mirrors and exhibit a series of new phenomena. Finally recent applications of switchable mirrors as smart coatings in electrochromic devices, as hydrogen indicators for catalytic and diffusion investigations, as active layer in fiber optic hydrogen sensors and as hydrogen absorption detectors in a combinatorial search for new lightweight hydrogen storage materials are briefly described.

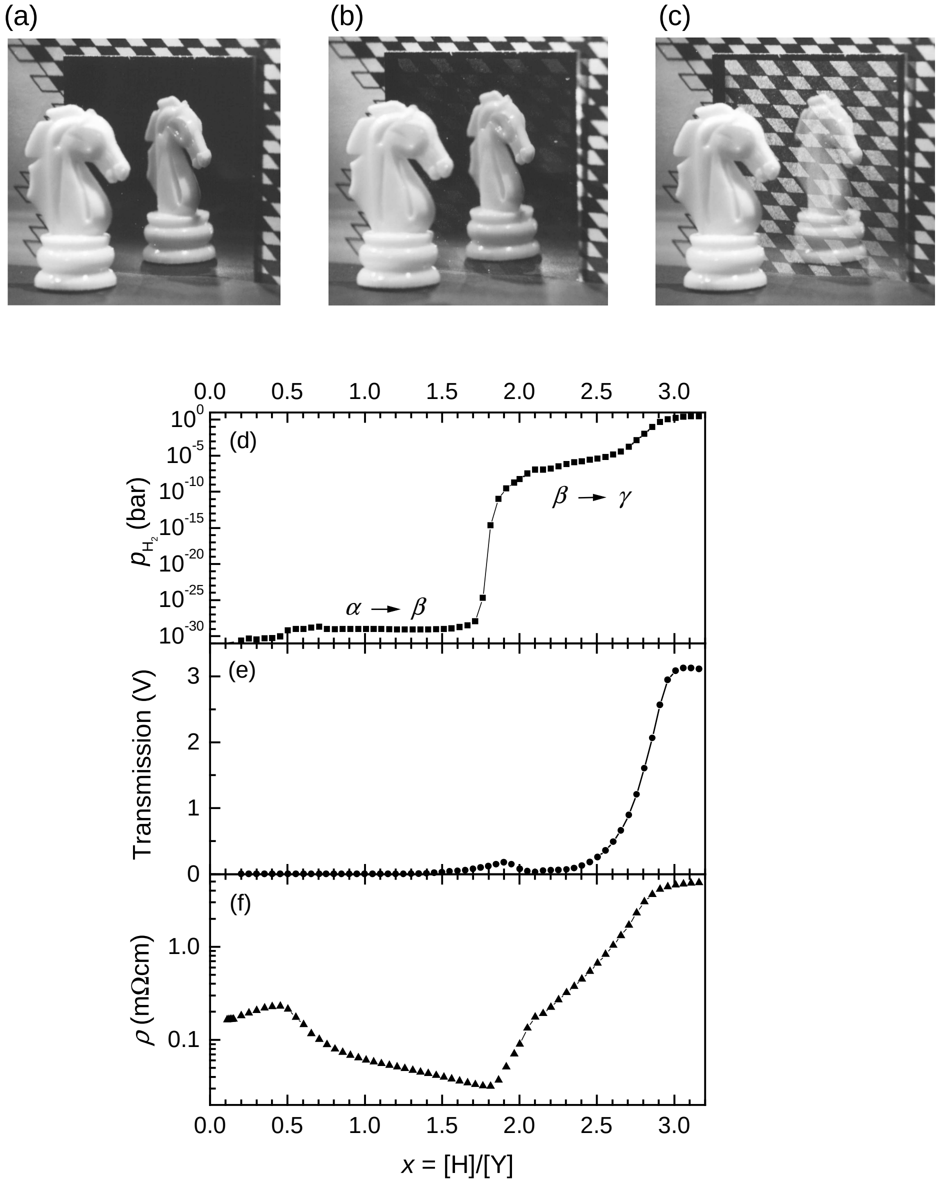

**Figure 1.1:** (a)-(c) Photographs of a switchable mirror in the as-deposited, dihydride and trihydride states. Furthermore, the pressure-composition isotherm (1 bar = $10^5$ Pa) (d) and hydrogen concentration dependence of the optical transmission (e) and electrical resisitivity (f) of a 300-nm-thick yttrium film capped with 15 nm palladium are shown. The optical transmission is measured at a photon energy $\hbar\omega = 1.96$ eV, corresponding to a wavelength $\lambda = 635$ nm. The weak transmission window of the $\beta$-phase around $x = 2$ and the transition to the transparent state in the $\gamma$-phase are clearly visible. The metal-insulator transition is not of structural origin. It occurs within the hexagonal phase at a composition of approximately $YH_{2.86}$. The resistivity first slightly increases when hydrogen dissolves in Y ($\alpha$-phase). The $\beta$-phase (dihydride) clearly has a lower resistivity and as soon as the $\gamma$-phase (trihydride) nucleates the resistivity increases to about 4 mΩcm. This value is limited by the metallic Pd cap layer which shortcuts the semiconducting $YH_{3-\delta}$ film. (From Refs. [74,90])

## 1.2 Preparation of switchable mirror thin films

The growth and microstructure of switchable mirror thin films involves specific aspects that need to be discussed before describing their physical properties. We focus first on Y, La and rare-earth films (for convenience all abbreviated as RE-films), deposited both in their metallic as well as in their hydride form. Some references to second-generation mirrors (Mg-RE) are included and third-generation switchable mirrors (Mg-TM) are shortly discussed separately.

### 1.2.1 Growth and microstructure of rare-earth (hydride) thin films

**Metallic RE-films**

Although the deposition and electrical characterization of RE and RE-hydrides was already reported in the seventies (see e.g. Curzon and Singh [21]), these films were not yet phase-pure, due to the limited quality of the vacuum systems of those days. Typically, for pure RE films the background pressure has to be below $10^{-5}$ Pa [76, 173]. The method of deposition seems not to be critical and both molecular beam deposition (MBD [76]), sputter deposition (SD [155, 156]) and pulsed laser deposition (PLD [22]) have been used. The purest metallic films are obtained by MBD, where the background pressure is lowest (typically $10^{-7}$ Pa). From the lattice expansion compare to pure Y one determines an as-deposited hydrogen content in $YH_x$ of $x \sim 0.08$ [76]. Thermodynamically, one would expect a higher hydrogen content, since the equilibrium Y-$YH_2$ plateau pressure is $\sim 10^{-34}$ Pa at room temperature [90]. At room temperature the polycrystalline films all tend to have a $[0001]_{\mathrm{hcp}}$ or $[111]_{\mathrm{fcc}}$ texture, i.e. the closed-packed layers are oriented parallel to the substrate plane.

From a fundamental point of view the underlying physical processes should preferably be investigated on single-crystalline or epitaxial films. Hayoz *et al.* [67] were able to grow highly ordered yttrium on the metallic substrate W(110). Taking the recipe originally developed by Kwo *et al.* [96], Wildes *et al.* [173] and Remhof *et al.* [133, 134] managed to form pure, epitaxial yttrium films on sapphire substrates using a Nb template layer. These approaches have the disadvantage that they complicate optical transmission and electrical transport measurements. This problem was solved by Nagengast *et al.* [93, 117] who showed that epitaxial yttrium films can be directly grown on (111)-$CaF_2$ substrates. Shortly after, Jacob *et al.* [81] showed that good epitaxiality could even be obtained by using $BaF_2$ substrates. This is remarkable since there is a 20 % lattice mismatch between Y and $BaF_2$. Due to the higher deposition temperature, the hydrogen impurity level of the epitaxial films is much lower than in polycrystalline films: $x = [H]/[Y] = 0.01 - 0.03$ [31, 173], as compared to $[H]/[Y]=0.08$ in polycrystalline films. It is suggested that some fluorine, however, is absorbed by the RE film and acts as a surfactant facilitating growth [68]. The large lattice mismatch with respect to the substrate ($\sim$5% in the case of $CaF_2$) causes the coherent film to relax after a certain critical thickness. As shown by Borgschulte *et al.* [15] this relaxation process is responsible for the formation of so-called ridges [60, 117]: strips of material with their c-axis parallel instead of perpendicular to the substrate. This stress-induced reorientation is due to $(10\underline{1}2)$-deformation twinning [89]. Indeed the as-grown density of ridges is much larger on films deposited on $CaF_2$ substrates as compared to Nb/sapphire substrates, moreover their density increases with film thickness. Formally, due to the ridges, the epitaxial films should be called bi-epitaxial since each of the twin orientations has a different substrate-film relation. The volume fraction of the ridges is however small, and for most purposes except the Hall effect [31] their effect can be neglected. When the metallic epitaxial films are hydrogenated the number of ridges increases, and an extended self-organized ridge network is formed, which delineates micron-sized triangular domains [86, 87]. Although hydrogen absorption involves a large expansion of the lattice and a change in lattice symmetry, the epitaxiality of the film remains intact. Details about the switching process of epitaxial $YH_x$ films are given in Section 1.3.5 on page 19.

### Cap layers

As-deposited RE films are very reactive. Exposing an uncovered film several hours to air already creates a 5 nm oxide layer while along grain boundaries oxygen is found at a depth of 150 nm [76, 110]. Therefore, palladium [76] and gold [173] cap layers are used which at same time act as catalysts for hydrogen dissociation and absorption [128]. To prevent the formation of a RE-Pd alloy (which blocks hydrogen transport) [14] these cap layers have to be deposited at room temperature. Alternatively, an intermediate (hydrogen transparent) thin oxide buffer layer is useful. In the case of La an intermediate $AlO_x$-layer is essential to prevent oxidation of La [54]. After using a combinatorial technique (see also Section 1.6.2 on page 49) to optimize the thickness of the Pd cap layer on Y, Van der Molen *et al.* [110] concluded that there is a well-defined critical thickness of 4 nm above which Pd can act as a catalyst for hydrogen absorption. This critical thickness is reduced to 2.7 nm, when an intermediate $YO_x$-layer is applied and to 0.5 nm with an 1.2-nm-thick $AlO_x$ layer [54]. Borgschulte *et al.* [16] concluded from a scanning tunnelling microscopy and spectroscopy study (STM/STS) that this critical cap layer thickness is related to an inactivation of Pd by encapsulation of the Pd islands by yttrium oxide or hydroxide. The substitution of Pd by cheaper, preferably transparent, catalytic cap layers is desirable, especially for smart window devices. In this respect, the catalytic properties of transition metal oxides [122] for storage materials could also prove to be useful for smart windows.

### In-situ deposition of RE-hydride films

RE films are generally loaded with hydrogen *after* deposition. To circumvent the associated generation of large stress [26], it is advantageous to grow the RE films as hydrides. The conditions for growth depend strongly on the technique used.

**a)** *Molecular beam deposition:* The in-situ formation of pure RE hydrides in MBD is difficult. The hydrogen source needs to be clean and also the vacuum system needs to be conditioned by a steady flow of hydrogen. Hydrogen liberates adsorbed species (oxygen, water) from the UHV-chamber walls. As a result, in dirty systems, $REO_x$-impurity phases are formed. Even when using up to $10^{-3}$ Pa molecular hydrogen and a substrate temperature of 800 K, a mixed oxide/hydride phase is obtained. Using an ultra-clean atomic hydrogen source with a direct line of sight in the vicinity of the substrate, Hayoz *et al.* [66] were able to prepare high quality $YH_2$ films in situ. Epitaxial films form at a substrate temperature of 500 K and a background pressure of $5 \cdot 10^{-4}$ Pa on W(110).

**b)** *Sputtering:* The in-situ deposition of RE hydride films is comparatively easy in sputter deposition. As shown by Van der Sluis and Mercier [155] GdMg-$H_5$ is formed when co-sputtering the metals in a 5:1 hydrogen/argon atmosphere at room temperature and a $10^{-1}$ Pa total pressure. To prevent arcing (due to the formation of insulating deposits) RF sources are used. The in-situ growth of the hydride phase probably benefits from the activated (atomic) hydrogen formed in the plasma.

**c)** *Pulsed laser deposition:* In PLD at elevated substrate temperatures, Lokhorst *et al.* [22, 103] found that RE hydrides can be made without adding hydrogen to the deposition chamber. In this case, the dihydride forms due to the fact that hydrogen dissolved in the RE-target is preferentially liberated during the ablation process. Structurally these films range from nanocrystalline to epitaxial depending on the deposition temperature and substrate used.

### 1.2.2 Ex-situ hydrogen loading

To transform the as-grown metallic films into hydrides they need to be exposed to hydrogen. This can be achieved by three methods:

**a)** *Gas loading* is the simplest and fastest procedure. It is well-suited for exploratory work but suffers from the fact that the amount of absorbed hydrogen cannot be directly determined. Gas loading can be extremely fast. For example GdMg-$H_2$ can be loaded to GdMg-$H_5$ at room temperature within 40 ms by applying a pressure of a few times $10^5$ Pa [62, 63]. The existence of kinetic barriers (e.g. stress, absorption or diffusion barriers) for hydrogen sorption is evident from the fact that a considerable overpressure (underpressure) is needed for the hydrogenation (dehydrogenation) reaction.

**b)** *Electrolytic loading* is the only technique that allows an easy and versatile *in situ* determination of the hydrogen concentration in a thin film. With an oxygen-free electrolyte it can be used to measure the hydrogen concentration in the films quantitatively and to determine pressure-composition isotherms [120]. At the solid/electrolyte interface the charge transfer reaction is represented by

$$H_2O + e^- \rightarrow H_{ad} + OH^-$$

Thus, there is a direct relation between the integrated current and the amount of hydrogen adsorbed. As the Pd cap layer is thin and as its plateau pressure at room temperature is over 1 mbar, the absorption by this layer is usually neglected. The potential of the Pd/RE electrode can be viewed as that of a Pd electrode in equilibrium with a low pressure hydrogen gas, of which the pressure is determined by the hydrogen concentration in the RE material underneath. Hence, the Pd/RE-electrode potential is directly related to the equivalent hydrogen pressure of the underlying RE hydride.

Electrolytic loading experiments were combined with optical transmission and reflection spectrometry as well as with electrical resistivity measurements by Kooij *et al.* [90]. They determined the hydrogen pressure-composition (p-c) isotherms of rare-earth hydrides over 30 orders of magnitude at room temperature. In Fig. 1.1 the room temperature p-c-isotherm of $YH_x$ for $0 < x < 3$ is given together with the optical transmission at 1.96 eV (635 nm) and the electrical resistivity. This shows that rare-earth metals such as Y have a strong hydrogen affinity. The dihydrides ($\beta$-phase) are already stable at very low pressures ($10^{-24}$ Pa for Y films [90], $10^{-25}$ Pa for La films [92] and $10^{-28}$ Pa for Gd films [25] at room temperature). The trihydrides ($\gamma$-phase) are formed at a pressure of about $10^{-1}$ Pa. Therefore, the reversibility is limited to the transition between the dihydride and trihydride phase under practical conditions. Only at very high temperatures (1000 K) it is possible to go back to metallic Y ($\alpha$-phase) [67].

Note, that compared to gas loading the total switching time increases to several minutes. Moreover, Notten *et al.* [120] report that the chemical stability of the Y-electrode is poor, especially when exposed to light.

**c)** *Chemical loading* of rare-earth films by immersion in an aqueous KOH-solution containing $NaBH_4$ has been demonstrated by Van der Sluis [154] for Gd. The redox reaction forms $BO_2^-$ and $GdH_3$. The attractive feature of this technique is that, due to the high redox-potential difference, it leads to almost stoichiometric trihydrides. The reaction is reversed by immersion in a 0.3% $H_2O_2$ aqueous solution.

### 1.2.3 Stress in polycrystalline and epitaxial thin films

Given the large lattice expansion, the fact that $REH_2$ films can be switched many times back and forth between the dihydride and trihydride phase is remarkable. To have reversible switching, plastic deformation has to be avoided. As shown by Pedersen *et al.* [127] Gd can be switched reversibly between well-defined stress-states of the dihydride and trihydride phases even though the stress involved is of the order of several GPa. Dornheim *et al.* [26] explained the relatively low net stress as the result of the fact that textured polycrystalline thin films benefit from a small in-plane tensile stress component. During the transformation from the dihydride to the trihydride phase mostly the distance between the closed-packed planes increases. Since the films have a texture such that these planes are parallel to the substrate most stress is relieved by an expansion of the film thickness. Clearly, to prevent hysteresis (see Section 1.3.3 on page 16) and long-term degradation, a switching material with zero lattice expansion is preferred. Van Gogh *et al.* [55] found such a zero-expansion alloy namely $La_{0.62}Y_{0.38}H_x$. It also exhibits the sharpest optical transition.

Epitaxial films switch also reversibly between the dihydride and trihydride state although some irreversible relaxation occurs during the first loading cycle (see Fig. 1.2). This irreversible relaxation is due to the ridges, which develop in addition to those already formed during deposition. The process through which an epitaxial film can accommodate high reversible strains/stresses without deterioration of its crystallinity was recently described by Kerssemakers *et al.* [86, 87]. Using *in situ* atomic force microscopy (AFM), they showed that reversible relaxation takes place

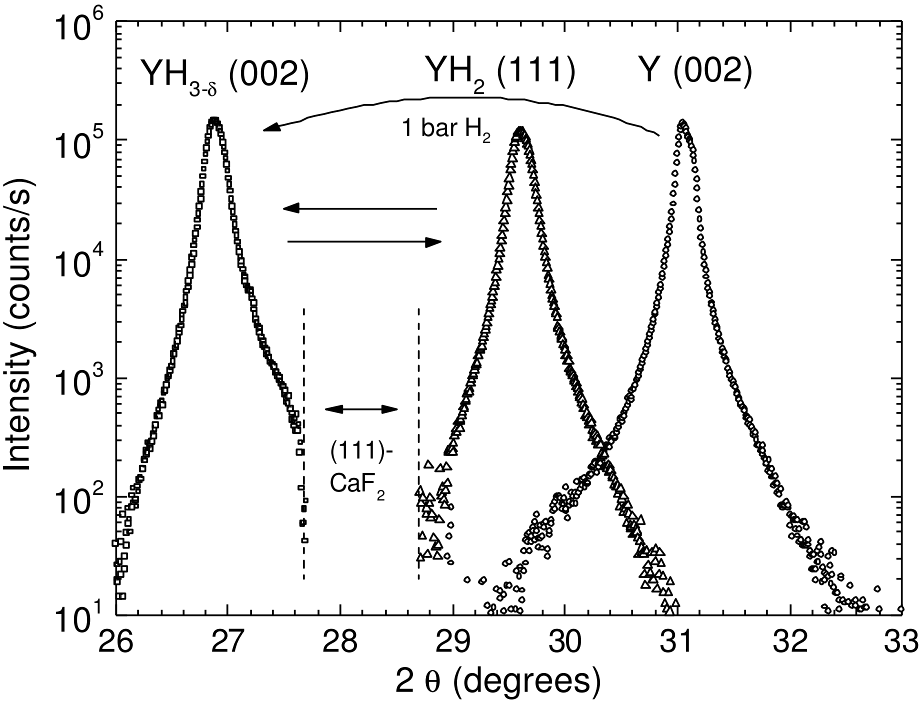

**Figure 1.2:** X-ray $\theta - 2\theta$ scan of a 300-nm-thick epitaxial Y film on (111) $CaF_2$ capped with 8 nm Pd, in-situ showing the development of the closed-packed lattice plane distance during reversible hydrogenation between the dihydride and trihydride state. Hydrogen loading is done in 1 bar $H_2$, unloading at 100°C in air. (From Ref. [117])

via the micron-sized triangular domains, which are defined by the ridge-network (see Sec. 1.3.5 on page 19). The domains expand one-by-one, homogeneously and essentially independently, during hydrogen absorption (see Figure 1.8(a) on page 26). From a transmission electron microscopy (TEM) study Kooi *et al.* [89] concluded that the reversible transition to and from the trihydride phase is greatly facilitated by numerous Shockley partial dislocations. These dislocations originate at the boundaries between two twin variants. These twins develop both within the triangles *and* within the ridges due to the phase transitions from the hcp phases Y and $YH_3$ to the fcc phase $YH_2$. This twin structure prevents an overall shape change associated with the symmetry change (see Fig. 11 of Ref. [89]).

### 1.2.4 Complex-metal-hydride thin films

The reversible switching of Mg-TM (TM=Ni, Co, Fe, Mn) films was discovered by Richardson *et al.* [138,139]. While in bulk samples hydrogenation requires high temperatures (500 to 600 K) and pressures of $10^5$ to $10^6$ Pa [12,130], for thin films it occurs readily at room temperature at low pressures when they are capped with a thin Pd layer. This class of materials does not involve rare-earth metals and might therefore be more resistant to oxidation than the earlier mirrors. This is especially important for applications.

As precursor for the complex metal-hydride the metal alloy of interest is sputtered or evaporated and subsequently capped with a thin Pd layer. The grain size of these films is small ($\sim 30$ nm). Complex hydrides of this type ($Mg_2NiH_4$, $Mg_2CoH_5$, $Mg_2FeH_6$) seem to form easily at room temperature at a few $10^2$ Pa of hydrogen, albeit in an x-ray amorphous form [101, 139]. The reversibility is quite remarkable given the large lattice expansion involved ($\sim 32$ %) and the large involved metal atom mobility. Note, that while $Mg_2Ni$ forms an alloy, corresponding $Mg_2Fe$ or $Mg_2Co$ compounds do not exist.

Very remarkable is that in these thin films the nucleation of the hydrogen-rich phase $Mg_2NiH_4$ starts preferentially near the film/substrate interface and not, as intuitively expected, close to the catalytic Pd layer at the surface of the sample [101, 102].

## 1.3 First-generation switchable mirrors: Rare-earth metal-hydride films

One of the most important aspects of the discovery of switchable mirrors is the fact that in the form of thin films rare-earth hydrides ($REH_x$) are amenable to a whole series of experiments, which were often impossible with bulk samples since hydrogen absorption resulted in a total disintegration of bulk samples.

In this section we show that the optical and electrical transition in $REH_x$ is reversible, continuous, robust and that it occurs in the visible [62]. It does also not depend on the isotope mass, i.e. the material shows the same features when loaded with deuterium as with hydrogen [53, 133]. Moreover, we show that the rare-earth-hydrides undergo a continuous quantum-phase transition [71, 72, 143]. Hysteretic effects are considered in Sec. 1.3.3. Although papers have appeared on e.g. Pr [113], Sm [95], Gd [6, 97] and Dy-hydrides [7] most investigations on switchable RE-hydrides are dealing with Y. In this way Y has become the archetypal material for the first-generation switchable mirrors. Scandium, although trivalent, does not form a trihydride under normal conditions (room temperature and $10^5$ Pa) [106].

### 1.3.1 Optical properties

In the Introduction we described how thin films of Y go from reflecting to transparent upon hydrogen absorption. From the photographs in Fig. 1.1 it is evident that this transition can be observed by the naked eye and that, consequently, it takes place in the visible part of the optical spectrum. The main optical changes from the reflecting to the transparent state occur smoothly and reversibly between the dihydride ($YH_2$) and the trihydride ($YH_3$) phase. The continuous evolution of reflection and transmission spectra during hydrogen loading between the dihydride ($x = 2$) and trihydride phase ($x = 3$) is displayed in Fig. 1.3 for a 300-nm-thick $YH_x$ layer capped with 15 nm Pd [90].

A typical feature of the dihydride phase is the weak transmission window in the red ($1.6 < \hbar\omega < 2.1$ eV for $YH_{2+\varepsilon}$ and $1.3 < \hbar\omega < 1.8$ eV for $LaH_{2+\varepsilon}$) at hydrogen concentrations $1.7 < x < 2.1$ [52] (see Figs. 1.1(b) and Fig. 1.3(a)). The existence of the dihydride transmission window is essential for the visualisation of hydrogen migration in switchable mirrors (see Section 1.6.1 on page 47). In the transparent trihydride phase, the material has characteristic colours e.g. yellow for $YH_{3-\delta}$ (absorption edge at 2.6 eV) and red for $LaH_{3-\delta}$ (absorption edge at 1.9 eV) [56]. Unfortunately, the optical contrast of the transition is reduced due to the Pd cap layer, which has a transparency of about 32% in the visible for a 12-nm thick layer [77]. Thus, for technological applications it is important to reduce the amount of Pd [4, 54, 110] or to use another more transparent material as cap layer (see Sec. 1.2.1).

Stoichiometric $YH_3$ cannot be obtained at $10^5$ Pa $H_2$ pressure. At most $YH_{2.9}$ is formed both during gas loading and electrochemical hydrogenation. This means that there are many vacancies that act essentially as donors [75, 118] and $YH_{2.9}$ is consequently a heavily-doped semiconductor. Stoichiometric $YH_3$ is only reached above 4 GPa [172]. High pressure studies of optical transmission spectra show that the semiconducting gap of $YH_3$ decreases markedly with increasing pressure but remains open until at least 25 GPa. Extrapolating the pressure dependence of the gap, an insulator-to-metal transition is expected at $55 \pm 8$ GPa.

Van Gogh *et al.* studied the optical properties of $La_{1-z}Y_zH_x$ with $0 < z < 1$ in great detail [56] and determined the dielectric function of these alloys. Fig. 1.4 shows the development of the dielectric function of $YH_x$ from the dihydride to the trihydride phase. For $1.9 < x < 2.1$ the film is in a single phase ($\beta$-phase) [131]. [1] In this concentration range interband transitions exist ($\varepsilon_2 > 0$ around 2.5 eV) below the plasma energy, which is typically at 4 eV. These interband transitions arise from the flat *d*-band of $YH_2$. The weak dihydride transmission window appears at the photon energy where $\varepsilon_1$ crosses zero and $\varepsilon_2$ is low ($1.6 < \hbar\omega < 2.1$ eV). During loading to the trihydride ($\gamma$-phase) three features are observed (see Fig. 1.4): (I) The disappearance of the free electron optical response (the large negative $\varepsilon_1$ at low photon energies that is typical for a metal is gradually reduced and replaced by positive $\varepsilon_1$) with increasing hydrogen concentration $x$. This means that our material changes from a metal into an insulator; (II) The suppression of interband absorption around 2.5 eV and, (III) A shift to lower energies of the second interband absorption peak in $\varepsilon_2$. The onset of interband absorption in the trihydride phase ($x = 2.9$) determines the final appearance of the film: $YH_3$ is yellow while $LaH_3$ is red. The photon energy at which $\varepsilon_2$ increases towards higher energy is the optical band gap of the material. For $YH_{2.9}$ this is 2.63 eV [56]. All $La_{1-z}Y_zH_x$ alloys exhibit the same features as $YH_x$ irrespective of the crystal structure of the phases. In particular, it does not matter whether the fully loaded trihydride films are cubic or hexagonal: they all are transparent and semiconducting. Thus, the switching behaviour is robust, in the sense that it is rather insensitive to chemical and structural disorder. Even the crystallographic phase appears irrelevant.

---

[1] Kooij *et al.* [91] stated erroneously that for $1.9 < x < 2.1$ thin films of $YH_x$ are in the coexistence region of the $\beta$-phase and $\gamma$-phase. Remhof *et al.* [131] and Kerssemakers *et al.* [86] confirmed that $YH_x$ follows the bulk phase diagram [164]. Thus, for $1.9 < x < 2.1$ the system is in the single $\beta$-phase and for $2.1 < x < 2.7$ in a mixed $\beta$-phase and $\gamma$-phase.

### 1.3.2 Electrical properties and the metal-insulator transition

The optical transition is always accompanied by an electrical transition from metallic to semiconducting when going from the dihydride to the trihydride phase (see Fig. 1.1(f)). This metal-insulator transition has also been investigated in detail. Van Gogh *et al.* [53] showed that the isotope mass is not important in the switching since $YH_x$ and $YD_x$ display the same electrical behaviour. The metal-to-insulator (MI) transition takes place at a hydrogen concentration of about 2.86 where the resistivity measured at room temperature diverges [53].

Very important was the observation that the metal-insulator transition in $YH_x$ occurs within a single structural phase and is not associated with a 'trivial' first-order phase transition. This can be concluded from the fact that for $x > 2.7$ yttrium hydride is in a single phase ($\gamma$-phase) [131] and as we have seen the MI transition occurs at $x = 2.86$. This is consistent with the observation that there is also a metal-insulator transition in Mg-stabilized cubic $YH_{3-\delta}$ [111] and in $LaH_x$ which remains fcc at room temperature for $2 < x < 3$. Even $La_{1-z}Y_zH_x$ alloys show the same behaviour independently of their crystallographic structure and their degree of structural disorder [56]. This is another demonstration of the robustness of the metal-insulator transition in rare-earth hydrides.

Intrigued by the possibility of a continuous quantum phase transition in $YH_x$, Hoekstra *et al.* investigated in great detail the temperature ($0.35 < \mathrm{T} < 293$ K) and concentration dependencies (for $0 < x < 3$) of the electrical resistivity $\rho$, charge carrier density n and magnetoresistance of polycrystalline $YH_x$ switchable mirrors in magnetic fields up to 14 T [71,72,143]. In Fig. 1.5 the conductivity $\sigma$ (=1/$\rho$) as a function of the temperature T is shown in a log-log scale for hydrogen concentrations between $x = 0.08$ and 2.93 [72]. The uppermost three curves with $\mathrm{n} > 10^{22}$ cm$^{-3}$ are for metallic $YH_x$ with $x < 2$. The curves relevant for a discussion of the MI transition are those with $\mathrm{n} < 2.5 \cdot 10^{19}$ cm$^{-3}$. For $x$ slightly smaller than 2.86 the curvature of the curves is positive, which according to scaling theories implies that they correspond to a metallic state. For $x$ larger than 2.90 their curvature is clearly negative. We conclude that somewhere between 2.86 and 2.90 the curvature vanishes and that, consequently, $\sigma$(T) is power-law in temperature T. This is the signature of a genuine metal-to-insulator transition. An unusually small power of 1/6 can be estimated from the slope of the curves in the critical region. The characteristic response of thin $YH_x$ films, is according to Hoekstra *et al.* connected to a *continuous* quantum phase transition a fundamental change of the ground state of the system as a function of a tuning parameter other than temperature T namely the charge carrier density n in this case. For this quantum phase transition, the critical charge carrier density $n_c$ is defined as the value at which the residual conductivity $\sigma(\mathrm{n},\mathrm{T}=0) \equiv \sigma_0(\mathrm{n})$ changes from a finite value in the metallic phase ($\mathrm{n} > \mathrm{n_c}$) to zero in the insulating phase ($\mathrm{n} < \mathrm{n_c}$). $YH_{3-\delta}$ is found to be a heavily doped semiconductor with a critical charge carrier density of $\mathrm{n_c}(0.35\ \mathrm{K}) = 1.39 \times 10^{19}$ cm$^{-3}$ at the metal-insulator transition.

Moreover, the electrical conductivity data over a wide temperature and hydrogen concentration range both in the metallic and insulating regions can be collapsed onto a single curve with the same, unusually large critical exponents [71,143]. These large critical exponents indicate the important role played by electron-electron interactions in the physics of switchable mirrors (see also Sec. 1.3.4 on page 17).

### 1.3.3 Hysteresis

Throughout this Chapter it is repeatedly stated that the optical switching in $YH_x$ is reversible between $x = 2$ and 3. What is meant is that this system can be switched from metallic to semiconductor and back to the original metallic state. When this transition is followed in detail one observes, however, that there is a giant hysteresis. This can be put in evidence in two different ways: (i) in a gas loading experiment (which does not allow a determination of the actual hydrogen concentration in a film) by plotting the optical transmission as a function of the simultaneously measured electrical resistivity [55], or (ii) by measuring the optical transmission as a function of the hydrogen concentration loaded electrolytically into a film [56,91]. A giant hysteresis is indeed found in $YH_x$ both in the pressure-composition isotherms and in transmission as a function of the hydrogen concentration $x$ (see Fig. 1.6) [91]. $LaH_x$, however, switches without any hysteresis at all (see Fig. 1.6(e)) [55, 56]. Furthermore, in $La_{1-z}Y_zH_x$ alloys the magnitude of the hysteresis depends strongly on their composition. For $z \leq 0.67$ when the material stays fcc - it vanishes altogether (see e.g. the p-c isotherm of $La_{0.55}Y_{0.45}$ in Fig. 1.6(d)). As shown by Van Gogh *et al.* [55] these hysteretic effects in La-Y alloys are related to the presence of a phase transition from fcc to hcp accompanied with a large uniaxial expansion. This leads to different stress states between absorption and desorption and therefore to $\beta$- and $\gamma$-phases with different hydrogen concentrations and thus different optical properties - during absorption and desorption [131]. Moreover, the optical transition is much sharper in $LaH_x$ than in $YH_x$ [55]. In single-phased La-Y alloys the sharpness of the optical transition seems to be related to the contraction or expansion of the material upon hydrogenation.

A closer look at the hysteretic effects in $YH_x$ reveals that there is a four orders of magnitude difference between the absorption and desorption plateau pressures. This corresponds to a difference of 10 kJ/mol H in enthalpy of formation. The transmission as function of $x$ and $\rho$ in combination with XRD and optical microscopy [131] shows that the intensity of the transmission window decreases within the single $\beta$-phase when going from $x = 1.9$ to 2.1. The same has been observed in epitaxial $YH_x$ films [86]. Moreover, from $x = 2.7$ to 2.9 no hysteresis is observed in transmission because the system is in the single $\gamma$-phase. The difference between absorption and desorption is that during absorption $\beta$-phase with $x = 2.1$ coexists with $\gamma$-phase with $x = 2.7$ while during desorption $\beta$-phase with $x = 1.9$ coexists with $\gamma$-phase with $x = 2.65$. The fact that the phase coexistence is influenced by the hydrogen loading history, as correctly described by Remhof *et al.*, is due to different stress states during loading and unloading [26, 131]. In single-phased materials such as $LaH_x$ there is no phase coexistence, but a continuous increase or decrease of the hydrogen content. Thus, no hysteresis will be observed.

Recently, Lokhorst *et al.* were even able to make hysteresis-free $YH_x$ films by pulsed laser deposition [22, 103]. These films are nanocrystalline and stay fcc during hydrogenation. Apparently, the randomly oriented grains are too small to be transformed to the hcp phase. The same has been observed in sputtered Gd films by Dankert *et al.* [36].

### 1.3.4 Theoretical models for the first-generation switchable mirrors

Although the occurrence of a metal-insulator transition could have been expected on the basis of (i) the pioneering work of Libowitz and co-workers (see Refs. [98, 99] and references therein), (ii) the extensive work of Vajda and co-workers (see Ref. [164] and references therein) and Shinar *et al.* [151, 152] and (iii) the early bandstructure calculations of Switendick on Y, YH, $YH_2$ and $YH_3$ [160, 161], the transparency of $YH_{3-\delta}$ discovered in 1995 by Huiberts *et al.* [73, 74] came as a great surprise, since in 1993 Wang and Chou [167, 168] and Dekker *et al.* [23] had all concluded from self-consistent band-structure calculations, that $YH_3$ was a *semi-metal* with, in fact, a very large band *overlap* (1.5 eV). These difficulties stimulated theorists to reconsider the $YH_x$ and $LaH_x$ sytems. Somewhat as for the high-$T_c$ superconductors two lines of thought were developed since 1995: (i) band-structure models including lattice (Peierls) distorsions and (ii) strong electron-correlation models.

#### Peierls distortion models

Kelly, Dekker and Stumpf [84] determined the ground state of $YH_3$ using density functional theory within the local-density approximation and the Car-Parrinello method. They found a broken-symmetry structure with a direct electronic gap of 0.8 eV. The value of the gap depends strongly on the exact position of H in the Y lattice. As calculations based on the local-density approximation systematically underestimate semiconducting energy gaps by about 1 eV, Kelly *et al.* considered their value as being consistent with the experimental optical data. Neutron scattering experiments on bulk (powders) and epitaxial $YH_{3-\delta}$ thin films by Udovic *et al.* [162, 163] and Remhof *et al.* [133] do not provide evidence for the occurrence of this broken-symmetry structure. Their data are compatible with the $P\bar{3}c1$ and $P6_3cm$ structures. Kierey *et al.* [88] find with Raman scattering that the structure of $YH_3$ is either $P6_3cm$ or $P6_3$ (the broken symmetry structure) not $P\bar{3}c1$. Żogał *et al.* [179] compare NMR data with electric-field gradient calculations and conclude that the $P6_3cm$ shows very good agreement better than $P\bar{3}c1$. Van Gelderen *et al.* [43] have shown recently by parameter-free calculations that also the $P6_3$ structure is compatible with the neutron diffraction data by Udovic. Thus, from all these experimental data we conclude that the space group of $YH_3$ is either $P6_3cm$ or $P6_3$. However, the absence of an isotope effect [53, 83] in both electrical and optical properties of $YH_x$ indicates that the exact position of the interstitial hydrogen (or deuterium) has essentially no effect on the ground state of $YH_x$. Another indication of the robustness of the ground state of $YH_3$ is that all La-Y alloys [56] switch optically as a function of hydrogen concentration, irrespectively of the chemical and structural disorder and also independently of the crystal symmetry of the trihydrides (fcc or hcp) [56, 111].

#### Electron correlation models

Already in 1995 Sawatzky suggested that electron correlation effects might explain the insulating ground state of $YH_3$ and $LaH_3$. Since then several electron correlation models have been proposed. Ng, Zhang, Anisimov and Rice [118, 119] propose the following mechanism for the metal-insulator transition in $LaH_x$. The removal of a hydrogen atom from insulating $LaH_3$ leaves a vacancy which effectively donates an electron to the conduction band. This electron is, however, expected to be so strongly localized (the radius of the vacancy state is estimated to be about 0.3 nm in contrast to typically 10 nm in standard semiconductors) that an impurity band can only form at very high doping level (about 20 % impurities). This explains why the metal-insulator transition occurs at large doping level around $x = 2.8$. Eder, Pen and Sawatzky [29] introduce a further ingredient in the theory. They show that the strong dependence of the hydrogen 1*s* orbital radius on the occupation number (the radius of the 1*s* orbital is about 3 times larger for the negative $H^-$ ion than for the neutral H atom), leads to the formation of localized singlet bound states involving one electron on the hydrogen and one on the neighbouring metal orbitals. This breathing hydrogen orbital leads to a strong occupation number dependence of the electron hopping ('breathing Hubbard model') integrals. Both Ng *et al.* and Eder *et al.* consider the effect of correlation on the hopping integrals, an effect that has not been taken into account by Wang and Chen [166].

The strong electron-correlation models are similar to some of the models developed in the theory of high-temperature superconductors based on copper-oxides. Instead of a linear combination of oxygen orbitals which couple to the copper 3*d* state in CuO, in $YH_x$ it is a linear combination of yttrium 4*d* orbitals which couple to the 1*s* state of the hydrogen. Locally the structure resembles then strongly that of an isolated $H^-$ ion in agreement with the chemical view of a highly polarizable hydrogen ion in ionic hydrides. Electromigration experiments by Den Broeder *et al.* [17] and Van der Molen *et al.* [112] confirm that hydrogen in $YH_{3-\delta}$ behaves like a negative ion. Infrared transmission spectra by Rode *et al.* [140,148] lead also to the conclusion that significant charge transfer from yttrium to hydrogen is taking place. They find that hydrogen does not enter as proton in the compound, but that it is negatively charged, with an effective charge of approximately -0.5 e. Furthermore, angular resolved photoemission spectroscopy (ARPES) data by Hayoz *et al.* [65] bear the signature of strongly correlated electron systems. And Hoekstra *et al.* [71,72,143] found unusually large critical exponents in scaling that hint to (strong) electron correlation (see Sec. 1.3.2 on page 15).

### Recent calculations

In the meantime new band-structure calculation methods beyond LDA have been used that treat correlation (many-body effects) such as GW and screened-exchange LDA. They all find gaps for both $YH_3$ and $LaH_3$ independent of the crystal structure (cubic or hexagonal) and the actual position of the hydrogen atoms (space groups $P\bar{3}c1$, $P6_3cm$, $P6_3$, etc.) (see Fig. 1.7).

Miyake *et al.* [109] find that the GW approximation (GWA) leads to an insulating ground state for $YH_3$ and their calculated dielectric function agrees reasonably well with the experimental data obtained by Van Gogh *et al.* [56]. Chang, Blase and Louie [20] conclude on the basis of their GW calculation that $LaH_3$ is a band insulator with a direct dipole forbidden band gap of 1.1 eV and an optical band gap of 3.6 eV. Wolf and Herzig [175,176] using screened-exchange LDA (sX-LDA) demonstrate that the direct gap of $YH_3$ is insensitive to the chosen structure of $YH_3$ (see Fig. 7). Van Gelderen *et al.* [41,42] conclude from parameter-free quasi-particle calculations within the GW approximation that $YH_3$ is essentially a conventional semiconductor. The unusually large error in the band structure made by LDA is traced to its poor description of the electronic structure of the hydrogen atom. Their GW results predict a fundamental band gap of only 1 eV and an optical gap of 2.6 eV in close agreement to optical measurements [56]. Alford *et al.* [3] have shown with GWA that both cubic $YH_3$ and $LaH_3$ are semiconducting. Finally, Wu *et al.* [178] recently studied hexagonal and cubic $YH_3$ and $LaH_3$ within the weighted-density approximation (WDA) and found a direct gap of 2.2 eV and a fundamental gap of 0.41 eV for hcp $YH_3$ and both cubic $YH_3$ and $LaH_3$ also show gaps. The authors conclude that the gap problem is not due to unusual correlations or quasiparticle corrections, but is a problem with the LDA and GGA exchange correlation functionals.

### 1.3.5 Specific properties of epitaxial switchable mirrors

#### Pixel-by-pixel switching

As described earlier (see Sec. 1.2.3 on page 11) *epitaxial* RE films deposited on (111)-$CaF_2$ substrates show a typical ridge structure [117]. The same was observed on other substrates, e.g. W [129] and Nb [59, 89]. The ridges mechanically decouple adjacent triangular domains [87]. Using *in situ* atomic force microscopy, combined with electrical resistivity and local optical transmission measurements, Kerssemakers *et al.* [85–87] discovered that micron-sized triangular domains switch one-by-one, homogeneously and essentially independently, during hydrogen absorption (see Fig. 1.8). These optically resolvable domains are delimited by an extended self-organized ridge network, created during the initial hydrogen loading [60, 117, 129]. The ridges have a higher effective hydrogen plateau pressure, i.e. they switch only after all domains have switched to the trihydride state. The ridges block lateral hydrogen diffusion and act as a sort of microscopic lubricant for the sequentially expanding and contracting domains. This block-wise switching results in a ‘Manhattan skyline’ in which the optical state is directly related to the local, structural lattice expansion. The domain tunability is of technological relevance since it opens the way to a pixel-by-pixel switchable pattern with a minimal amount of inactive surface area.

Also in polycrystalline films *local* optical inhomogeneities are observed in the two-phase region [131]. However, the ridges are a typical feature in epitaxial films only. Due to their unfavorable crystallographic orientation, their switching occurs at a significantly larger hydrogen pressure. However, on a *macroscopic* scale, both polycrystalline and epitaxial switchable mirrors exhibit the same optical properties [56]. This is in sharp contrast with their electrical transport properties, which are markedly different. Enache *et al.* [31] found that at all hydrogen concentrations the electrical resistivity $\rho$ of the epitaxial films is substantially lower than that of polycrystalline films.

The as-deposited epitaxial Y films have a residual-resistivity-ratio of typically 14 and a low residual resistivity of 5.2 $\mu\Omega$cm at 4.2 K. The temperature dependence of $\rho$ is essentially the same as for single-crystalline yttrium. The charge carrier density determined from Hall effect measurements is also similar to that of yttrium single crystals (i.e. $3.53 \cdot 10^{22}$ $cm^{-3}$ at 220 K). These features indicate that the quality of MBE deposited epitaxial Y films is excellent. The temperature dependence of the optical transmission at $\hbar\omega = 1.8$ eV in the dihydride state resembles that of the conductivity, i.e. $1/\rho$. These features are well described by a Drude model for free electrons, in which the only temperature dependent parameter is the electron scattering time [31]. The values for the optical gap of the epitaxial and polycrystalline $YH_3$ films prepared under similar conditions (i.e., 1 bar $H_2$ at 300 K) are comparable [31, 56]. Due to the ridges, the electrical resistivity of these films are very different: for example at 220 K, 8 mΩcm for epitaxial $YH_3$ and 40 mΩcm for polycrystalline films. This is due to a difference in effective charge carrier density. The later switching of the ridges corresponds to a smaller average value of the H concentration in the epitaxial $YH_{3-\delta}$ films (i.e. under the same loading conditions the effective $\delta$ is larger in epitaxial than in polycrystalline films). The electrical transport properties of epitaxial $YH_3$ films are path-controlled by the ridges. This is clearly revealed by Hall effect measurements in magnetic fields up to 5 T: in sharp contrast to the isotropic electrical resistivity, the charge carrier density exhibits an in-plane anisotropy that is also temperature dependent.

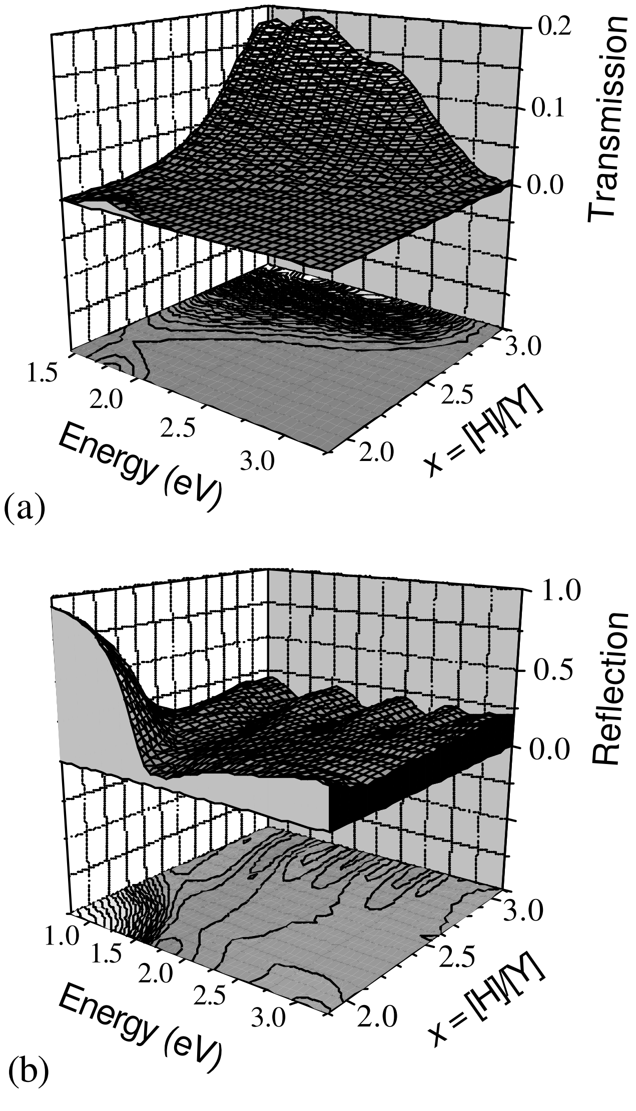

**Figure 1.3:** Optical transmission (a) and reflection (b) of a 300 nm Y/15 nm Pd film as a function of hydrogen concentration *x* and photon energy during the second electrolytic loading from the dihydride to the trihydride state. In the lower part of the graphs contour plots are shown. The maximum transmission is limited by the Pd cap layer. (From Ref. [90])

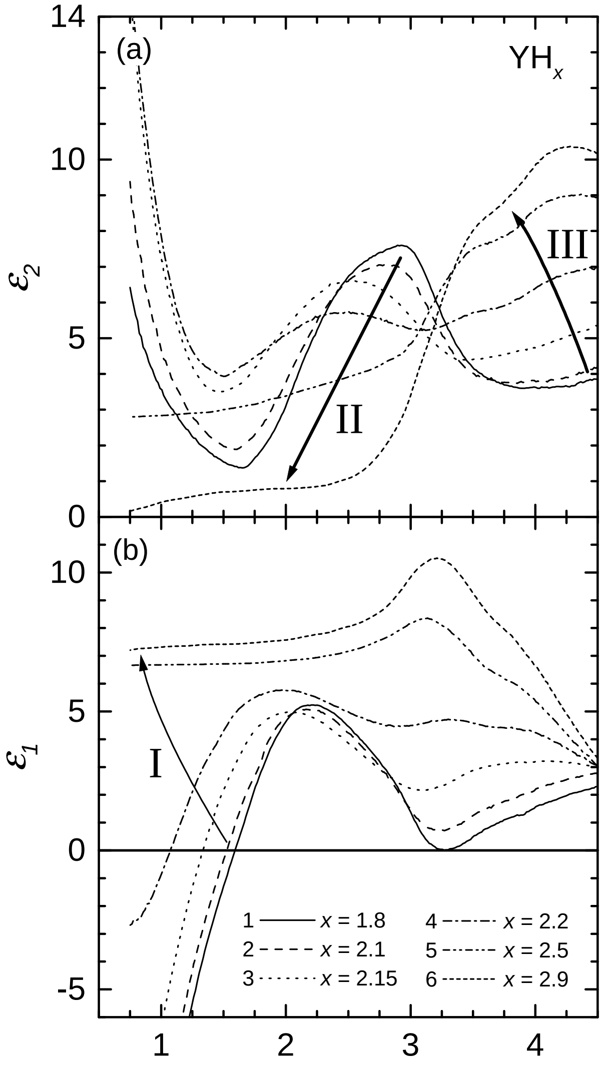

**Figure 1.4:** Hydrogen concentration dependence of (a) the complex ($\varepsilon_2$) and (b) the real ($\varepsilon_1$) part of the dielectric function for YH$_x$. Similar dependencies are observed in La$_{1-z}$Y$_z$H$_x$ alloys although the trihydrides La$_{1-z}$Y$_z$H$_3$ with $z \leq 0.67$ remain cubic while for $z \geq 0.86$ they are hexagonal. (From Ref. [56])

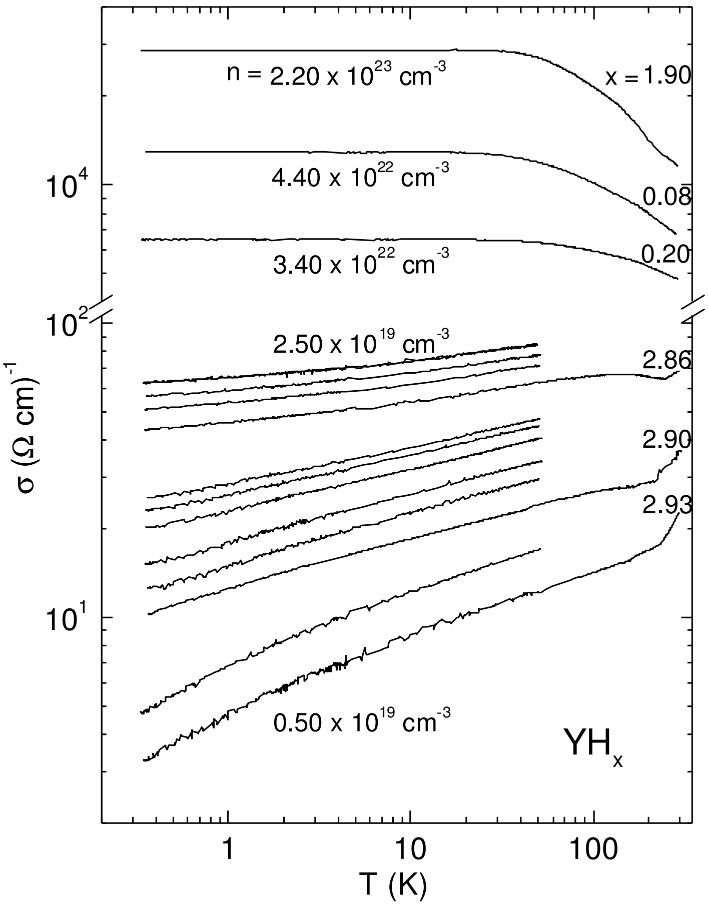

**Figure 1.5:** Conductivity $\sigma$ as a function of temperature T for a $YH_x$ film at a series of charge carrier densities n(T=0.35K). The metal-insulator transition is tuned by a combination of hydrogen gas loading (curves up to 300 K) and UV illumination (curves up to 50 K). Unlabeled curves have n = (0.75, 0.89, 1.07, 1.18, 1.45, 1.51, 1.64, 1.88, 2.12, and 2.32) $\times 10^{19}$ $cm^{-3}$. The hydrogen concentration is indicated on the right. (From Ref. [72])

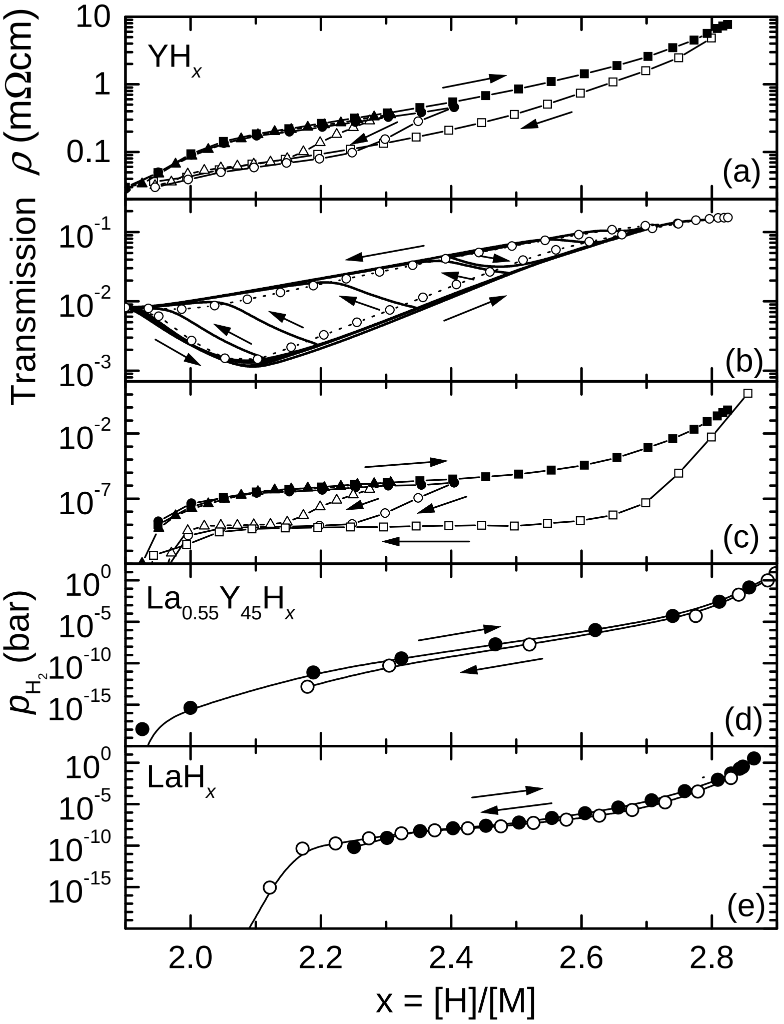

**Figure 1.6:** Hysteresis in the p-c-isotherms (c) and hydrogen concentration dependence of the electrical resistivity (a) and transmission (b) of $YH_x$ during a hydrogen loading (filled circles) – unloading cycle (open circles). The giant hysteresis (factor $10^4$) in the plateau pressure of the p-c-isotherm of $YH_x$ is absent in $LaH_x$ and $La_{0.55}Y_{0.45}H_x$ alloys (lower two panels (d) and (e)). (From Refs. [56, 91])

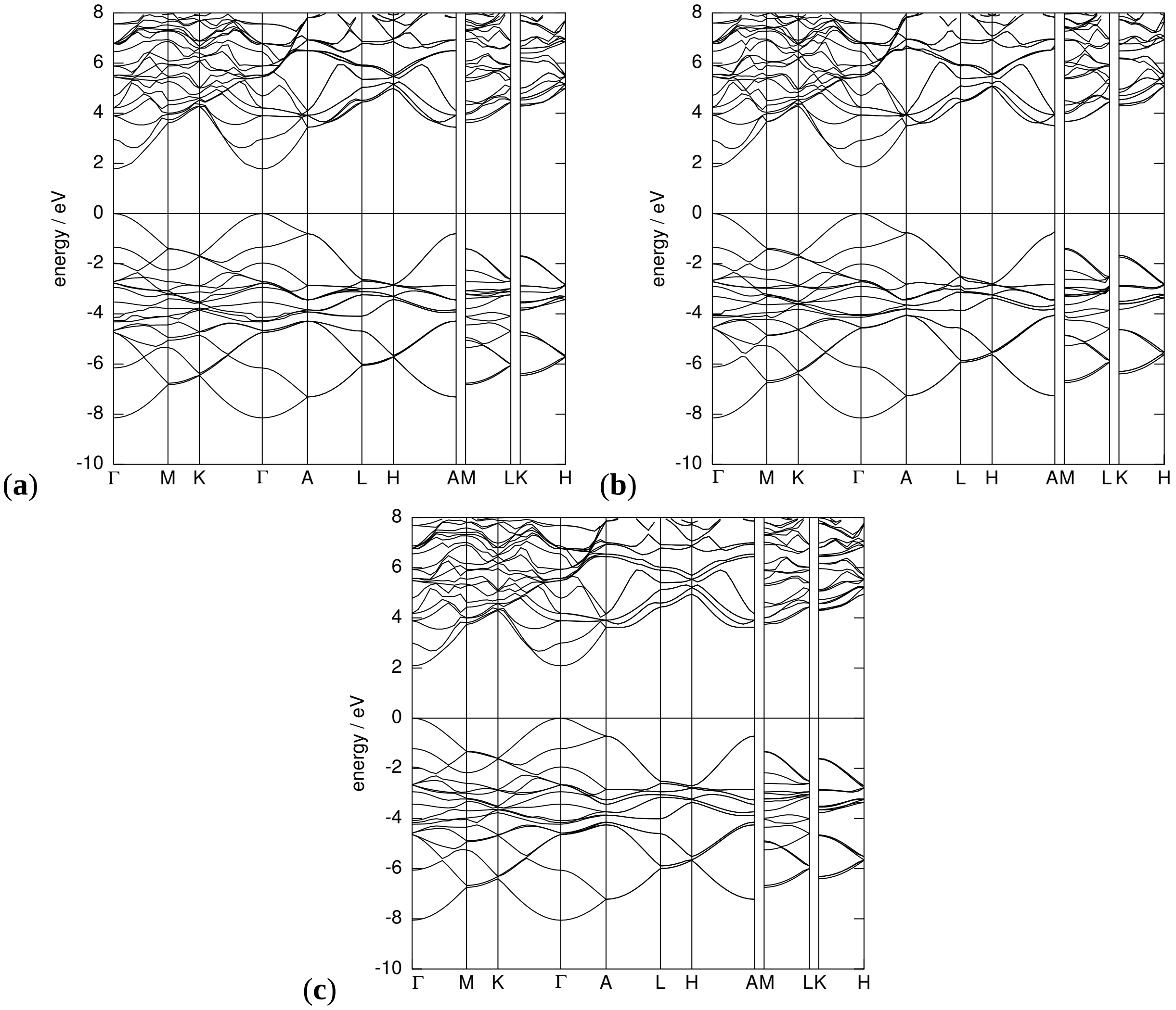

**Figure 1.7:** Band structures calculated by Wolf and Herzig [175, 176] using screened-exchange LDA (sX-LDA) for hexagonal $YH_3$ with space group (a) P$\bar{3}$c1 (b) P$6_3$cm (c) P$6_3$. These band structure calculations demonstrate that the direct gap of $YH_3$ is insensitive to the chosen structure of $YH_3$. (From Refs. [175, 176])

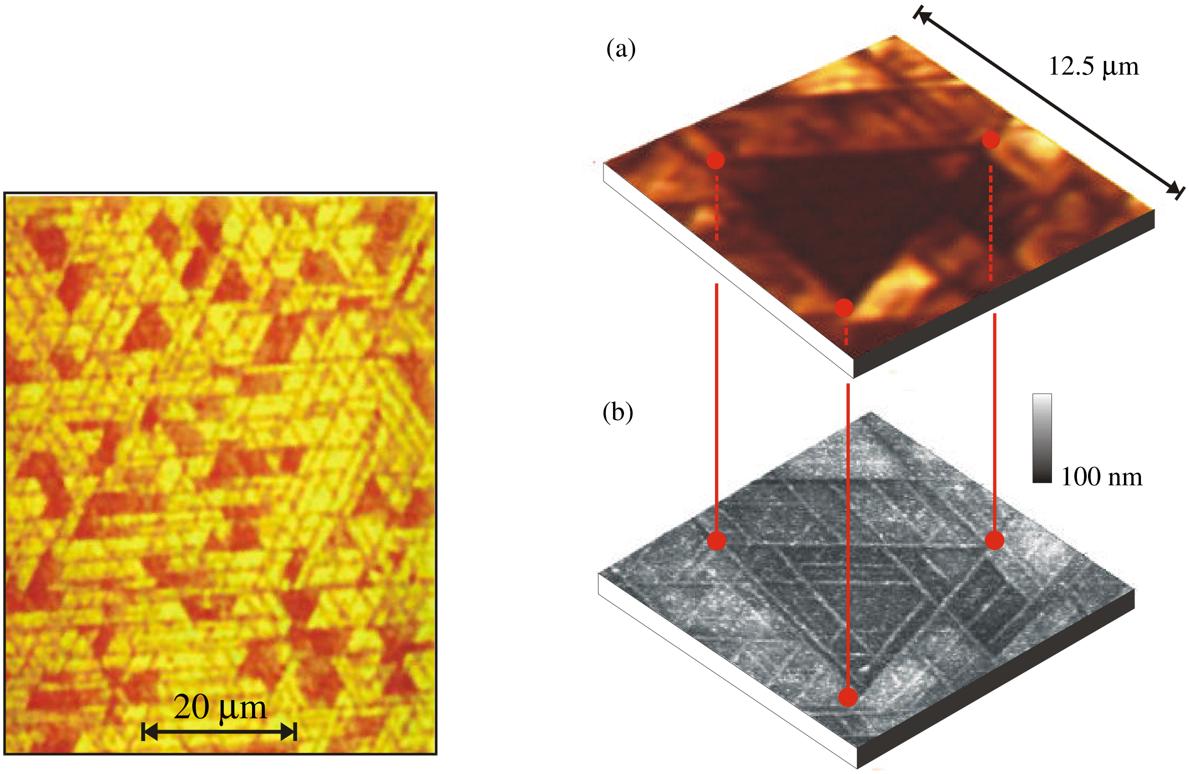

**(A)** **(B)**

**Figure 1.8:** (A) Optical domain switching. Real-colour optical micrograph in transmitted light of a 400-nm-thick Y film capped with 7 nm of Pd. After loading to the trihydride phase $YH_{3-\delta}$, the hydrogen content is slowly lowered. The yellowish transparent $YH_{3-\delta}$ film switches back domain by domain to reddish opaque $YH_2$. The domains are bounded by a triangular network of reddish opaque lines. (B) One-to-one correlation between optical and structural texture. (a) Optical micrograph in transmitted light of a dihydride/trihydride mixed-phase region of a 150-nm-thick Y/$CaF_2$ film capped with 20 nm of Pd. The image is $12.5\times12.5\ \mu m^2$. The large triangle is almost entirely in the electrically conducting and opaque dihyride phase ($YH_2$). The bright yellow regions are in the transparent trihydride phase ($YH_3$). (b) AFM micrograph of the same area as in (a). A triangular network of ridges bounds micrometer-sized flat domains of various heights (dark is low, white is high). The surface topography closely matches the optical pattern in (a), indicating that domains are in different stages of switching from $YH_2$ (opaque, contracted domains) to $YH_3$ (transparent, expanded domains). (From Ref. [87])

## 1.4 Second-generation switchable mirrors: Magnesium-rare-earth films

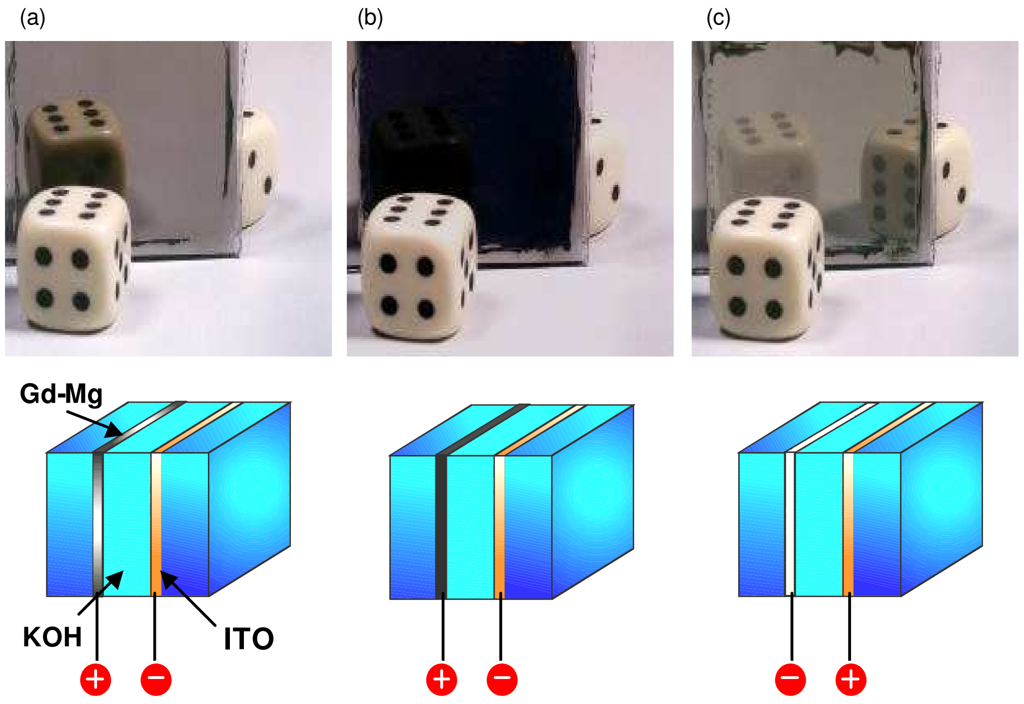

**Figure 1.9:** The three optical states of a liquid electrolyte Gd-Mg switchable mirror: (a) shiny metallic at positive voltage (∼2 V), (b) strongly absorbing at ∼1 V and (c) transparent and insulating at negative voltages (-2 V). In this device the Gd-Mg layer deposited on a glass substrate is used as the negative electrode for hydrogen loading. The counter electrode is made of a transparent but conducting indium-tin-oxide (ITO) layer deposited on glass. The liquid electrolyte is a 1 M KOH solution in water. (From Ref. [63])

For technological applications it is desirable to switch from a metallic state to a transparent state that is colour neutral instead of the coloured rare-earth trihydrides ($REH_3$). To achieve this, alloying a RE with a metal for which the heat of hydride formation is similar to that of the $REH_2$ - $REH_3$ transition and with a band gap large enough to have a fully transparent hydride, is an option. A group at Philips Research discovered in 1997 [156] that magnesium fulfils both demands [30]. This opened the way to the second-generation switchable mirrors. These alloys turned out to be also of fundamental importance since Mg-containing alloys exhibit a series of remarkable properties: (i) they disproportionate into $REH_x$ and $MgH_x$ and exhibit a microscopic shutter effect [116], (ii) $MgH_2$ stabilizes $YH_3$ in a cubic structure [111], and (iii) all MgRE-$H_x$ exhibit a highly absorbing, black intermediate state [48]. In Fig. 1.9 pictures of the reflecting, absorbing and colour neutral, transparent states are shown for a Gd-Mg alloy film. Further tailoring of the optical properties is achieved in multilayers of RE and Mg. As Mg plays a key role and, as we shall see later, can form Mg and $MgH_2$ inclusions in MgRE-$H_x$ we describe first the physical properties of $MgH_2$.

### 1.4.1 Optical properties of $MgH_2$

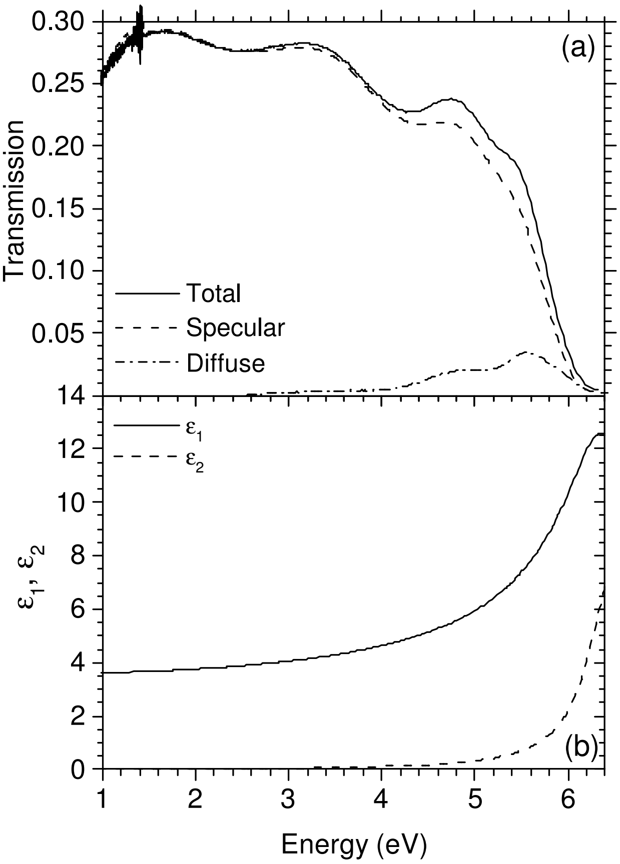

**Figure 1.10:** (a) Total (solid line), specular (dashed line), and diffuse (dashed dotted line) transmission as a function of photon energy for a 150-nm-thick $MgH_2$ film capped with 12 nm Pd and loaded at 100°C in 10 MPa hydrogen. (b) Real ($\varepsilon_1$) and imaginary part ($\varepsilon_2$) of the dielectric funtion for $MgH_2$ determined from ellipsometry and transmission data. (From Ref. [77])

Mg is considered to be one of the most important candidates for the reversible storage of hydrogen due to its lightweight, low cost and high hydrogen storage capacity (7.6 wt.% of hydrogen). However, only little is known about the intrinsic physical properties of the Mg-$MgH_2$ system. This triggered Isidorsson *et al.* [77] to study the optical properties of $MgH_2$ thin films in detail. $MgH_2$ turns out to be a colour neutral, highly transparent insulator with an optical band gap of 5.6 eV in close agreement with recent GW band structure calculations [2].

As shown by Krozer, Kasemo and others, the hydrogenation of Mg to $MgH_2$ is not straightforward [94, 144]. Palladium capped Mg films exhibit unusual kinetics due to the formation of a blocking $MgH_2$ layer at the interface between Pd and Mg. This $MgH_2$ layer prevents hydrogen from diffusing into the underlying unreacted metallic Mg. Its formation can be circumvented by starting hydrogenation at relatively low ($10^2$ Pa) $H_2$ pressure at a temperature of 100°C. Magnesium films with thicknesses up to 150 nm can be transformed to $MgH_2$ in this way [144,171]. To make sure that Mg is completely transformed to $MgH_2$ up to 10 MPa $H_2$ was used in the optical studies [77].

In Fig. 1.10(a) the total, specular and diffuse (scattered) transmission are shown for a 150-nm-thick $MgH_2$ film capped with 12 nm Pd. As expected the transmission only drops at high energies far beyond the visible part of the optical spectrum. The occurrence of diffuse transmission is due to surface roughness of the film. The diffuse transmission, $T_d$, has a strong wavelength dependence and is proportional to $(\hbar\omega)^4$. It decreases strongly above the band gap as the film starts to absorb light. Therefore, it is easiest to determine the band gap $E_g$ from this curve and one obtains $E_g = 5.6 \pm 0.1$ eV [77]. The dielectric function of $MgH_2$ is given in Fig. 1.10(b). In contrast to $YH_3$ and the other RE trihydrides, in $MgH_2$ there is no interband absorption below the band gap (i.e. $\varepsilon_2$=0). This means that the transmission of a $MgH_2$ film capped with Pd is only limited by the absorption in the metallic Pd film.

### 1.4.2 The microscopic shutter effect

In contrast to the binary $REH_x$ switchable mirror films which have a weak red transparency window in their metallic dihydride phase (see Sec. 1.3.1 on page 13), rare-earth alloys containing magnesium are remarkable for the large optical contrast [116, 125, 156] between their metallic dihydride and transparent trihydride phase. It has been shown by several techniques that this is due to a disproportionation of the Mg-RE alloy [24, 25, 80, 116]. This disproportionation is induced by the great hydrogen affinity of RE metals that form dihydrides already at very low hydrogen pressures (see Fig. 1.1(d) on page 7) Thus, while the RE-dihydride phase is formed, Mg separates out, remaining in its metallic, reflecting state. Upon further loading, insulating (transparent) $MgH_2$ is formed together with $REH_3$. In this way Mg acts essentially as a microscopic optical shutter [116]. It enhances the reflectivity of these switchable mirrors in their metallic state, suppresses the dihydride transmission window of their $REH_2$ phase (see Fig. 1.11) and increases their optical gap and transparency in their transparent state (see Fig. 1.14) [156]. The optical transmission ratio for thin films over the whole visible wavelength range can thus be increased to more than $10^3$ (theoretically $10^9$) [141] when at least 30 at.% Mg is added. This is the concentration where the dihydride transmission window disappears. $YH_x$ and the other RE hydrides only have a contrast of 10 between the dihydride and trihydride.

Di Vece *et al.* [24,25] studied $Mg_yGd_{1-y}H_x$ alloys in detail. In Fig. 1.11 pressure-composition isotherms are shown together with the transmission at 1.85 eV (670 nm) [25]. $GdH_x$ behaves like $YH_x$ (see Fig. 1.7). The first plateau around $10^{-27}$ Pa corresponds to the transformation of $\alpha$-Gd to $\beta$-$GdH_2$. A transparency window appears in transmission. The transition from $\beta$-$GdH_2$ to transparent $\gamma$-$GdH_3$ occurs at much higher pressures (around 1 Pa $H_2$).[2] For $y = 0.30$ and 0.62 a plateau at low hydrogen concentration is also observed with an enthalpy of formation close to that of $GdH_2$. The concentration range of this plateau suggests that all Gd is transformed to $GdH_2$. The disproportionation occurring in these Mg-Gd alloys results thus in gadolinium dihydride and pure magnesium clusters. The second (sloping) plateau corresponds to the formation of $MgH_2$ and $GdH_3$ since in thin films both have approximately the same enthalpy of formation. X-ray absorption fine structure (XAFS) studies indicate that upon hydrogen loading the coordination number of gadolinium by magnesium decreases markedly, thus confirming segregation [24].

Von Rottkay *et al.* [141] determined the index of refraction $n$ and the coefficient of absorption $k$ for several Mg-RE alloys (RE=Er, Gd, Sm). They found that $k$ of $Mg_{0.5}RE_{0.5}H_{2.5}$ (in the transparent state) is quite low at energies below the band gap (typically $k = 10^{-3}$). This leads to the conclusion that the transparency of these films is mainly limited by the Pd cap layer just as in $MgH_2$.

Van der Molen *et al.* [111] investigated the shift of the band gap in $Mg_zY_{1-z}H_x$ films as a function of alloy composition. For fully hydrogenated $Mg_zY_{1-z}H_{3-z}$ films with $0.10 \leq z \leq 0.50$ in which only fcc $YH_3$ and $MgH_2$ are present, the optical band gap $E_g^{\text{opt}}$ increases almost linearly with increasing $z$ ($\Delta E_g^{\text{opt}}/\Delta z = 1.1$ eV). Since the resistivity $\rho$ increases almost exponentially with $z$ from $z = 0$ to $z = 0.25$, they conclude that there is a change in some characterisitic energy parameter. With the simple relation $\rho(z) = \rho(z = 0)\exp[E_g^{\rho}(z)/2k_BT]$ they find that $\Delta E_g^{\rho}/\Delta z = 1.6$ eV. It is conceivable that the band structure of $YH_{3-\delta}$ changes due to quantum confinement (QC) effects since the grain size decreases from 18 nm (at $z = 0$) to only 4 nm (at $z = 0.3$) and the smaller the cluster, the higher the energy levels. The authors estimate theoretically that $\Delta E_g^{\text{QC}}/\Delta z = 1$ eV in reasonable agreement with their optical and electrical data.

### 1.4.3 Cubic $YH_3$

Van der Molen *et al.* [111] found that cubic (fcc) $YH_3$ can simply be stabilized by addition of Mg. They studied $Mg_yY_{1-y}$ thin films with $0 < y < 0.5$ in detail. X-ray diffraction showed that for $y \geq 0.10$ only fcc $YH_3$ is present in fully hydrogenated samples. Interestingly, the volume change upon loading from $YH_2$ to $YH_3$ is positive for all $y$ in contrast to the predicitons by Sun *et al.* [159]. This is consistent with the results obtained for $La_{1-z}Y_zH_x$ [56]. However, these samples show no segregation upon hydrogen loading, i.e. Y and La stay homogeneously mixed on an atomic scale. $La_{1-z}Y_zH_x$ expands for $y > 0.36$ and is cubic up to $y = 0.67$. This suggests strongly that if fcc $YH_3$ exists its volume should be larger that that of fcc $YH_2$.

In the two-phase fcc-hcp $YH_3$ region ($y < 0.1$), the optical gap does not change significantly with $y$, although hcp $YH_3$ is increasingly substituted by fcc $YH_3$. Since $MgH_2$ is a large-gap insulator ($E_g = 5.6$ eV, see Sec. 1.4.1 on page 28), this is only possible if the optical properties of fcc $YH_3$ are comparable to those of hcp $YH_3$. Therefore, this strongly suggests that fcc $YH_3$ is a large-gap semiconductor very similar to hcp $YH_3$. This is substantiated by electrical resistivity

---

[2] The slope of the p-c isotherm in Fig. 1.11(a) for concentrations between 1.5 and 3 suggests that a fcc-hcp transition in $GdH_x$ might be absent in these sputtered films. This is in agreement with measurements by Dankert *et al.* [36] on sputtered Gd.

data [111]. That fcc $YH_3$ is semiconducting is another demonstration of the robustness of the metal-insulator transition in the rare-earth hydrides

In Fig. 1.12 p-c isotherms together with the optical transmission at $\hbar\omega = 1.85$ eV ($\lambda =$ 670 nm) are shown as a function of $\Delta x$, the amount of hydrogen per metal atom that is desorbed for both $YH_{3+\Delta x}$ and $Mg_{0.1}Y_{0.9}H_{2.9+\Delta x}$ [51]. The plateau in Fig. 1.12(a) is due to the coexistence of hcp $YH_3$ and fcc $YH_2$. On the other hand, there is no plateau in Fig. 1.12(b) since $YH_x$ remains cubic as discussed above. Another consequence of the absence of the fcc-hcp phase transition is seen in Fig. 1.12(b): a steepening of the optical transition upon hydrogen desorption compared to pure $YH_x$. This is in agreement with the observations in fcc $La_{1-z}Y_zH_x$ alloys [55]. As a consequence of this $Mg_{0.1}Y_{0.9}H_{2.9}$ shows a much larger thermochromic effect than $YH_3$ [51].

### 1.4.4 Black state due to coexistence of Mg and $MgH_2$

Mg-containing rare-earth hydrides exhibit in addition to a transparent and a reflecting state, a state that has a low reflection and a very low transmission, i.e. it has a black appearance [5, 48, 61, 156]. These alloys can therefore be switched through the three fundamental optical states of matter by merely changing their hydrogen content. The key ingredient is the coexistence of nanograins of metallic Mg and insulating (dielectric) $MgH_2$ [48].

We discuss now the black state of MgY-$H_x$. Figures 1.13(a,b) show the reflection and transmission of a 200-nm-thick $Mg_{0.5}Y_{0.5}$ film on quartz covered with 10 nm Pd during loading in $10^3$ Pa $H_2$. From the measured reflection, $R$, and transmission, $T$, the absorption, $A$, is calculated, with $A = 1RT$ (see Fig. 1.13(c)). Apart from a reflecting and a transparent state there exists a highly absorbing, black state as well. The black state, which corresponds to the hill in $A$, occurs when the reflection is low and the film is just becoming transparent. Over the entire visible part of the spectrum the absorption is 85 to 90%. After correction for the Pd cap layer and the quartz substrate still 70-80% absorption is left. This is exceptionally high since we are looking (through the transparent substrate) at a smooth interface between the substrate and the film (and not at a rough surface such as in Si or Ni-P black [18, 177]). Moreover, it is not a narrow absorption line but it spans a wide energy range form the ultraviolet to the near-infrared. The same is observed in Mg-Gd [5, 156], Mg-La [48, 80] and Mg-Sc [47, 126] films and in Mg/Y and Mg/Ni multilayers [50]. Thus, it is a general feature of Mg-RE films with Mg playing a major role.

Recently, Giebels *et al.* [48] observed that thin pure Mg films can have a highly absorbing, black state as well. For this, Mg films need to be hydrogenated carefully at elevated temperatures (50-100°C) and be rather thin ($\leq$ 100 nm). In order to observe the black state it is very important that the film is loading (or unloading) homogeneously, i.e. $MgH_2$ (or Mg) nucleates everywhere in the sample. This confirms early reports by Hjörvarsson [69] on a black state in $MgH_x$ films.

At the black state structural x-ray diffraction data indicate that Mg is transforming to $MgH_2$ both in Mg-RE films [80] and in pure Mg. A sharp increase in the resistivity can be observed as soon as the reflection drops, i.e. when the absorption increases dramatically [48]. This points to percolation phenomena. The optical and electrical behaviour of these films can be reconstructed using Bruggeman's effective medium approximation [19] for a Mg-$MgH_2$ composite [48]. It shows that the coexistence of Mg and $MgH_2$ grains plays an essential role.

The unique feature of the switchable mirror systems considered here is that they can switch from a metallic, reflecting film via a black, highly absorbing state near the percolation threshold to a transparent and insulating material by simply changing the hydrogen concentration in a given sample. In all other metal-dielectric composites (such as Au-glass, Ag-glass and Co-$Al_2O_3$ [11]) a new sample has to be made for every desired volume percentage of metal in the dielectric.

### 1.4.5 Tailoring optical properties using multilayers

Giebels *et al.* [49] showed that multilayers offer much freedom to tailor the optical properties by playing with their periodicity. Multilayers have superior reflection in the low-hydrogen state (when the sample is unloaded). In the transparent fully loaded state the absorption edge of the mulitlayers with the same overall composition is shifted in energy on increasing the individual layer thicknesses. Figure 1.14 shows the reflection and transmission spectra of the unloaded respectively, fully loaded state for multilayers with layer thicknesses ranging from 2 to 10 nm and an overall composition of $Mg_{0.6}Y_{0.4}$. For comparison spectra of $YH_x$ and a disordered alloy of the same composition are added. The character of the two different materials, $YH_x$ and $MgH_x$, can clearly be distinguished. $YH_2$ exhibits a large dip in reflection around 1.75 eV (see Fig. 1.14(a)) and is even slightly transparent around this energy, while the Mg-Y alloy and multilayers have superior reflection due to the highly reflective Mg. In the fully loaded state (see Fig. 1.14(b)) Giebels *et al.* [49] observe a clear difference between the fully loaded disordered alloy and the multilayers in contrast to observations by Van der Sluis [153]. With decreasing layer thickness the absorption edge of the multilayers shifts in energy from that observed in $YH_3$ to the edge of the alloy. This hints at changes in the band structure of the $YH_x$ layers when the layer thickness becomes thinner, in the same manner as in the alloys (see Sec. 1.4.2 on page 29 and Ref. [111]). This may be the result of quantum confinement effects.

Moreover, the optical contrast of multilayers is much higher than for pure $YH_x$ and their optical switching does not suffer from hysteretic effects. X-ray diffraction shows that $YH_x$ in multilayers still undergoes a fcc-hcp transition when going from the dihydride to the trihydride in contrast to Mg-Y alloys of the same composition. In Fig. 1.15 the p-c isotherm between the low- (unloaded) and high-hydrogen (fully loaded) states for a 10 nm multilayer is shown. Only one plateau is observed. This plateau corresponds to the coexistence of $YH_2$ and $YH_3$ as well as Mg and $MgH_2$. Strikingly, there is still a hysteresis of two orders of magnitude in the pressure-composition isotherm, but there are no hysteretic effects in the optical transmission.

By selecting appropriate multilayer periods, samples can be built that switch much faster than alloys with a comparable Mg content [153]. An optimal Mg layer thickness of 1.12 nm is found for a composition $Mg_{0.40}Gd_{0.60}$. The switching time is reduced to 0.08 s compared to 0.65 s for the alloy. However, when the Mg layer is increased to 4.45 nm the switching time (80 s) is considerably longer than in the corresponding alloy. The enhanced kinetics of multilayers is even more pronounced for higher Mg contents. For instance, a $Mg_{0.80}Gd_{0.20}$ alloy has a switching time (at room temperature) of about 20 minutes whereas a multilayer with the same average composition and 1.12 nm thick Mg layers has a switching time of only 70 s.

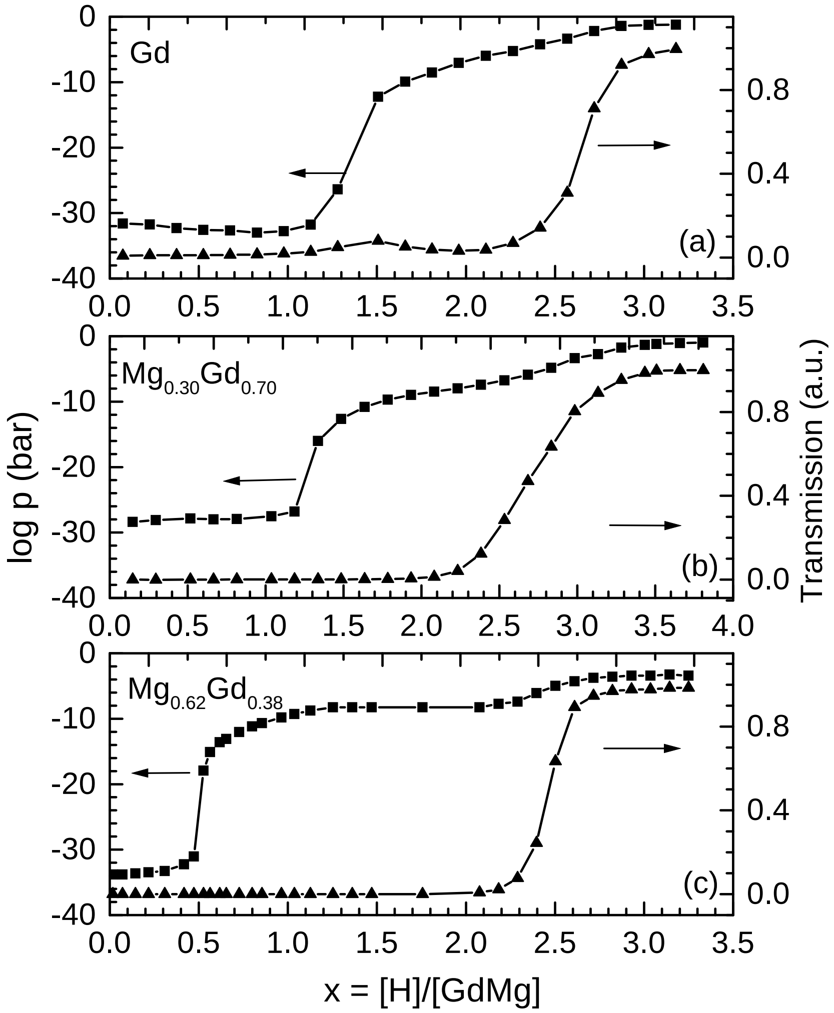

**Figure 1.11:** Pressure-composition isotherms (squares) for (a) Gd, (b) $Mg_{0.3}Gd_{0.7}$, and (c) $Mg_{0.62}Gd_{0.38}$ alloys as determined electrochemically. The corresponding normalized transmission at 1.85 eV (triangles) is also shown. (1 bar = $10^5$ Pa) (From Ref. [25])

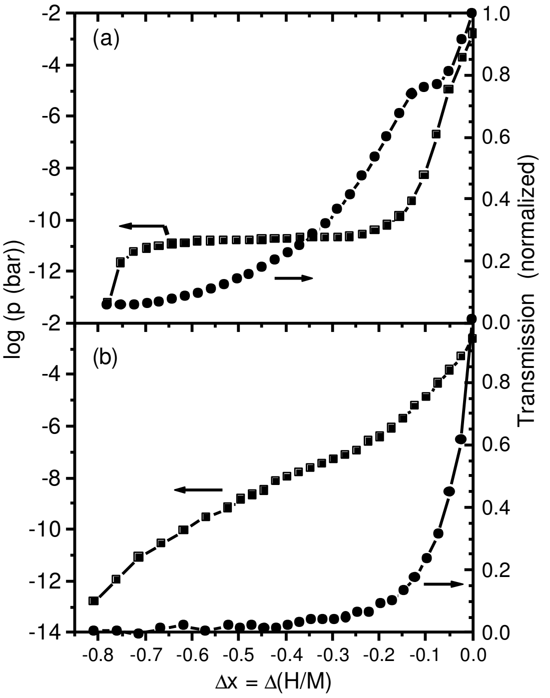

**Figure 1.12:** Pressure-composition isotherms (squares) as determined by Giebels *et al.* [51] at 30°C of (a) $YH_{3-\Delta x}$ and (b) $Mg_{0.1}Y_{0.9}H_{2.9-\Delta x}$ as a function of $\Delta x$, the amount of hydrogen per metal atom that is desorbed. The measurements are performed electrochemically in the third desorption cycle. Also shown is the normalized transmission at 1.85 eV ($\lambda = 670$ nm) (circles). At $\Delta x = 0.0$ the sample is fully loaded with hydrogen, around $\Delta x = -0.8$ the sample is unloaded. (1 bar = $10^5$ Pa) (From Ref. [51])

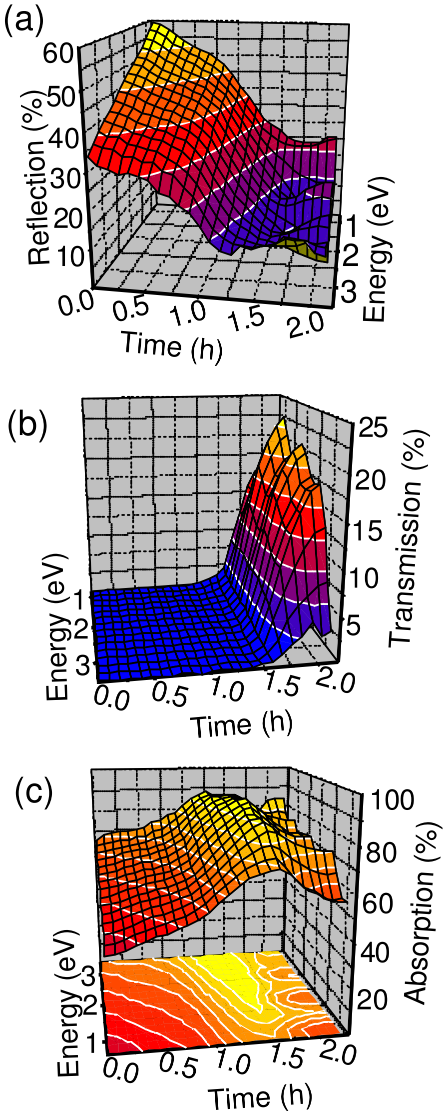

**Figure 1.13:** (a) Reflection, (b) transmission and (c) absorption of a 200-nm-thick $Mg_{0.5}Y_{0.5}$ film on quartz covered with 10 nm Pd during loading in $10^3$ Pa $H_2$. The time is given in hours. At $t = 2.2$ h the sample is fully loaded with hydrogen. The overall composition is then approximately $Mg_{0.5}Y_{0.5}H_{2.5}$. (From Ref. [48])

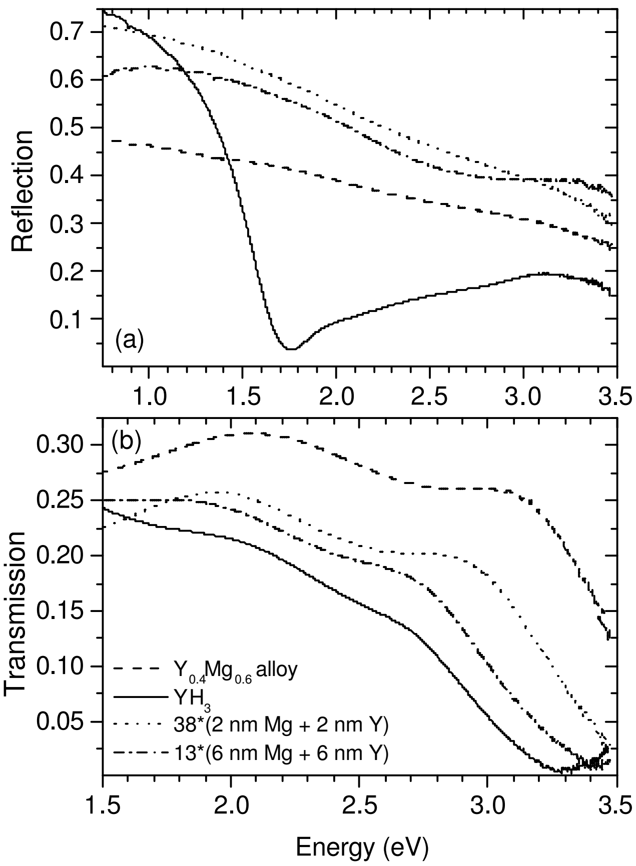

**Figure 1.14:** (a) Reflection spectra after hydrogen desorption, and (b) transmission spectra in the fully loaded state of a disordered $Mg_{0.6}Y_{0.4}$ alloy, Mg/Y multilayers with the same overall composition, and Y. The films all have a total thickness of 300 nm and are capped with 10 nm Pd. (From Ref. [49])

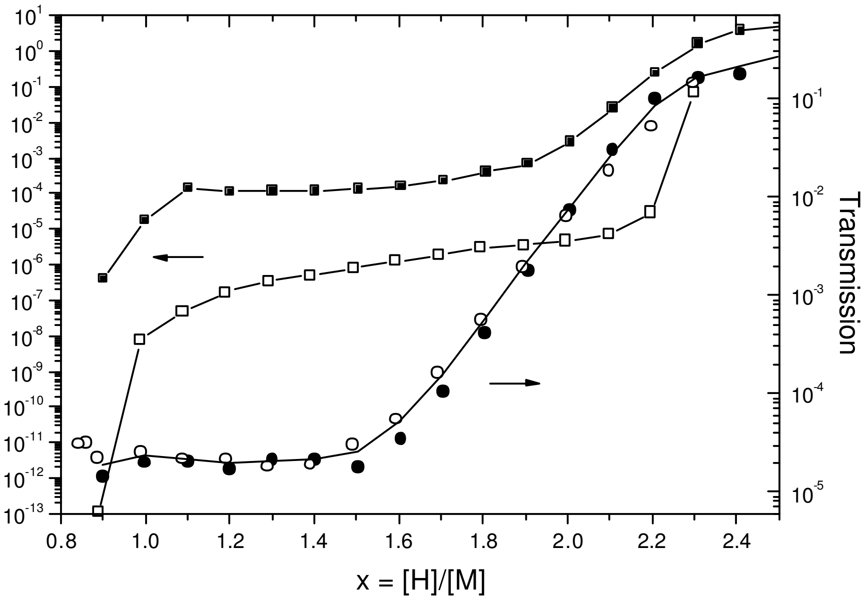

**Figure 1.15:** Pressure-composition isotherm determined electrochemically (squares) of a 15∗(10 nm Mg + 10 nm Y) multilayer capped with 10 nm Pd between the unloaded ($YH_2$ and Mg) and fully loaded state ($YH_3$ and $MgH_2$) as a function of the hydrogen concentration per metal atom, $x =$H/M. Also shown is the transmission (circles) at 635 nm (1.96 eV). The filled symbols refer to hydrogen absorption and the open ones to desorption. (1 bar = $10^5$ Pa) (From Ref. [49])

## 1.5 Third-generation switchable mirrors: Magnesium-transition-metal films

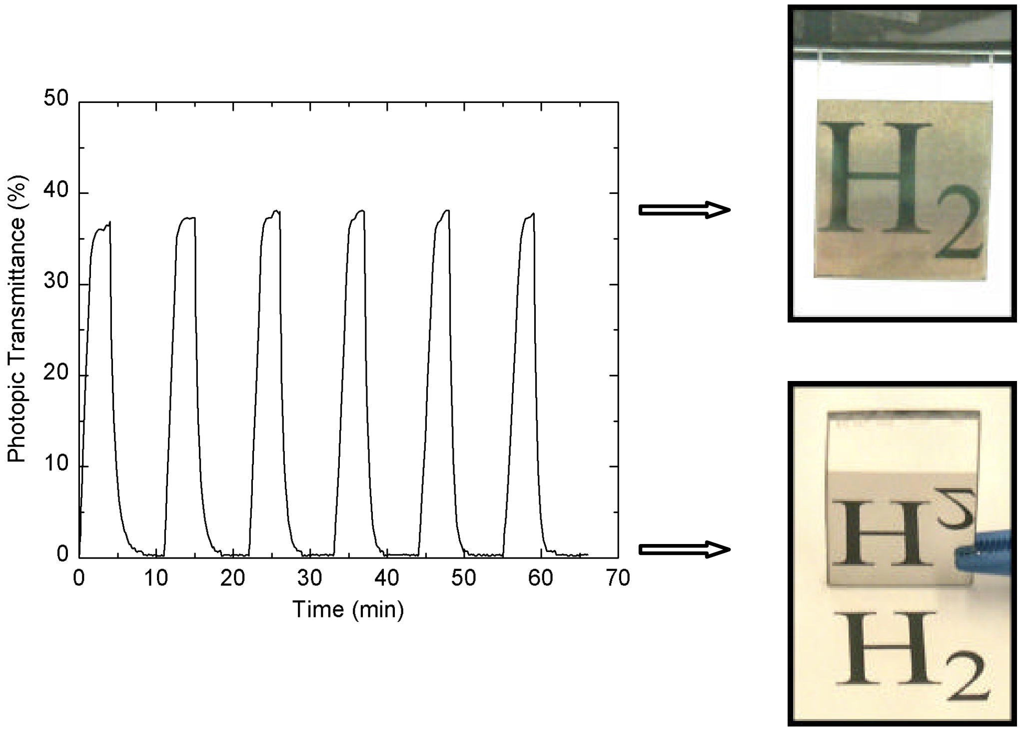

**Figure 1.16:** Optical transmission of a 40-nm-thick Mg-Ni-$H_x$ film evaporated on ITO/glass and capped with 5 nm Pd during electrochemical loading-unloading cycles in 8 M KOH/1 M LiOH. The upper photograph shows transparent Mg-Ni hydride, the lower photograph is Mg-Ni in the reflecting state. (From Ref. [137])

Richardson *et al.* [137, 138] reported in 2000 that alloys of Mg and Ni exhibit also optical switching as a function of H concentration (see Fig. 1.16). At first sight this does not seem to be of major importance since it has been known for decades that $Mg_2Ni$ reacts readily with gaseous hydrogen to form $Mg_2NiH_4$ [130] that is considered to be an attractive material for storage purposes. The reaction occurs by formation of $Mg_2NiH_4$ from the hexagonal intermetallic compound $Mg_2Ni$ upon hydrogen absorption. The hydrogen solubility range of the hexagonal $Mg_2Ni$ is limited to 0.3, i.e. it extends up to a composition $Mg_2NiH_{0.3}$ [130, 158]. The hydride $Mg_2NiH_4$ is the only stable ternary compound known for the Mg-Ni-H system. This compound shows a well-defined stoichiometry, essentially independent of temperature and hydrogen partial pressure. During heating under a $H_2$ pressure of one atmosphere $Mg_2NiH_4$ undergoes a structural phase transition at 510 K to a cubic high-temperature form with the metal atoms in an antifluorite-type structure [40, 44, 145]. The low-temperature form of $Mg_2NiH_4$ is monoclinic albeit with only slight distortions from the antifluorite lattice [44, 180].

The discovery of Richardson *et al.*, however, is important for two reasons. First, it demonstrated that Mg-Ni films absorb very easily hydrogen. While in bulk samples hydrogenation requires high temperatures (500 to 600 K) and pressures of $10^5$ to $10^6$ Pa [12, 130], for thin films it occurs readily at room temperature at low pressures when they are capped with a thin Pd layer. Secondly, it opened the way to the *third-generation* switchable mirrors. This class of materials does not involve rare-earth metals and might therefore be more resistant to oxidation than the earlier mirrors. This is especially important for applications. So far all alloys of Mg with the transition metals (TM) Ni, Co, Fe, Mn, V have been found to switch with hydrogen [139] (see Fig. 1.19 on page 44).

As for the 1st and 2nd generation switchable mirrors, thin films provide us with a unique possibility to determine the intrinsic physical properties of $Mg_2NiH_x$ and other so-called complex metal-hydrides such as $Mg_2CoH_5$ and $Mg_2FeH_6$. A first indication that the physics of $Mg_2NiH_4$ is not trivial is that until very recently the position of H in $Mg_2NiH_4$ was not known precisely. By combining total energy calculations with experimental data García *et al.* [39] conclude that in the HT phase the four H are arranged around a Ni atom in a tetrahedrally distorted square planar configuration. The negatively charged complex $(NiH_4)^{4-}$ is ionically bound to the $Mg^{2+}$ ion. For the LT phase Myers *et al.* [115] found from an energy minimalization that hydrogen is in an almost perfect tetrahedron. As a whole every added hydrogen removes one electron [32] from the conduction band of $Mg_2NiH_x$ as expected on the basis of the so-called anionic model for hydrogen in Groups I, II and III of the periodic table [114].

### 1.5.1 Electrical properties and the metal-insulator transition

Enache *et al.* [32] have investigated the temperature (between 2 K and 280 K) and concentration (for $0 < x < 4$) dependencies of the electrical resistivity, charge carrier density and magnetoresistance of $Mg_2NiH_x$ switchable mirrors. Although the electrical resistivity increases by almost three orders of magnitude between metallic $Mg_2Ni$ and transparent $Mg_2NiH_4$ (see Fig. 1.17) the charge carrier concentration n decreases only gradually from typically $10^{23}$ $cm^{-3}$ to $10^{21}$ $cm^{-3}$. These metallic-like features indicate that $Mg_2NiH_{4-\delta}$ prepared at room temperature under $1.3 \times 10^5$ Pa $H_2$ is a heavily-doped semiconductor [13, 32]. The estimated non-stoichiometry is $\delta = 0.05$. By combining Hall effect, electrical resistivity and electrochemical data, it is shown that n varies like $(4-x)$, which confirms that the role played by hydrogen in the host lattice is that of a negatively charged $H^-$ ion. In the limit $\delta \to 0$, $Mg_2NiH_4$ is a semiconductor. This is in agreement with the electronic ground state of the low-temperature $Mg_2NiH_4$ phase calculated by Myers *et al.* [115] (see Fig. 1.18).

For $0.3 < x < 4$ the hydrogen concentration dependence of the electrical resistivity of $Mg_2NiH_x$ can be modelled with an effective medium theory. From such an analysis Enache *et al.* concluded that the metallic $Mg_2NiH_{0.3}$ and $Mg_2NiH_4$ inclusions needed to be very flat ellipsoids with their small axes perpendicular to the plane of the film. This implies that a $Mg_2NiH_x$ film exhibits metallic behaviour up to high hydrogen since the flat metallic inclusions short-circuit the sample.

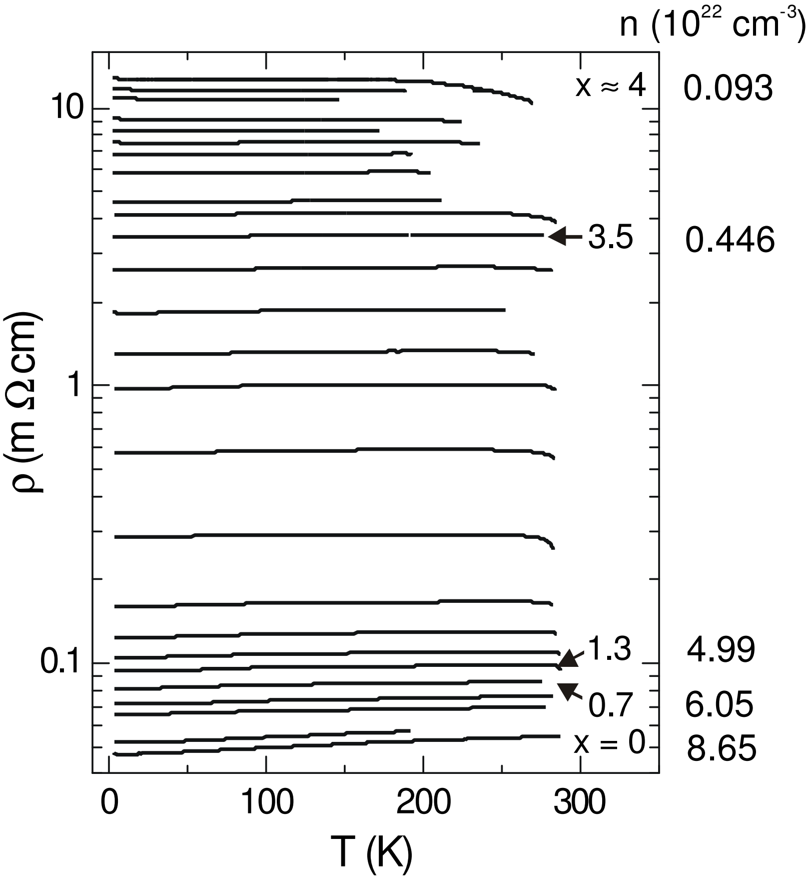

**Figure 1.17:** Electrical resistivity $\rho$ of a 232-nm-thick $Mg_2NiH_x$ film (with $0 < x < 4$) covered with 2 nm Pd as a function of temperature . The curves corresponding to $Mg_2NiH_x$ samples with concentrations $x = 0, 0.7, 1.3, 3.5$ and $\approx 4$ are indicated explicitly. The decreasing electrical resistivity above 220 K is due to hydrogen loss during warming up of the film. (From Ref. [32])

### 1.5.2 Optical properties

There have been several fragmentary reports on the optical properties of $Mg_2NiH_4$ in the past. Reilly and Wiswall noted already in 1968 [130] that bulk $Mg_2NiH_4$ was a dark red solid, Lupu *et al.* [104] determined a band gap of 1.68 eV for both the low-temperature (LT) and high-temperature (HT) phases from resistivity data and reflection measurements on powder samples, Selvam *et al.* [149] measured two gaps near 2.0 eV and 2.4 eV, the direct respectively the indirect gap of $Mg_2NiH_4$, and Fujita *et al.* [38] found a gap of $\approx 1.3$ eV in a $Mg_2NiH_4$ film from resistivity data and optical absorption measurements for both the LT and HT phases. The large spread in these values is a direct indication of one major difficulty with these materials, i.e. the controlled deposition of films with well-defined composition and morphology (see also Section 1.6.2 on page 49). Richardson *et al.* measured the optical transmission and reflection only for as-deposited

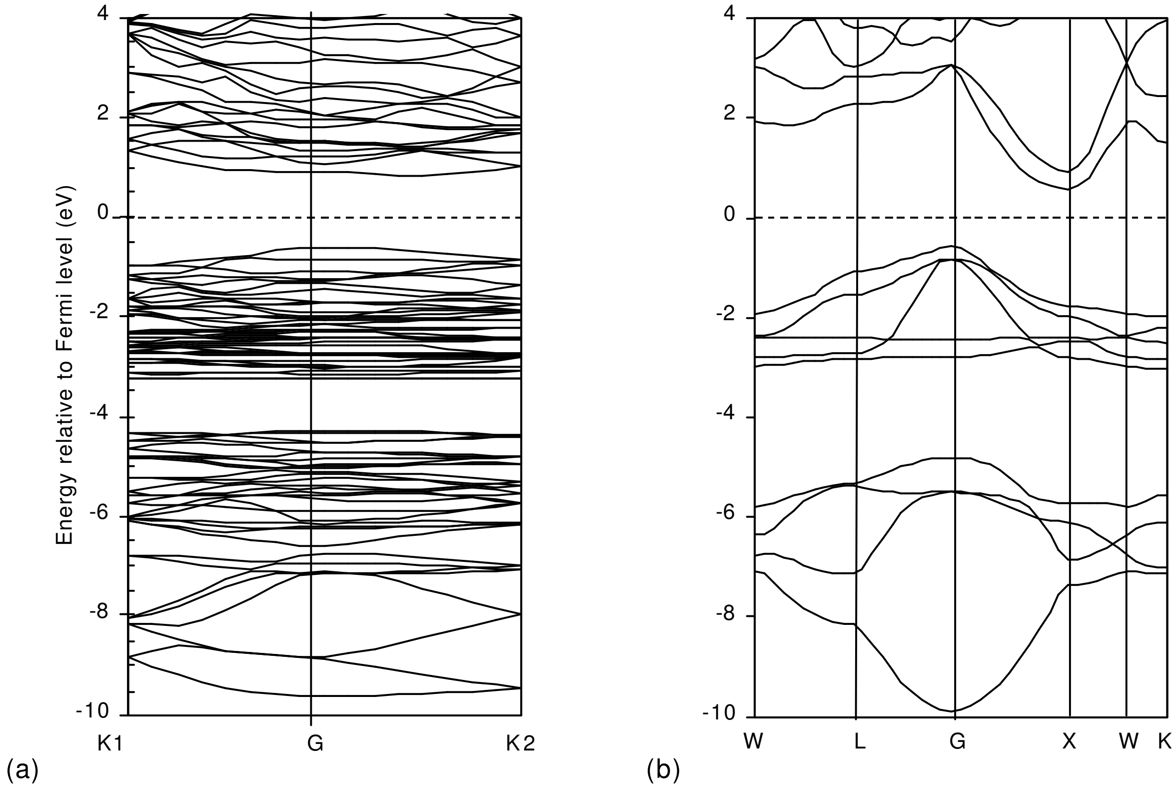

**Figure 1.18:** Electronic band structures for $Mg_2NiH_4$ calculated with LDA in (a) the low-temperature monoclinic phase and (b) the high-temperature cubic phase with undistorted tetrahedral $NiH_4$ complexes. (From Ref. [115])

films and fully hydrogenated films (see Fig. 1.19). In many cases these films were very much Mg-rich [138, 139]. For films with a composition close to $Mg_2NiH_4$ Isidorsson *et al.* [78] estimated from transmission edge measurements a gap of 1.6 eV in reasonable agreement with the band structure calculations of Myers *et al.* [115] and Haussermann *et al.* [64].

The first detailed study of hydrogen concentration dependence of the optical properties of $Mg_2NiH_x$ was done by Isidorsson *et al.* [79]. They measured the reflection and transmission together with the electrical resistivity of a 232-nm-thick $Mg_{2.1}NiH_x$ film capped with 2 nm Pd during slow loading with hydrogen. These measurements revealed a curious behaviour of the reflection at low hydrogen concentration. Above $x = 0.3$ the reflection drops markedly and reaches a minimum at $x = 0.8$, i.e. at a hydrogen-to-metal ratio of less than 0.3.[3] The optical transmission remains very low (typically 0.001) until $x$ is approaching 4. The electrical resistivity at the minimum in reflection is still relatively low, typically below $100\mu\Omega$cm. The Hall effect data indicate

---

[3] The estimated hydrogen concentration in the original publication by Isidorsson *et al.* [79] was too low. At the time the authors were convinced that the drop in reflection occurred for $0.2 < x < 0.3$. Lohstroh *et al.* [101] have shown that the black state corresponds to an overall hydrogen concentration of $0.3 < x < 0.8$.

that the charged carrier concentration is still rather high, typically $7 \times 10^{22}$ cm$^{-3}$. This seems to be mutually incompatible since metals have always a large reflectance. This stimulated a large effort by Lohstroh *et al.* [101, 102] in order to understand the mechanism leading to this peculiar behaviour.

### 1.5.3 Black state due to self-organized layering

An important clue about the origin of the black state in $Mg_2NiH_x$ came from a visual observation from the front and backsides of the same sample during hydrogen loading [102]. Figure 1.20 displays photographs taken from two pieces of the same sample (a) in the metallic state and (b) black $Mg_2NiH_{0.8}$, respectively. The sample on the left hand side is viewed through the substrate and on the right hand side the Pd cap layer faces the front. Without hydrogen, both sides are shiny reflecting, and the small difference in appearance is mainly due to the different media for the incoming light (sapphire on the left hand side and air on the right hand side). After hydrogen is introduced at a pressure of 1600 Pa, it takes a couple of minutes for $Mg_2NiH_x$ to become black when viewed through the substrate. Surprisingly, $Mg_2NiH_x$ keeps its metallic lustre when observed from the Pd side. Note, that the Pd cap layer (5 nm) has a rather high transparency ($T > 40\%$) and hence the $Mg_2NiH_x$ layer underneath contributes significantly to the observed reflection. These photographs demonstrate vividly that the originally homogenous $Mg_2Ni$ film starts to react with hydrogen at the substrate-film interface [101, 102]. Further H-uptake causes the hydrogen-rich layer to grow at the expense of the metallic part until eventually the entire film has switched to $Mg_2NiH_4$. This double layer model is compatible with the x-ray absorption spectroscopy data by Farangis *et al.* on Mg-Ni (see Fig. 2 in Ref. [37]) where they see that while the Mg-Ni peak gradually decreases, the Mg-Ni hydride peak increases.

This unusual loading sequence is also supported by the data in Fig. 1.21 that represents the evolution of the reflection from the substrate side as a function of hydrogen loading. Due to the transparency of $Mg_2NiH_4$ the reflection exhibits typical interference fringes when the optical path length of the light that is reflected between the two interfaces (substrate-$Mg_2NiH_4$ and $Mg_2NiH_4$-$Mg_2NiH_{0.3}$, respectively) is a multiple of the wavelength. With increasing hydrogen concentration the increasing $Mg_2NiH_4$ thickness yields to a shift of the interference fringes towards lower energies as well as to a smaller difference between adjacent maxima until the entire sample has switched. In contrast, the reflection viewed from the Pd side is unchangingly high. The increasing thickness of the evolving $Mg_2NiH_4$ layer can be directly determined from the experimental reflection data. During hydrogen unloading reflection, transmission and resistivity go through the same stages as during loading but, of course, in reversed order.

The mechanism leading to the black state described above is not an exotic peculiarity of the $Mg_2NiH_x$ system. It is also observed in other Mg-based alloys (Mg-Co, Mg-Fe and Mg-Co-Ni). The spatial separation of the hydrogen uptake (in the catalytic Pd layer) and the nucleation of the new phase ($Mg_2NiH_4$, $Mg_2CoH_5$ and $Mg_2FeH_6$) in the vicinity of the film substrate interface seems inherent to these systems. The black state is robust in the sense that it appears in sputtered films as well as in UHV evaporated films and the choice of the substrate is also not crucial i.e. $Al_2O_3$, glass, ITO, $SiO_2$ and $CaF_2$ can be used.

It is important to note here that the black state observed in Mg-TM hydrides is fundamentally different from that of Mg-RE hydrides described in Section 1.4.4 on page 31. In the Mg-RE hydrides a spatial disproportionation into Mg and $REH_2$ islands is induced once and for all during the *first* hydrogen loading. These islands are finely dispersed throughout the film. In the Mg-TM hydrides a macroscopic and reversible layering is the essential feature.

The fact that all films investigated could easily be loaded at room temperature at pressures well below $10^5$ Pa demonstrates the importance for the hydrogen loading process of the small grain size typical for these thin films. The fact that the hydrogenation starts from the bottom of the film, suggests some catalytic activity of the film/substrate interface. This suggests new strategies for the optimization of catalysts in, for example, nanostructured hydrogen storage materials. In this respect an appropriately catalyzed $Mg_2FeH_6$ is interesting since it has a relatively high hydrogen capacity: 5.7 wt% and 171 kg $H/m^3$.

As discussed in Section 1.8.2 on page 60 the switching from a mirror to a black absorber offers also interesting possibilities for applications as smart coatings in solar collectors and antiglare rear-view mirrors or as sensing layer in optical fiber hydrogen detectors. The fact that the switching takes place at a low hydrogen-to-metal ratio is a favourable factor for the cycleability of a device.

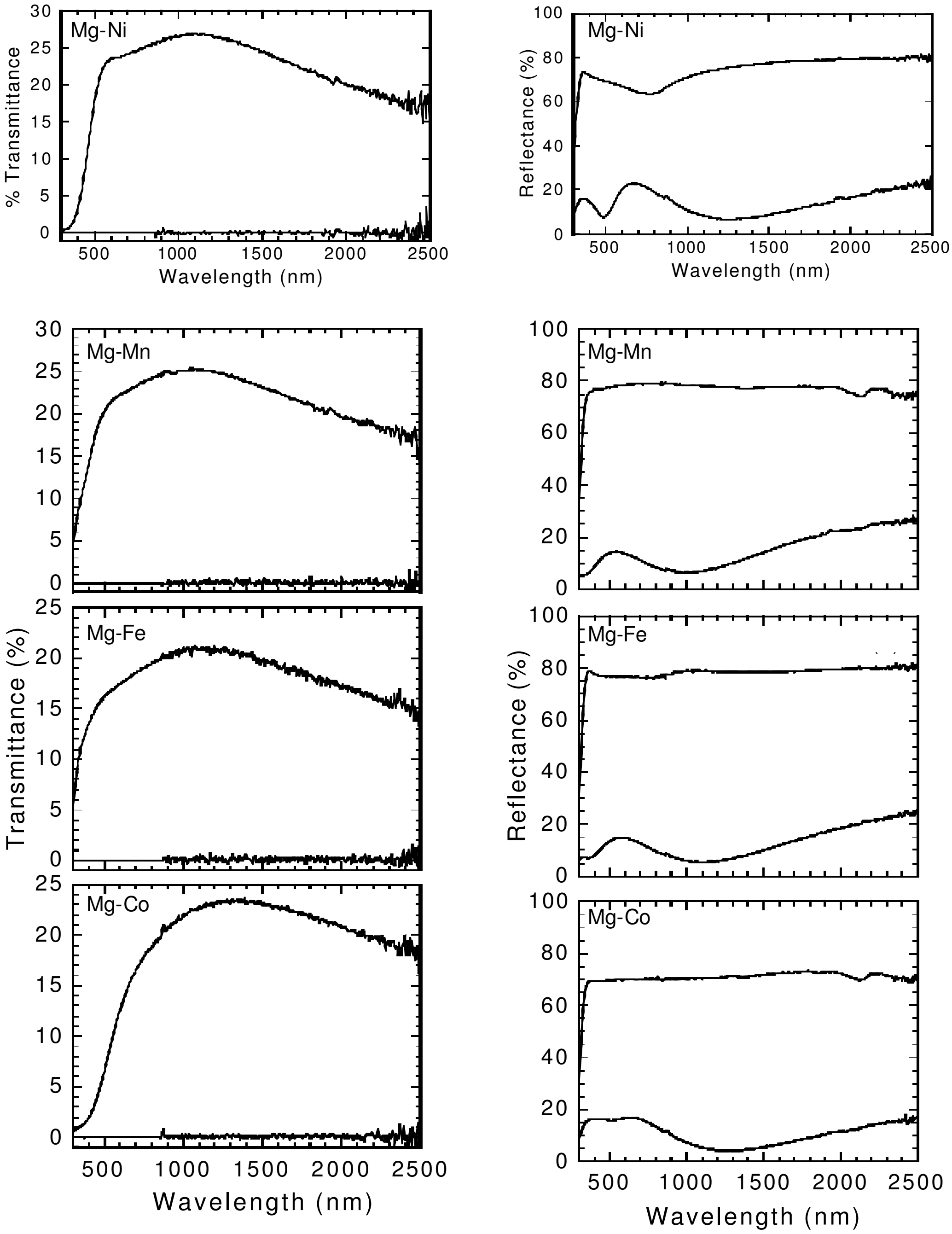

**Figure 1.19:** Visible and near-infrared reflection and transmission spectra of 80 nm Mg-Ni, 60 nm Mg-Mn, 40 nm Mg-Fe, and 40 nm Mg-Co films (Mg:TM 6:1) with 7-nm-thick Pd overlayers on glass substrates in the metallic and fully hydrogenated states. Spectra were recorded from the substrate side. (From Refs. [138, 139])

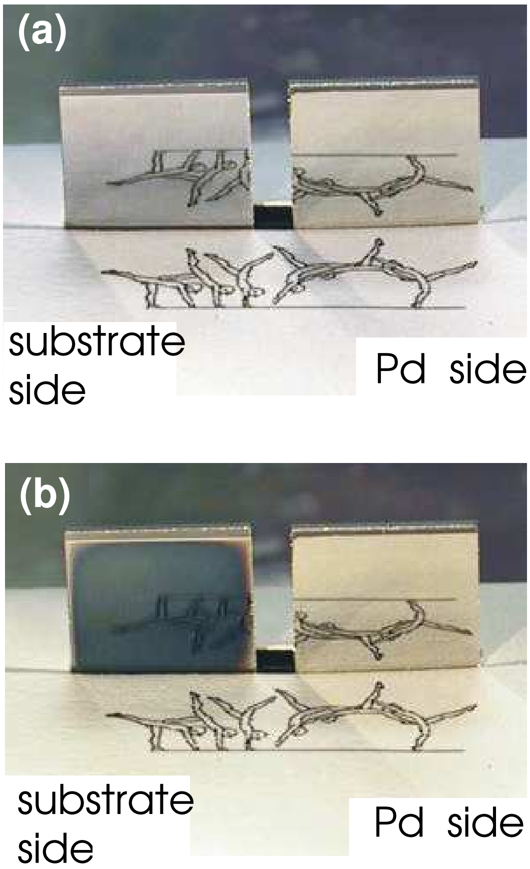

**Figure 1.20:** Photographs of two identical films 200 nm $Mg_2Ni$ / 5 nm Pd on sapphire. On the left hand side we look at the film through the substrate and on the right hand side from the Pd layer side. (a) As-deposited, (b) in 1600 Pa $H_2$ at room temperature. Upon exposure to hydrogen the 'substrate' side of the sample becomes black while the 'Pd' side stays metallic. The difference in appearance is not due to the thin metallic Pd cap layer but due to the nucleation of the hydrogen-rich phase $Mg_2NiH_4$ at the film-substrate interface. (From Ref. [102])

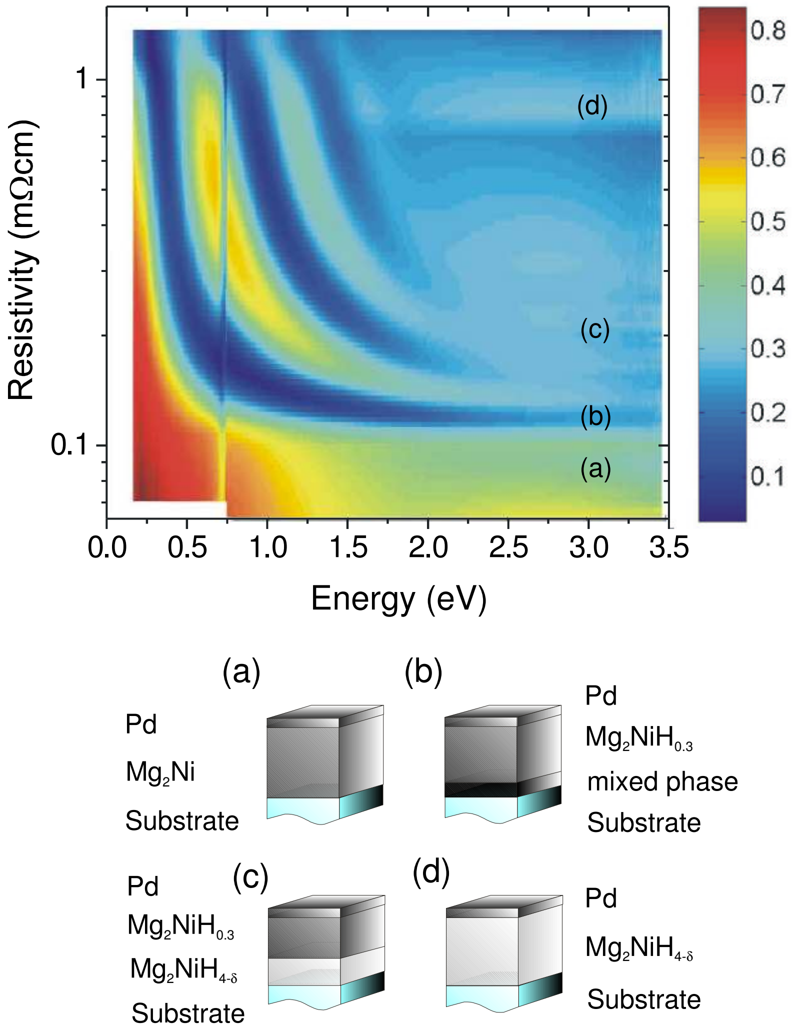

**Figure 1.21:** Intensity map of the reflection $R$ (measured through the substrate) during hydrogen uptake of a sample 250 nm $Mg_2Ni$ / 7 nm Pd. At low resistivity (i.e. in the metallic state) $R$ is high. At around $\rho = 130\mu\Omega$cm ($x \sim 0.8$) $R$ exhibits a deep minimum over the entire visible wavelength regime. A double layer system $Mg_2NiH_{0.3}$-$Mg_2NiH_4$ is formed and subsequently interference minima and maxima appear. As the transparent layer increases in thickness these interference fringes shift to lower energies. The hydrogen induced layering of the film is schematically indicated at four characteristic hydrogen concentrations (a)-(d). (From Refs. [101, 102])

## 1.6 Applications of switchable mirrors to materials science problems

### 1.6.1 Switchable mirrors as indicator layers

One of the striking properties of hydrogen in metals is its large mobility. Already at room temperature the H diffusion coefficient can be as high as $10^{-5}$ $cm^2/s$, i.e., a value almost comparable to diffusion in liquids. Diffusion of hydrogen in metals has also attracted considerable theoretical attention, because it is fast even at low temperatures, involves only simple jumps between interstitial sites, and is ideal for the investigation of isotope effects when H is replaced by deuterium or tritium. A review of experimental data and techniques used so far to measure hydrogen diffusivity in bulk samples is given by Völkl and Alefeld [165]. Most of these methods are not applicable to thin films as they are either hampered by the influence of the substrate e.g., in Gorsky effect or by the rather small volume of the film e.g. in quasi-elastic neutron scattering. Consequently, relatively little is known about hydrogen diffusion in thin metallic films and multilayers. Furthermore, very little is known about long range diffusion of hydrogen in metals such as yttrium, lanthanum and rare-earths metals, for the simple reason that these materials are reduced to powders at high hydrogen concentrations. As mentioned in the Introduction, thin films of these materials do not suffer from this drawback. The understanding and manipulation of hydrogen transport through films is, however, important for the control and optimization of coatings and thin-film devices such as hydrogen detectors, metal-hydride switchable mirrors or tunable magnetic elements. The fact that switchable mirror films have optical properties that depend strongly on hydrogen concentration offers the possibility to use them as two dimensional hydrogen concentration indicators. The simplest application is to monitor hydrogen diffusion in switchable mirrors themselves. Another possibility is to deposit a thin switchable mirror on a sample of interest that might be opaque. In such a configuration hydrogen diffusion can be observed through a coloration change in the switchable mirror indicator. Several examples of indicator applications are described below.

#### Diffusion and electromigration in switchable mirrors

One can exploit the characteristic features of the transmission spectra of switchable mirrors to monitor hydrogen diffusion optically in a non-invasive way. The first experiments by Den Broeder *et al.* [17] were done on yttrium by using a film produced in the following way (see Fig. 1.22). First, an yttrium film is evaporated under ultrahigh vacuum conditions onto a transparent substrate (sapphire or quartz). Subsequently, a several nm thick palladium pattern (consisting for example of a disk or one or more strips) is evaporated *in situ* on top of yttrium. When brought into contact with air yttrium oxidizes, forming a thin $Y_2O_3$ layer that is impermeable to hydrogen atoms. However, areas covered with Pd do not oxidize and remain permeable for hydrogen. In a typical experiment, hydrogen gas ($10^5$ Pa) is introduced into the chamber containing the sample. The chamber that is equipped with optical windows and a temperature control system is placed onto the positioning table of an optical microscope. Using a white lamp behind the cell optical transmission changes are monitored optically. In contact with $H_2$, the yttrium underneath the palladium pattern immediately starts absorbing hydrogen atoms and within a few seconds transparent $YH_{3-\delta}$ is formed under the Pd-covered region. Further hydrogen uptake can only take place if H diffuses out laterally into the Y underneath the transparent $Y_2O_3$ layer. For the disk geometry chosen in Fig. 1.22 hydrogen diffuses radially. As the hydrogen concentration $x$ decreases from essentially 3 beneath the Pd disk to 0 far from it, several hydride phases are formed. As each phase has a characteristic optical transmission, H diffusion leads to the formation of typical rings that expand with time $t$ as $\sqrt{t}$. The inner ring corresponds to the $\gamma$-$YH_{3-\delta}$ phase and the outer ring to the $\beta$-$YH_2$ phase, with its weak transparency window for red photons (1.8 eV). It is this characteristic optical feature that makes it possible to observe real-time hydrogen diffusion at room temperature.

The same technique can be used to study electromigration of hydrogen in a switchable mirror [17, 112]. A nice example is shown in Fig. 1.23 for an yttrium film that is simultaneously loaded with hydrogen from the left and the right through Pd pads. In absence of an electrical current (top panel) the diffusion pattern is symmetric. In the presence of a current a clear asymmetry is induced (middle panel). The asymmetry is increased by increasing the current (lower panel). These experiments show unambiguously that hydrogen behaves like a negative ion in $YH_x$. This is in agreement with the infrared data of Rode *et al.* [140] and the strong electron correlation models of Ng *et al.* [118, 119] and Eder *et al.* [29] (see Section 1.3.4 on page 17).

### Visualization of hydrogen diffusion in opaque materials

The technique described above for $YH_x$ is obviously not directly applicable to systems that are opaque. However, one should realize that a material such as $YH_x$ exhibits also characteristic changes in its reflection (see Sec. 1.3.1 on page 13). Remhof *et al.* [132] demonstrated that hydrogen diffusion in materials such as vanadium could be monitored optically in reflection by using samples as shown in Fig. 1.24(a). A vanadium stripe of 10-mm length, 1-mm width and a thickness of typically 100 nm is covered with a thin layer of yttrium as an optical indicator for hydrogen diffusion. The indicator thickness is typically 30 nm. One end of this V/Y sandwich is covered *in situ* with a 10-nm-thick Pd cap layer. When brought into air a thin oxide layer forms on the uncovered yttrium. Loading with hydrogen proceeds via the Pd stripe. The subsequent lateral hydrogen diffusion occurs mainly through vanadium, since H uptake cannot occur via the superficially oxidized Y and since hydrogen diffusion is several orders of magnitude faster in vanadium than in yttrium. The lateral migration of hydrogen in vanadium away from the Pd-covered region can easily be monitored optically as a change in the reflection of the Y indicator layer. Figure 1.24(b) depicts a snapshot at $t = 10^4$ s after the Y/V sandwich was exposed to a hydrogen atmosphere of $10^2$ Pa at T=473 K. The Pd-covered part, where the hydrogen enters the samples and the lateral diffusion starts, is at the top of the photo. The optical discontinuity within the indicator corresponds to the boundary between the silvery gray low concentration $\alpha$-$YH_{0.2}$ phase and the blue (in reflection) dihydride phase $\beta$-$YH_{1.9}$. This diffusion front has moved by approximately 0.9 cm within $10^4$ s. This indicates that the diffusion coefficient is of the order of $10^{-4}$ $10^{-5}$ cm$^2$/s, which is indeed very fast, in agreement with measurements on bulk samples. It should be pointed out here that reliable values for the diffusion coefficient can only be derived from simultaneous optical measurements on Y/V sandwiches with various thickness ratios in order to take into account the hydrogen leaking from the film under investigation (here V) to the indicator layer (here Y). With such an analysis Remhof *et al.* [132] determined D=1.2 × $10^{-5}$ $cm^2/s$ at T=473 K for a hydrogen concentration H/V=0.62. Furthermore, the photographs in Fig. 1.24(b) indicate clearly that the overall diffusion rate of hydrogen in an Y/V sandwich depends on the thickness ratio of the two metallic layers. This means that the effective diffusion coefficient of a film can be tuned. In a patterned thin film this opens the opportunity to locally vary the hydrogen mobility and to investigate the behaviour of hydrogen diffusion fronts when they are crossing the interface between two media with different diffusion coefficients [135,136]. As an example we show the results obtained by Remhof *et al.* for a circular diffusion front generated in a 'slow' medium (see Fig. 1.25). When it hits the boundary with a 'fast' medium the front bulges out and a mushroom shaped pattern is formed. The deformation of the diffusion front can be investigated in great detail and compared to theoretical calculations [150]. The results of this type of experiments is also relevant for the propagation of so-called diffusion waves (see e.g. Refs. [105,123]).

## 1.6.2 Combinatorial research

### Use to optimize catalytic cap layers/buffer layers

The hydrogenation process of a metal-hydride $MH_x$ capped by a catalyst layer is a complicated process [146]. Hydrogen molecules absorb at the catalyst surface (physisorption), split in chemisorbed hydrogen atoms, diffuse into the catalyst subsurface layers, diffuse towards the $MH_x$ boundary and cross the catalyst/$MH_x$ boundary.

To optimize catalytic layers one needs to study the interaction of two layers. To speed-up the optimization procedure of catalyst/metal-hydride layers Van der Molen *et al.* [110] introduced a combinatorial approach, using so-called matrix samples (see insert in Fig. 1.26). Using a shadow mask, they deposited two orthogonal stepped thickness gradients of both the switching metal (in this case yttrium or lanthanum) and the catalyst layer (palladium) and created in this way $\sim$ 200 different plaquettes on the same substrate. Monitoring the optical transmission during hydrogen loading, the behaviour of these $\sim$ 200 plaquettes is recorded. From a comparison the optimal layer thicknesses for the parameters of interest (i.e. for a short switching time, large optical contrast, reversibility, etc.) are easily obtained (see Fig. 1.26). Indeed a well-defined critical Pd-thickness was found (see Section 1.2.1). The stepped matrix samples have the advantage that the optimal combination of layer thicknesses can easily be distinguished from the plaquette position on the matrix sample.

With this technique it was also possible to look for appropriate buffer layers between the metal-hydride and Pd to prevent interdiffusion and oxidation [54]. In the case of La switchable mirrors is was found that an $AlO_x$ layer with a very well defined thickness (between 0.9 and 1.2 nm) is able to inhibit Pd/La interdiffusion and oxidation of La without significantly hampering hydrogen absorption.

### Search for new lightweight hydrogen storage materials

In the standard approach followed so far, the exploratory search for new lightweight hydrogen storage materials is very time consuming since a bulk sample needs to be made for each chosen composition. However, metal-hydrides and even complex metal-hydrides are easily formed at room temperature from the elements, when a thin film of the corresponding metal composition is exposed to hydrogen. Thin films are therefore perfectly suited to study the reversible formation of complex hydrides from the elements. By making thin films with controlled gradients in the local chemical composition of three or more constituents, one may study the hydrogenation of typically $10^4$ samples simultaneously since the hydrogenation process can be monitored optically. Here one exploits the hydrogen concentration dependence of optical properties of metal-hydrides. Since at least 90% of all complex metal-hydrides found so far have a band gap, the transparency is a good indicator for the presence of a (complex) hydride phase. For the fabrication of gradient samples Dam *et al.* [35] use a sputtering system with several off-axis sources, which can be tilted towards and away from the substrate (see Fig. 1.27). Depending on the tilt angle, the thickness of a particular component increases up to 7-fold over a diameter of a 3 inch wafer.

Using Mg-Al and Mg-Ni as model systems, Dam *et al.* found that the well-known $Mg_2NiH_4$ and $Mg(AlH_4)_2$ hydrides indeed show up as transparent regions with a well-defined compositional width after hydrogenation. Reversible optical switching (and hence reversible hydrogen loading) was found in both systems over a very wide Mg-rich compositional range [35]. Another combinatorial approach is chosen by Olk *et al.* [124] who analyze the hydrogen sorption process by detecting the changes in the infrared emissivity during hydrogenation. This method basically detects both temperature changes (hence the enthalpy of formation) and changes in the optical properties of the material. They show that the hydrogen loading temperature of Mg-Ni-Fe alloys depends significantly on the composition.

Not every lightweight complex metal-hydride is suited for reversible hydrogen storage. The combination with PEM fuel cells dictates for example a hydrogen gas pressure of $1-3\cdot10^5$ Pa at $T< 373$ K. In addition, the kinetics must be fast enough to fill a tank with 5 kg of hydrogen within 2 minutes. The goal is to find a hydrogen storage material (combination) with a hydrogen-mass density larger than 7.5 wt%, a volume density larger than 62 kg/m$^3$ and suitable ab/desorption characteristics (typically a few times $10^5$ Pa hydrogen equilibrium pressure at 100°C) [33, 147]. To meet these objectives, one studies the effect of additives to stabilize or destabilize the crystal structure or to catalyze the sorption process. In a thin-film approach, the effect of substitutions on the loading behaviour is easily studied by co-depositing an additional gradient of a suitable element. To optimize the kinetic properties the gradient layers can be combined with various cap layers. Once the most promising spots have been identified, their local chemical composition, crystal structure and surface morphology are determined with Rutherford backscattering spectrometry, focused beam x-ray scattering and AFM, respectively. Thus the combinatorial thin-film-gradient technique is an efficient tool to optimize both the hydrogen content and the kinetics of the sorption reaction in both new and known complex metal-hydrides.

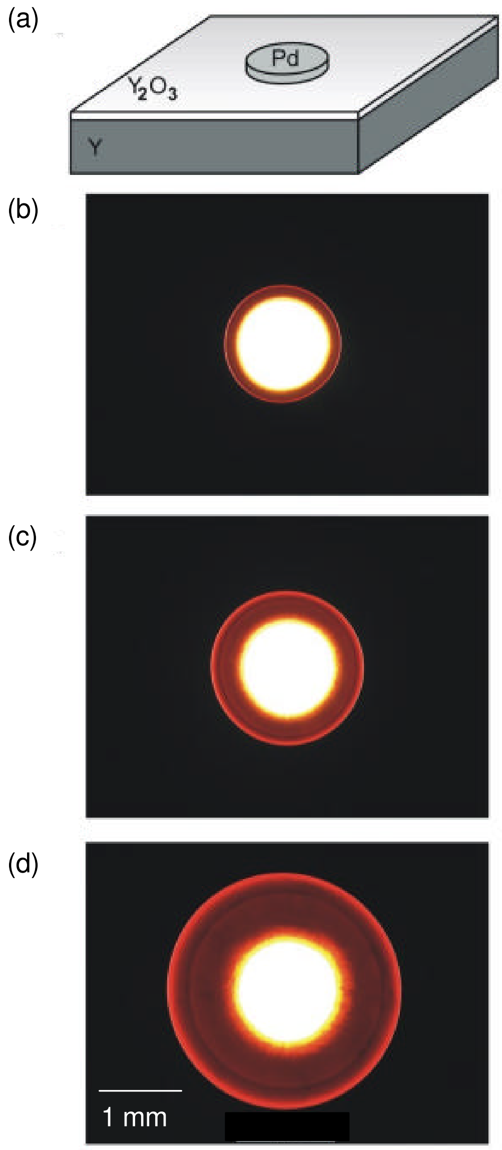

**Figure 1.22:** Radial hydrogen diffusion in yttrium observed visually. Microscope photographs in transmitted light of (a) a 300-nm-thick yttrium film on sapphire, covered by a 30-nm thick palladium disk of 1.1 mm diameter at various times $t$ after introduction of $H_2$ ($10^5$ Pa). Within a few seconds transparent $\gamma$-$YH_{3-\delta}$ is formed beneath the Pd, which adsorbs and dissociates hydrogen. The remaining Y surface has been oxidized, making it impermeable for hydrogen. (b) The diffusion profile after 1 day, (c) after 5 days, and (d) after 23 days at 60°C. The red outer ring is due to the weak transparency window at $\hbar\omega = 1.8$ eV, characteristic of the dihydride $\beta$-$YH_2$ phase, while the dark surrounding region is non-transparent metallic $\alpha$-$YH_x$. (From Ref. [17])

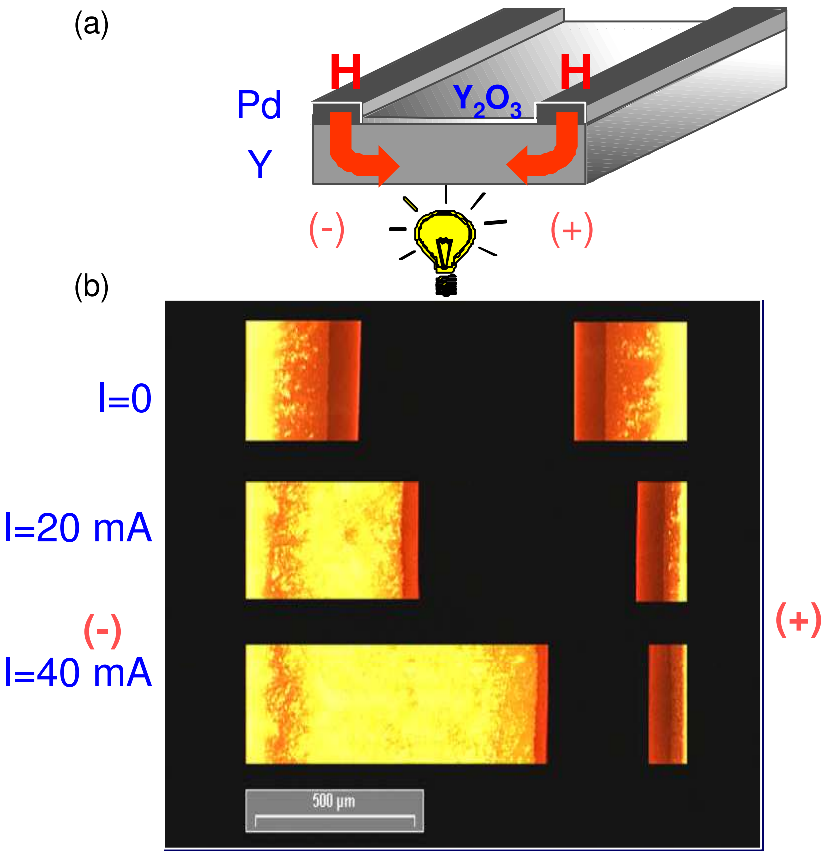

**Figure 1.23:** Electromigration of hydrogen in a (a) 200-nm-thick, 1.5-mm-wide Y film on sapphire, covered on the left and right by 30-nm-thick Pd-strips. At $t = 0$ $H_2$ gas (at $10^5$ Pa) is introduced and hydrogen is allowed to migrate for 12:10 h at 110°C. (b) In the absence of an electric current (I=0) the resulting diffusion profiles are symmetric. The lower two profiles show the hydrogen fronts when a d.c. current (I = 20 mA and 40 mA, respectively) has been applied from right (+) to left (-). The asymmetry in the profiles is due to the force created by the electric field on the hydrogen atoms, and proves the negative effective valence of H in $YH_{3-\delta}$. We note that the effect of electromigration on the $\beta$-phase growth is relatively small due to its lower resistivity. Therefore, it grows faster than $YH_{3-\delta}$ at the positive side of the sample, but shrinks to minimal size at the negative side, where it is almost overtaken by the accelerated $YH_{3-\delta}$ phase. The scale bar corresponds to 500 $\mu$m. (From Ref. [17])

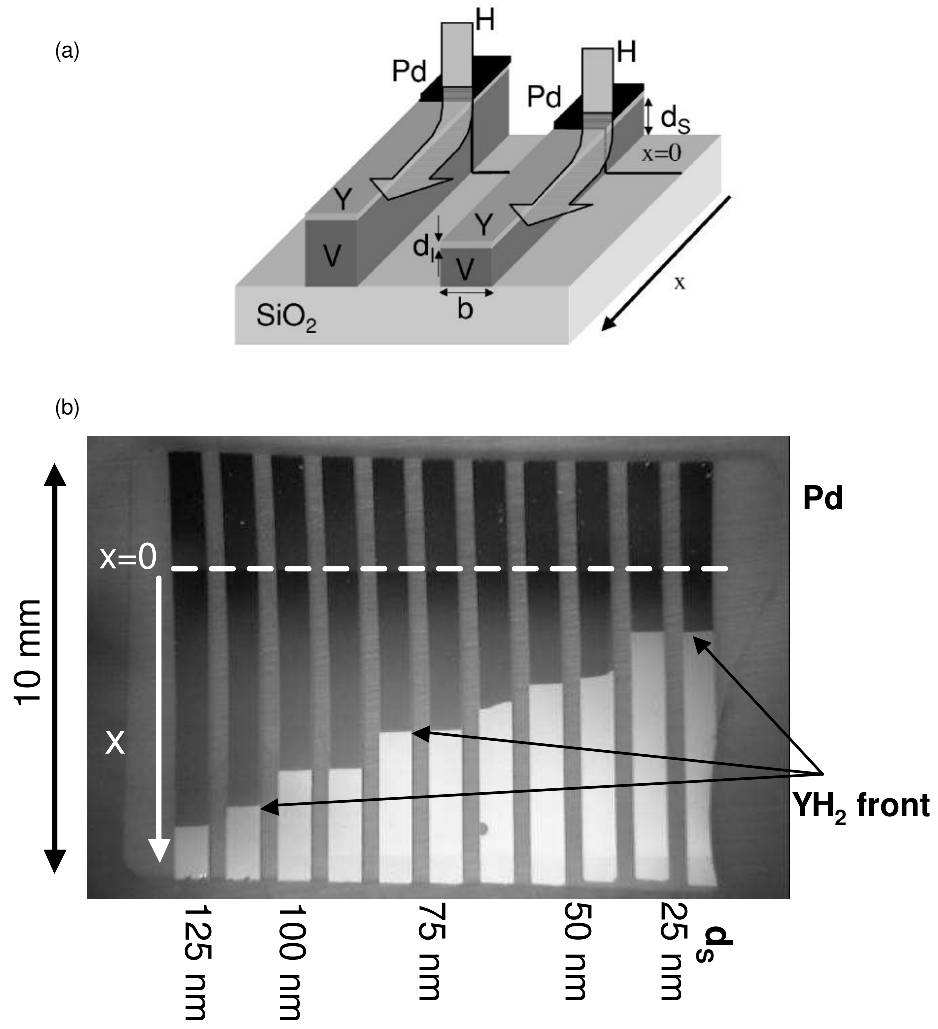

**Figure 1.24:** (a) Schematic sample design used by Remhof *et al.* [132] to measure optically hydrogen diffusion in vanadium. Yttrium-covered vanadium stripes ($1 \times 10$ mm$^2$) of thickness 25 to 125 nm are deposited onto an SiO$_2$ substrate ($15 \times 10 \times 0.53$ mm$^3$). On one end the stripes are partially covered with a Pd cap layer to enable gas phase H loading. The actual sample shown in (b) consists of 11 stripes. The thickness of the vanadium stripes decreases from 125 nm to 25 nm from left to right. The sample is loaded in a hydrogen atmosphere ($p_{H_2} = 100$ Pa, $T = 473$ K) for $10^4$ s. The 11 composite V/Y stripes take up H via the Pd layer, which is located at the upper part of the photo. Lateral H migration occurs along the stripes away from the Pd-covered part. Within the Y-indicator layer, the presence of H leads to the formation of the YH$_2$ phase, which appears blue in reflection. Note the influence of the V thickness on the mobility of the YH$_2$ front in the indicator. The non-constant thickness of the 2nd, 7th, and the 9th vanadium stripes leads to a deformation of the diffusion front. (From Ref. [132])

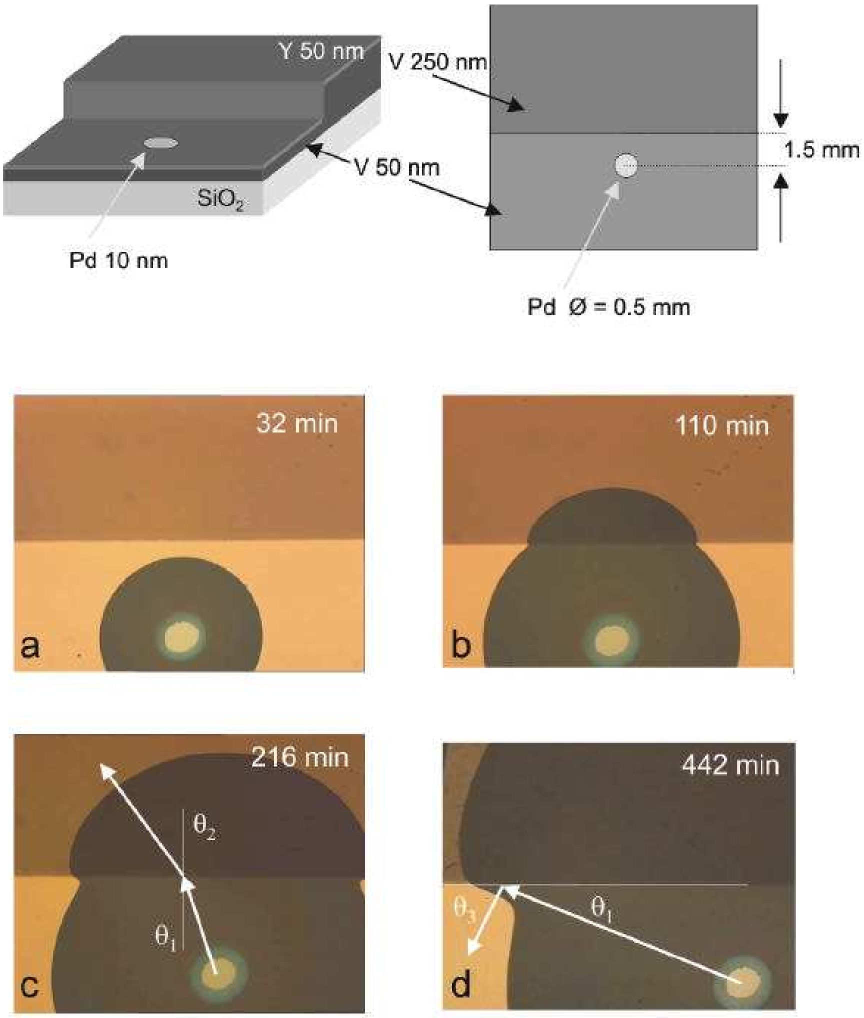

**Figure 1.25:** Top panels: Schematic representation of the sample used to investigate hydrogen diffusion from a slow medium to a fast medium. Hydrogen enters the sample via the Pd dot in the lower half of the sample, 1.5 mm away from the interface. Photographs: Each image covers a 5.6×4.5 mm$^2$ area of the sample. They are recorded in reflection 37 min, respectively 110 min after the sample has been brought into contact with a hydrogen atmosphere of $10^5$ Pa at 373 K. The originally circular diffusion front is heavily deformed as soon as it hits the interface between the two media. On the basis of such investigations Remhof *et al.* [135] concluded that there were some analogies between diffusion and geometric optics (for example Snell's law is valid in (c)). (From Ref. [135])

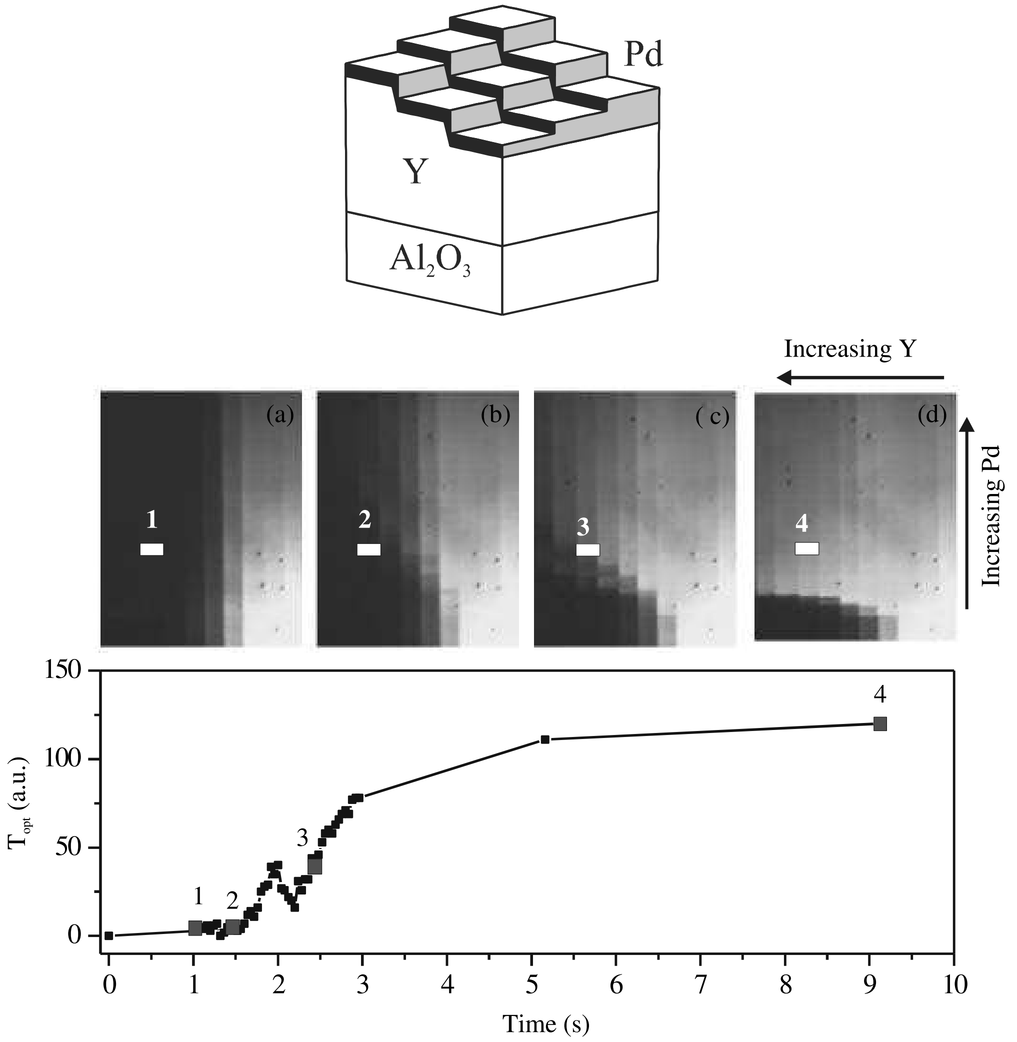

**Figure 1.26:** Time dependence of the optical transmission of a Pd/YH$_x$ matrix sample during hydrogenation. The top panel is a schematic representation of a matrix sample. Four stages of the optical transmission of a matrix sample are shown in (a)-(d). The yttrium and Pd thicknesses increase from 0 to 150 nm and 1 to 25 nm respectively. In the lower panel the optical transmission versus time of one arbitrarily chosen plaquette (marked white, $d_{Pd} = 10$ nm, $d_Y = 100$ nm) is given. (From Ref. [110])

**Figure 1.27:** Photograph of the sputtering chamber showing six magnetron sources. Five of them are covered with a shutter, one is uncovered (on the left) showing the magnets within the source. The sources are at various tilt-angles.

## 1.7 Switchable mirror based devices

### 1.7.1 Electrochromic devices

Electrochromism is the reversible change in optical properties that occurs when a material is electrochemically oxidized or reduced [142]. This working definition includes a change in optical properties anywhere in the solar (and even in some cases the microwave) range. In addition to the active electrochromic layer, a device consists of an electrolyte and a counter electrode, which may or may not be electrochromic. The electrolyte should be a good ionic conductor and electrically insulating in order to be non-volatile.

At first sight the large change in optical transmission found in switchable mirrors seems comparable to that observed in other electrochromic materials such as hydrogen or lithium intercalated transition-metal-oxide films [57]. However, the simultaneous occurrence of metallic reflectivity, high absorption over a large part of the solar spectrum, and colourless transparency in the visible part of the optical spectrum in the same material (e.g. in Mg-RE, see Sec. 1.4) is not found in other electrochromics. As far as we know, these are unique properties of metal-hydrides. Well-known electrochromic materials such as $WO_3$, Prussian blue or viologen switch reversibly from a transparent to an absorbing state, which is active over a limited wavelength range only [57]. The intercalated blue bronzes $H_xWO_3$ change e.g. from a transparent colourless insulator at $x \approx 0$ to a transparent but deep blue semiconductor at $x \sim 0.3$. The high contrast of the metal-hydrides between the metallic reflecting state and the semiconducting transparent state, indicates that gasochromic devices based on this materials could be much thinner (e.g. $\sim 100$ nm) than the $WO_3$-layers used so far [174]. Interestingly, in the transparent trihydride state the switchable mirrors are in their oxidized state ($Y^{3+}$), which make them complementary to $WO_3$ which is coloured in its reduced state ($W^{6+}$ mixed with $W^{5+}$) [8].

#### Device demands

Clearly, a feasible device needs to withstand a large number of switching cycles. To prevent mechanical damage to the device, lattice expansion during switching should be minimized. The expansion-free switching of the $Y_{0.38}La_{0.62}$-alloy is in this respect very promising. Additionally, the absence of hysteresis in these alloys (see Sec. 1.3.3 on page 16) is advantageous for a predictable operation of an electrochromic device.

The power needed to switch the optical properties of a window determines to a large extent the applicability of an electrochromic device. The coloration efficiency of a device is given by the ratio of the change in optical density $\Delta(\mathrm{OD}) = \log T_1(\lambda)/T_2(\lambda)$, with $T(\lambda)$ the transmission at a certain wavelength in the reduced and the oxidized state, respectively, divided by the amount of charge (or hydrogen in this case) DQ to be moved in/out of the active layer per unit area (CE=Δ(OD)/DQ) [57]). Clearly, to minimize the power needed for the switching of an electrochromic device, it is advantageous if the change in transmission is induced by a small amount of charge. Ouwerkerk [125] measured a CE = -37 $cm^2C^{-1}$ in a 200 nm $Sm_{0.3}Mg_{0.7}H_x$ film. Values of $|$ CE $|> 100$ are feasible since the minimum charge needed is only $\sim 40$ mC/$cm^2$ and the $\Delta(\mathrm{OD}) = 4$ measured is limited by pinholes rather than intrinsic properties. The disadvantage of the metal-hydrides is the fact that these materials so far need to be protected by a Pd cap layer, which reduces the maximum effective transparency to about 40%.

### Towards an electrochromic device

Compared to gasochromic switching, which can be as fast as 40 ms in GdMg-$H_x$, the insertion of an electrolyte drastically increases the switching time. In the case of liquid electrolyte devices (see Fig. 1.9 on page 27) the minimal switching time is of the order of minutes. Using a 2 M KOH solution, Ouwerkerk [125] showed reversible switching in a Pd-capped 200-nm $Sm_{0.3}Mg_{0.7}H_x$ thin film. Janner *et al.* [82] have studied the cycling durability of Gd-Mg switchable mirrors in 1 M KOH. After an initial decrease in the switching time, it increases again at the end of the lifetime. The increase in switching time is related to delamination and the formation of an oxide layer at the metal-hydride electrolyte interface. Additional protective layers proved to be unsuccessful so far. Strain problems could be reduced by depositing the metal-hydride directly in the fully hydrogenated state.

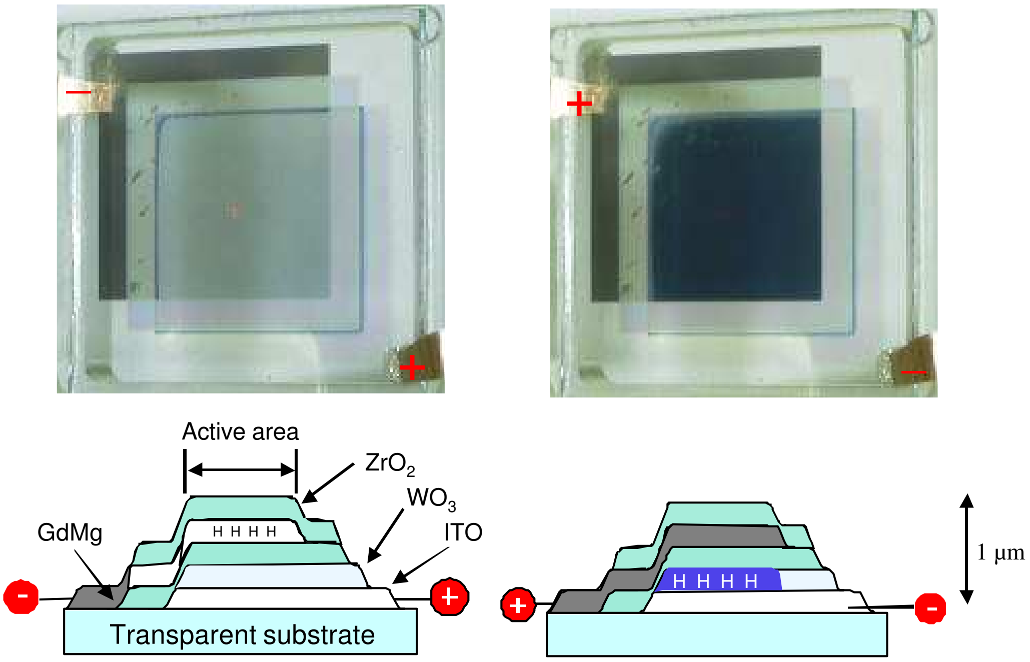

**Figure 1.28:** Schematic cross-sections and photographs of an all-solid-state switchable mirror [155] in two optical states: (a) at negative applied voltage both the GdMg-$H_x$ switchable mirror and the $WO_3$ storage electrode are in their transparent state; (b) at positive voltage GdMg is metallic and $WO_3$ dark blue.

The first all-solid-state metal-hydride switchable mirror device [5] had switching times of up to 16 hrs and used GdMg as active layer, hydrated $ZrO_2$ as electrolyte and $H_xWO_3$ as counter electrode and hydrogen storage layer. The transparent metal-hydride is formed when 3 V is applied with respect to the $WO_3$ layer. The large currents involved lead the authors to assume that the long switching times are due to electric shorts in the hydrated $ZrO_2$. In an inverted device ($WO_3$ as bottom electrode/H storage layer, see Fig. 1.28) Van der Sluis *et al.* [155] showed that the switching time can be reduced to 5 minutes, although the full switching cycle is still of the order of 1 hour. The devices switch reversibly up to 400 consecutive cycles. Some degradation occured, but this could be compensated by increasing the switching time. The self-discharge was negligible resulting in a retention time of over a year. Unfortunately, these results were not reproduced so far. However, many improvements are possible. The Zr-based electrolyte [108] may not be ideal since it transports protons, while within metal-hydrides such as $YH_x$ or $REH_x$ we are dealing with $H^-$. Alternatively, Y-doped $CaF_2$ might be used as a $H^-$ conducting electrolyte in conjunction with a suitable $H^-$ based counter electrode.

### 1.7.2 Thermochromic devices

As shown by Giebels *et al.* [51] the temperature dependence of the equilibrium plateau pressures of metal-hydrides can be used for an (*open*) thermochromic device. Especially $Y_{0.9}Mg_{0.1}$ samples appear to be promising since Mg suppresses the fcc-hcp transition of the $REH_2$-$REH_3$ transition. Because of this more hydrogen is desorbed upon heating and thus the transparency change is much larger and varies almost linearly with temperature. An alternative scheme for an electrochromic device is proposed by Lokhorst *et al.* [34]. They use two *encapsulated* metal-hydride layers with a slightly different temperature dependence of the hydrogen plateau pressure. Any temperature change results then in a redistribution of the hydrogen over the two layers.

The switchable metal-hydrides are clearly different from other traditional (metal-insulator) thermochromic systems [57] such as the vanadium oxides ($VO_2$, $V_5O_5$) . The change in contrast in the visible during the transition is much larger than in $VO_2$, which switches predominantly at wavelengths larger than 600 nm (2.1 eV).

## 1.8 Applications of metal-hydride-based devices

### 1.8.1 Smart windows

Smart coatings can play an important role in reducing the energy consumption of buildings and cars. In the US about 30% of the primary energy consumption is used for heating/cooling/lighting of residential and office buildings [27]. By regulating the heat balance while maintaining outward visibility enormous energy savings are feasible. Several active and passive window coatings have been proposed so far [58]. In general one would like to regulate the solar power input, while maintaining visibility. Hence the optical properties of the visible range should be different from those of the long wavelength range of the solar spectrum. Alternatively, heat dissipation is controlled by the emissivity around 0.1 eV (8 $\mu$m; 373 K black-body radiation). Windows with low thermal losses (e.g. based on $SnO_2$) should transmit over the whole solar range and reflect energies below 0.5 eV (2.5 $\mu$m). To minimize heat input while maintaining outward visibility, one could use windows reflecting light between 0.5-1.65 eV (2.5 $\mu$m 750 nm). This would reduce the cooling need for buildings dramatically. The fact that switchable metal-hydrides are able to block incoming radiation over the whole solar spectrum, make them of interest to use in cars, e.g. to reduce the thermal load of parked cars.

### 1.8.2 Switchable absorbers

Devices based on Mg-Ni films have a potential as variable reflectance coatings. Recently Van Mechelen *et al.* [107] showed that these materials have an optical absorption contrast over the solar range of a factor 2, comparing the metallic $Mg_2Ni$ to the ‘black’ $Mg_2NiH_{0.8}$-state. As the black-body emissivity at 100°C is smaller than 15% for this material, the ‘black state’ is an interesting heat absorber. There is a present need for such variable reflectance metal-hydride (VAREM) coatings particularly for use in combined photovoltaic cells/thermal solar collector devices. These devices consist essentially of a photovoltaic cell on top of a thermal solar collector [28]. Under certain conditions (high solar energy influx and low warm water consumption) the temperature of such devices can be well above 150°C. This leads to a reduced total efficiency and (in case plastic components are used) to an irreversible degradation of the photovoltaic component. This problem can be circumvented by depositing a VAREM between the photovoltaic cell and the thermal collector. When the thermal load of the system becomes too high, the VAREM is driven into its metallic reflecting state. In the opposite situation it is switched to its black absorbing state. In these devices VAREM coating can also be used to reduce heat radiation losses during night hours. The active control of the optical properties of a VAREM is also beneficial to heat collecting walls inside buildings: these so-called Trombé-walls [1] allow an optimal use of solar energy during all parts of the day in all seasons.

### 1.8.3 Fiber optic hydrogen sensors

Societal acceptance is a key ingredient for the implementation of a future hydrogen based economy. As this acceptance depends essentially on safety of operation there is a great need for sensitive, selective, fast, reliable, stable and cheap hydrogen sensors. Currently, commercial hydrogen detectors are not useful for widespread use, particularly in transportation, because they are rather bulky, not stable over a long period of time and expensive. Furthermore, most of the sensors available commercially are based on electrical measurements at the sensing point. This might be undesirable in potentially explosive environments. These disadvantages can be circumvented by using optical detectors in which the end of an optic fiber is coated with a hydrogen sensitive layer. The changes induced in the optical properties of this layer during absorption of hydrogen are detected optically at the other end of the fiber. Compared to other hydrogen sensors, optical fiber sensors have the advantage to be simple yet very sensitive, cheap, insensitive to electromagnetic noise, explosion-safe, and to allow multiple sensing with one central (remote) detector. This is the key-advantage over conventional detectors that make optical sensors cost competitive. Furthermore, optic fibers are more resistant to corrosion than standard electrical wires.

| | | |
|---|---|---|
| 1. | Hydrogen concentration in air: | 0-10 % (for safety detectors)<br>0-100 % (for sensors) |
| 2. | Operating temperature: | -25 to 100° |
| 3. | Response time: | 1 s or less for 90 % full scale |
| 4. | Long time stability: | more than 1 year |
| 5. | Selectivity: | hydrogen specific |
| 6. | Pollutant resistant: | especially to hydrocarbons, $H_2S$ |
| 7. | Insensitivity to humidity | |
| 8. | Low price | |

To be competitive with other hydrogen sensors the coatings to be developed must satisfy at least the following performance targets:

Several groups are presently developing fiber optic hydrogen sensors. For example at the National Renewable Energy Laboratory (NREL) researchers have obtained interesting results with fibers coated with a $WO_3$ film at the sensing end [10, 157]. This originally transparent material is coloured blue when absorbing hydrogen. However, presence of water molecules is essential for its switching [45, 46]. This limits its application range to temperatures above 0°C. This problem can be avoided if metal-hydride switchable mirrors are used as sensing coating. In this context the Mg-TM hydrides are particularly interesting since their reflection decreases strongly already at low hydrogen concentrations as shown in Fig. 1.20 for $Mg_2NiH_x$. In such a material coloration does not depend on the presence of water and, since hydrogen diffusion is sufficiently fast over a large temperature range (-40 to +90 °C) such sensors should remain operational below 0°C.

### 1.8.4 Batteries

Notten *et al.* [121] discovered recently a very large (reversible) storage capacity of 5.6 wt.% (1500 mAh/g) in $Mg_{0.8}Sc_{0.2}Pd_{0.024}$ pellets in a 6-M-KOH electrolyte at 25°C. This is about 4 times more than in conventional Ni-MH batteries such as $LaNi_5H_6$. Their research was inspired by the switchable mirrors research on Mg-RE films done before at Philips Research Laboratories in Eindhoven [125, 153, 156]. To achieve such a large storage capacity Sc has to become $ScH_3$. This is rather surprising since pure Sc does not load to the trihydride phase at atmospheric pressure. Only at 300 MPa hcp $ScH_3$ is formed [9]. Giebels *et al.* [50] confirmed the formation of $ScH_3$ recently in thin-films of Mg-Sc. These films become very transparent when the Mg content is larger than 65 at.%. They behave as Mg-Y and Mg-La switchable mirrors, i.e. they show a black state and a shift of the band gap with excess Mg.

## 1.9 Conclusions and Outlook

In this Chapter we have described the remarkable optical properties of switchable metal-hydride films. So far three generations of switchable mirrors have been discovered. The first-generation concerns the hydrides of the rare-earths and yttrium and lanthanum. The transparency of these materials posed intriguing questions about the origin of the insulating state to theorists. In the second and third generations magnesium plays an essential role. Alloyed with rare-earths it leads to colour neutral films when fully hydrogenated. There is an intriguing highly absorbing state, the black state, which occurs at intermediate hydrogen concentrations. Essential for the high absorption is the coexistence of Mg and $MgH_2$ grains. Alloyed with the transition metals Ni, Co, Fe, and Mn, magnesium forms complex metal-hydrides that exhibit also the three fundamental optical states of matter, i.e. reflecting, absorbing and transparent. In these third-generation switchable mirrors, the mechanism leading to the black state involves a self-organized double layering of $Mg_2NiH_x$. Surprisingly, during hydrogenation $Mg_2NiH_4$ nucleates first in a thin layer at the interface to the substrate. Further hydrogen uptake yields to a growth of that layer at the expense of the remaining metallic layer on top.

The results presented in this Chapter show also the tremendous advantage of thin films compared to bulk metal-hydrides. During hydrogen absorption the films retain their structural integrity. In contrast to bulk samples they are not reduced to powder when they react with hydrogen, although the volume changes can be considerable (for example 32% in the case of $Mg_2NiH_4$ and $MgH_2$). This makes it possible to investigate in detail the intrinsic physical properties (electrical resistivity, charge carrier density, optical properties, etc.) of these materials.

The thin-film geometry makes it also possible to investigate and optimize catalytic layers. In many cases Pd works fine and makes it possible, for example, to hydrogenate $Mg_2Ni$ at room temperature with hydrogen at pressures of a few hundred Pa. The possibility to study in detail the effect of catalytic cap layers is very important for all applications where reaction kinetics is important: energy storage, electrochromic devices, etc.

By using matrix-samples or films with large compositional gradients it will be possible to monitor optically the reaction of hydrogen with a great number of different samples evaporated on the same substrate. This will allow a highly efficient combinatorial exploration of new lightweight hydrogen storage materials. Thin films of light-metals (for example alanates) will soon be investigated optically.

Although various devices have been demonstrated until now, their performance needs still to be drastically improved. This will require a major research and development effort.

# Bibliography

[1] URL `http://www.nrel.gov/buildings/highperformance/trombe_walls.html`

[2] J. A. Alford and M. Y. Chou, *First principles study of the electronic structure and optical properties of* $MgH_2$, Bulletin of the American Physical Society, **48** (1), 300 (2003)

[3] J. A. Alford, M. Y. Chou, E. K. Chang, and S. G. Louie, *First-principles studies of quasi-particle band structures of cubic* $YH_3$ *and* $LaH_3$, Phys. Rev. B, **67**, 125110 (2003)

[4] R. Armitage, M. Cich, M. Rubin, and E. R. Weber, *A method to pattern Pd over-layers on GdMg films and its application to increase the transmittance of metal hydride optical switches*, Appl. Phys. A (2000)

[5] R. Armitage, M. Rubin, T. Richardson, N. O'Brien, and Yong Chen, *Solid-state gadolinium-magnesium hydride optical switch*, Appl. Phys. Lett., **75** (13), 1863–1865 (1999)

[6] I. Aruna, B. R. Mehta, L. K. Malhotra, and S. M. Shivaprasad, *A color-neutral, Gd nano-particle switchable mirror with improved optical contrast and response time*, Adv. Mater., **16** (2), 169–173 (2004)

[7] D. E. Azofeifa and N. Clark, *Optical and electrical changes of hydrogenated Dy films*, J. Alloys Compd., **305**, 32–34 (2000)

[8] K. Bange, *Colouration of tungsten oxide films: A model for optically active coatings*, Solar Energy Mater. Solar Cells, **58** (1), 1–131 (1999)

[9] I. O. Bashkin, E. G. Ponyatovskii, and M. E. Kost, *Phase transformations in hydrides of rare-earth metals under pressure II. The Sc-H and Yb-H systems under high hydrogen pressure*, Phys. Status Solidi B, **87**, 369–372 (1978)

[10] D. K. Benson, C. E. Tracy, G. Hishmeh, P. Ciszek, and S.-H. Lee, *Low-cost fiber optic chemochromic hydrogen detector*, Proceedings of the 1998 U.S. DOE Hydrogen Program Review, NREL/CP-570-25315 (1998)

[11] S. Berthier, *Fonction diélectrique des milieux inhomogènes*, Ann. Phys. Fr., **13**, 503–595 (1988)

[12] H. Blomqvist, *Magnesium ions stabilizing solid-state transition metal hydrides*, Ph.D. thesis, Stockholm University (2003)

[13] H. Blomqvist and D. Noréus, *Mechanically reversible conductor–insulator transition in* $Mg_2NiH_4$, J. Appl. Phys., **91** (8), 5141–5148 (2002)

[14] A. Borgschulte, M. Rode, A. Jacob, and J. Schoenes, *Alloy formation of Y with Pd investigated by photoemission and electron diffraction*, J. Appl. Phys., **90** (3), 1147–1154 (2001)

[15] A. Borgschulte, S. Weber, and J. Schoenes, *Interfacial reaction during the epitaxial growth of yttrium on* $CaF_2$*(111)*, Appl. Phys. Lett., **82** (17), 2898–2900 (2003)

[16] A. Borgschulte, R. J. Westerwaal, J. H. Rector, B. Dam, R. Griessen, and J. Schoenes, *The effect of the strong metal-support interaction on hydrogen sorption kinetics,* submitted to Phys. Rev. B

[17] F. J. A. den Broeder, S. J. van der Molen, M. Kremers, J. N. Huiberts, D. G. Nagengast, A. T. M. van Gogh, W. H. Huisman, N. J. Koeman, B. Dam, J. H. Rector, S. Plota, M. Haaksma, R. M. N. Hanzen, R. M. Jungblut, P. A. Duine, and R. Griessen, *Visualization of hydrogen migration in solids using switchable mirrors,* Nature (London), **394**, 656–658 (1998)

[18] R. J. C. Brown, P. J. Brewer, and M. J. T. Milton, *The physical and chemical properties of electroless nickel-phosphorus alloys and low reflectance nickel-phosphorus black surfaces*, J. Mater. Chem., **12**, 2749–2754 (2002)

[19] D. A. G. Bruggeman, *Berechnung verschiedener physikalischer Konstanten von heterogene Substanzen – I. Dielektrizitätskonstanten und Leitfähigkeiten der Mischkörper aus isotropen Substanzen*, Ann. Phys. (Leipzig), **24**, 636–679 (1935)

[20] E. K. Chang, X. Blase, and S. G. Louie, *Quasiparticle band structure of lanthanum hydride*, Phys. Rev. B, **64**, 155108–1–155108–5 (2001)

[21] A. E. Curzon and O. Singh, *Thin film studies of yttrium, yttrium hydrides and yttrium oxide*, J. Phys. F.: Metal Phys., **8**, 1619–1625 (1978)

[22] B. Dam, A. C. Lokhorst, A. Remhof, M. C. R. Heijna, J. H. Rector, D. Borsa, and J. W. J. Kerssemakers, *In situ preparation of* $YH_2$ *thin films by PLD for switchable mirrors,* J. Alloys Compd., **356-357**, 526–529 (2003)

[23] J. P. Dekker, J. van Ek, A. Lodder, and J. N. Huiberts, *The gap in* $YH_3$ *and its lattice structure,* J. Phys.: Condens. Matter, **5**, 4805–4816 (1993)

[24] M. Di Vece, A. M. J. van der Eerden, J. A. van Bokhoven, S. Lemaux, J. J. Kelly, and D. C. Koningsberger, *X-ray absorption fine structure study of the structural and electronic properties of the GdMg hydride switchable mirror*, Phys. Rev. B, **67**, 035430 (2003)

[25] M. Di Vece, S. J. M. Zevenhuizen, and J. J. Kelly, *Optical switching properties from isotherms of Gd and GdMg hydride mirrors*, Appl. Phys. Lett., **81** (7), 1213–1215 (2002)

[26] M. Dornheim, A. Pundt, R. Kirchheim, S. J. van der Molen, E. S. Kooij, J. Kerssemakers, R. Griessen, H. Harms, and U. Geyer, *Stress development in thin yttrium films on hard substrates during hydrogen loading*, J. Appl. Phys., **93** (11), 8958–8965 (2003)

[27] M. S. Dresselhaus and I. L. Thomas, *Alternative energy technologies*, Nature (London), **414**, 332–337 (2001)

[28] Stichting Energieonderzoek Centrum Nederland (ECN), Dutch patent application NL 1020281, International patent application PCT/NL03/00233

[29] R. Eder, H. F. Pen, and G. A. Sawatsky, *Kondo-lattice–like effects of hydrogen in transition metals*, Phys. Rev. B, **56** (16), 10115–10120 (1997)

[30] F. H. Ellinger, C. E. Holley, Jr., B. B. McInteer, D. Pavone, R. M. Potter, E. Staritzky, and W. H. Zachariasen, *The preparation and some properties of magnesium hydride*, J. Am. Chem. Soc., **77**, 2647–2648 (1955)

[31] S. Enache, T. Leeuwerink, A. F. Th. Hoekstra, A. Remhof, N. J. Koeman, B. Dam, and R. Griessen, *Electrical and optical properties of epitaxial* $YH_x$ *switchable mirrors*, submitted to Phys. Rev. B

[32] S. Enache, W. Lohstroh, and R. Griessen, *Temperature dependence of magnetoresistance and Hall effect in* $Mg_2NiH_x$ *films*, Phys. Rev. B, **69**, 115326 (2004)

[33] United States Department of Energy (DOE), *Hydrogen posture plan* (2004), URL `http://www.eere.energy.gov/hydrogenandfuelcells/`

[34] A. C. Lokhorst *et al.*, to be published in J. Alloys Compd.

[35] B. Dam *et al.*, to be published in J. Alloys Compd.

[36] O. Dankert *et al.*, (unpublished)

[37] B. Farangis, P. Nachimuthu, T. J. Richardson, J. L. Slack, R. C. C. Perera, E. M. Gullikson, D. W. Lindle, and M. Rubin, *In situ x-ray absorption spectroscopy study of hydrogen absorption by nickel-magnesium thin films*, Phys. Rev. B, **67**, 085106 (2003)

[38] Y. Fujita, M. Yamaguchi, and I. Yamamoto, *Electrical and optical properties of* $Mg_2NiH_4$ *films*, Z. Phys. Chem. Neue Folge, **163**, 633–634 (1989)

[39] G. N. García, J. P. Abriata, and J. O. Sofo, *Calculation of the electronic and structural properties of cubic* $Mg_2NiH_4$, Phys. Rev. B, **59** (18), 11746–11754 (1999)

[40] Z. Gavra, M. H. Mintz, G. Kimmel, and Z. Hadari, *Allotropic transitions of* $Mg_2NiH_4$, Inorg. Chem., **18** (12), 3595–3597 (1979)

[41] P. van Gelderen, P. A. Bobber, P. J. Kelly, and G. Brocks, *Parameter-free quasiparticle calculations for* $YH_3$, Phys. Rev. Lett., **85** (14), 2989–2992 (2000)

[42] P. van Gelderen, P. A. Bobbert, P. J. Kelly, G. Brocks, and R. Tolboom, *Parameter-free calculation of single-particle electronic excitations in* $YH_3$, Phys. Rev. B, **66**, 075104 (2002)

[43] P. van Gelderen, P. J. Kelly, and G. Brocks, *Phonon spectrum of* $YH_3$*: Evidence of a broken symmetry structure*, Phys. Rev. B, (63), 100301(R) (2001)

[44] J. Genossar and P. S. Rudman, *Structural transformation in* $Mg_2NiH_4$, J. Phys. Chem. Solids, **42**, 611–616 (1981)

[45] A. Georg, W. Graf, R. Neumann, and V. Wittwer, *Mechanism of the gasochromic coloration of porous* $WO_3$ *films*, Solid State Ionics, **127**, 319–328 (2000)

[46] A. Georg, W. Graf, R. Neumann, and V. Wittwer, *The role of water in gasochromic* $WO_3$ *films*, Thin Solid Films, **384**, 269–275 (2001)

[47] I. A. M. E. Giebels and R. Griessen, *Insulating cubic* $ScH_{3-\delta}$ *stabilized by Mg doping*, in preparation

[48] I. A. M. E. Giebels, J. Isidorsson, and R. Griessen, *Highly absorbing black Mg and rare-earth-Mg switchable mirrors*, Phys. Rev. B, **69**, 205111 (2004)

[49] I. A. M. E. Giebels, J. Isidorsson, E. S. Kooij, A. Remhof, N. J. Koeman, J. H. Rector, A. T. M. van Gogh, and R. Griessen, *Highly reflecting* $Y/Mg\text{-}H_x$ *multilayered switchable mirrors*, J. Alloys Compd., **330-332**, 875–881 (2002)

[50] I. A. M. E. Giebels, W. Lohstroh, M. Bjurman, and R. Griessen, *Highly absorbing state in Mg/Y and Mg/Ni multilayers*, (unpublished)

[51] I. A. M. E. Giebels, S. J. van der Molen, R. Griessen, and M. Di Vece, *Thermochromic effect in*$YH_{3-\delta}$ *and* $Mg_{0.1}Y_{0.9}H_{2.9-\delta}$, Appl. Phys. Lett., **80** (8), 1343–1345 (2002)

[52] A. T. M. van Gogh and R. Griessen, *Dihydride transmission quenching in switchable* $La_{1-z}Y_zH_x$ *mirrors*, J. Alloys Compd., **330-332**, 338–341 (2002)

[53] A. T. M. van Gogh, E. S. Kooij, and R. Griessen, *Isotope effects in switchable metal-hydride mirrors*, Phys. Rev. Lett., **83** (22), 4614–4617 (1999)

[54] A. T. M. van Gogh, S. J. van der Molen, J. W. J. Kerssemakers, N. J. Koeman, and R. Griessen, *Performance enhancement of metal-hydride switchable mirrors using* $Pd/AlO_x$ *composite cap layers*, Appl. Phys. Lett., **77** (6), 815–817 (2000)

[55] A. T. M. van Gogh, D. G. Nagengast, E. S. Kooij, N. J. Koeman, and R. Griessen, *Quenching of giant hysteresis effects in* $La_{1-z}Y_zH_x$ *switchable mirrors*, Phys. Rev. Lett., **85** (10), 2156–2159 (2000)

[56] A. T. M. van Gogh, D. G. Nagengast, E. S. Kooij, N. J. Koeman, J. H. Rector, R. Griessen, C. F. J. Flipse, and R. J. J. G. A. M. Smeets, *Structural, electrical and optical properties of* $La_{1-z}Y_zH_x$ *switchable mirrors*, Phys. Rev. B, **63**, 195105–1–195105–21 (2001)

[57] C. G. Granqvist, *Handbook of Inorganic Electrochromic Materials* (Elsevier, Amsterdam, 1995)

[58] C. G. Granqvist and V. Wittwer, *Materials for solar energy conversion: an overview*, Sol. Energy Mater. Solar Cells, **54**, 39–48 (1998)

[59] E. J. Grier, M. L. Jenkins, A. K. Petford-Long, R. C. C. Ward, and M. R. Wells, *Misfit dislocations of epitaxial (110) niobium || (11$\bar{2}$0) sapphire interfaces grown by molecular beam epitaxy*, Thin Solid Films, **358**, 94–98 (2000)

[60] E. J. Grier, O. Kolosov, A. K. Petford-Long, R. C. C. Ward, M. R. Wells, and B. Hjörvarsson, *Structural changes to epitaxial (0001) holmium layers during hydrogen loading*, J. Phys. D: Appl. Phys., **33**, 894–900 (2000)

[61] R. Griessen, *Schaltbare Spiegel aus Metallhydriden*, Phys. Blätter, **53** (12), 1207–1209 (1997)

[62] R. Griessen, *Switchable Mirrors*, Europhys. News, **32** (2), 42 (2001)

[63] R. Griessen and P. van der Sluis, *Schaltbare Spiegel – Elektronenkorrelationen in der Anwendung*, Physik in userer Zeit, **32**, 76–83 (2001)

[64] U. Häussermann, H. Blomqvist, and D. Noréus, *Bonding and stability of the hydrogen storage material* $Mg_2NiH_4$, Inorg. Chem., **41**, 3684–3692 (2002)

[65] J. Hayoz, C. Koitzsch, M. Bovet, D. Naumovic, L. Schlapbach, and P. Aebi, *Electronic structure of the* $YH_3$ *phase from angle-resolved photoemission spectroscopy*, Phys. Rev. Lett., **90** (19), 196804 (2003)

[66] J. Hayoz, Th. Pillo, M. Bovet, A. Züttel, St. Guthrie, L. Schlapbach, and P. Aebi, *Preparation and characterization of clean, single-crystalline* $YH_x$ *films (*$0 \leq x \leq 2.9$*) on W(110)*, J. Vac. Sci. Technol. A, **18** (5), 2417–2431 (2000)

[67] J. Hayoz, S. Sarbach, Th. Pillo, E. Boschung, D. Naumović, P. Aebi, and L. Schlapbach, *Observation of the reversible H-induced structural trnsition in thin Y films via x-ray photoelectron diffraction*, Phys. Rev. B, **58** (8), 4270–4273(R) (1998)

[68] J. Hayoz, J. Schoenes, L. Schlapbach, and P. Aebi, *Switchable yttrium–hydride mirrors grown on* $CaF_2$ *(111): A x-ray photoelectron spectroscopy and diffraction study*, J. Appl. Phys., **90** (8), 3925–3933 (2001)

[69] B. Hjörvarsson, (private communication)

[70] B. Hjörvarsson, C. Chacon, H. Zabel, and V. Leiner, *Adjustable magnetic interactions: the use of hydrogen as a tuning agent*, J. Alloys Compd., **356-357**, 160–168 (2003)

[71] A. F. Th. Hoekstra, A. S. Roy, and T. F. Rosenbaum, *Scaling at the Mott-Hubbard metal-insulator transition in yttrium hydride*, J. Phys.: Condens. Matter, **15** (9), 1405–1413 (2003)

[72] A. F. Th. Hoekstra, A. S. Roy, T. F. Rosenbaum, R. Griessen, R. J. Wijngaarden, and N. J. Koeman, *Light induced metal–insulator transition in a switchable mirror*, Phys. Rev. Lett., **86** (23), 5349–5352 (2001)

[73] J. N. Huiberts, *On the road to dirty metallic atomic hydrogen*, Ph.D. thesis, Vrije Universiteit Amsterdam (1995)

[74] J. N. Huiberts, R. Griessen, J. H. Rector, R. J. Wijngaarden, J. P. Dekker, D. G. de Groot, and N. J. Koeman, *Yttrium and lanthanum hydride films with switchable optical properties*, Nature (London), **380**, 231–234 (1996)

[75] J. N. Huiberts, R. Griessen, R. J. Wijngaarden, M. Kremers, and C. van Haesendonck, *Logarithmic divergence of the electrical resistivity in the metal hydride* $YH_{3-\delta}$, Phys. Rev. Lett., **79** (19), 3724–3727 (1997)

[76] J. N. Huiberts, J. H. Rector, R. J. Wijngaarden, S. Jetten, D. de Groot, B. Dam, N. J. Koeman, R. Griessen, B. Hjörvarsson, S. Olafsson, and Y. S. Cho, *Synthesis of yttriumtrihydride films for ex-situ measurements*, J. Alloys. Compd., **239**, 158–171 (1996)

[77] J. Isidorsson, I. A. M. E. Giebels, H. Arwin, and R. Griessen, *Optical properties of* $MgH_2$ *measured in situ by ellipsometry and spectrophotometry*, Phys. Rev. B, **68**, 115112 (2003)

[78] J. Isidorsson, I. A. M. E. Giebels, M. Di Vece, and R. Griessen, *Electrochromism of Mg-Ni hydride switchable mirrors*, Proc. SPIE, **4458**, 128–137 (2001)

[79] J. Isidorsson, I. A. M. E. Giebels, R. Griessen, and M. Di Vece, *Tunable reflectance Mg-Ni-H films*, Appl. Phys. Lett., **80** (13), 2305–2307 (2002)

[80] J. Isidorsson, I. A. M. E. Giebels, E. S. Kooij, N. J. Koeman, J. H. Rector, A. T. M. van Gogh, and R. Griessen, *Structural, optical and electronic properties of* $LaMgH_x$ *switchable mirrors*, Electrochim. Acta, **46**, 2179–2185 (2001)

[81] A. Jacob, A. Borgschulte, and J. Schoenes, *Epitaxial yttrium growth mode on* $BaF_2$ *(111) and* $CaF_2$ *(111)*, Thin Solid Films, **414**, 39–42 (2002)

[82] A-M. Janner, P. van der Sluis, and V. Mercier, *Cycling durability of switchable mirrors*, Electrochim. Acta, **46**, 2173–2178 (2001)

[83] P. J. Kelly, J. P. Dekker, and R. Stumpf, *Kelly, Dekker, and Strumpf reply*, Phys. Rev. Lett., **79** (15), 2921 (1997)

[84] P. J. Kelly, J. P. Dekker, and R. Stumpf, *Theoretical prediction of the structure of insulating* $YH_3$, Phys. Rev. Lett., **78** (7), 1315–1318 (1997)

[85] J. W. J. Kerssemakers, S. J. van der Molen, R. Günther, B. Dam, and R. Griessen, *In situ monitoring of optical and structural switching in epitaxial* $YH_x$ *switchable mirrors*, J. Alloys Compd., **330-332**, 342–347 (2002)

[86] J. W. J. Kerssemakers, S. J. van der Molen, R. Günther, B. Dam, and R. Griessen, *Local switching in epitaxial* $YH_x$ *switchable mirrors*, Phys. Rev. B, **65**, 075417 (2002)

[87] J. W. J. Kerssemakers, S. J. van der Molen, N. J. Koeman, R. Günther, and R. Griessen, *Pixel switching of epitaxial* $Pd/YH_x/CaF_2$ *switchable mirrors*, Nature (London), **406**, 489–491 (2000)

[88] H. Kierey, M. Rode, A. Jacob, A. Borgschulte, and J. Schoenes, *Raman effect and structure of* $YH_3$ *and* $YD_3$ *thin epitaxial films*, Phys. Rev. B, **63**, 134109 (2001)

[89] B. J. Kooi, E. Zoestbergen, J. Th. M. De Hosson, J. W. J. Kerssemakers, B. Dam, and R. C. C. Ward, *Mechanism of the structural phase transformations in epitaxial* $YH_x$ *switchable mirrors*, J. Appl. Phys., **91** (4), 1901–1909 (2002)

[90] E. S. Kooij, A. T. M. van Gogh, and R. Griessen, *In situ resistivity measurements and optical transmission and reflection spectroscopy of electrochemically loaded switchable* $YH_x$ *films*, J. Electrochem. Soc., **146**, 2990–2994 (1999)

[91] E. S. Kooij, A. T. M. van Gogh, D. G. Nagengast, N. J. Koeman, and R. Griessen, *Hysteresis and the single-phase metal-insulator transition in switchable* $YH_x$, Phys. Rev. B, **62** (15), 10088–10100 (2000)

[92] E. S. Kooij, J. Isidorsson, and I. A. M. E. Giebels, (unpublished)

[93] E. S. Kooij, J. H. Rector, D. G. Nagengast, J. W. J. Kerssemakers, B. Dam, R. Griessen, A. Remhof, and H. Zabel, *Growth and hydrogenation of epitaxial yttrium switchable mirrors on* $CaF_2$, Thin Solid Films, **402**, 131–142 (2002)

[94] A. Krozer and B. Kasemo, *Hydrogen uptake by Pd-coated Mg: Absorption–decomposition isotherms and uptake kinetics*, J. Less-Common Met., **160**, 323–342 (1990)

[95] P. Kumar, R. Philip, G. K. Mor, and L. K. Malhotra, *Influence of palladium overlayer on switching behaviour of samarium hydride thin films*, Jpn. J. Appl. Phys., **41**, 6023–6027 (2002)

[96] J. Kwo, M. Hong, and S. Nakahara, *Growth of rare-earth single crystals by molecular beam epitaxy: The epitaxial relationship between hcp rare earth and bcc niobium*, Appl. Phys. Lett., **49** (6), 319–321 (1986)

[97] M. W. Lee and C. H. Lin, *Determination of the optical constants of the $\gamma$-phase $GdH_3$ thin films*, J. Appl. Phys., **87** (11), 7798–7801 (2000)

[98] G. G. Libowitz, *Electronic properties of the rare earth hydrides*, Ber. Bunsen. Phys. Chem., **76** (8), 837–845 (1972)

[99] G. G. Libowitz and J. G. Pack, *Electrical resistivity of nonstoichiometric cerium hydride single crystals,* J. Chem. Phys., **50** (8), 3557–3560 (1969)

[100] W. Lohstroh, F. Leuenberger, W. Felsch, H. Fritzsche, and H. Maletta, *Hydrogen-controlled interlayer exchange coupling in Fe/$LaH_x$ multilayers*, J. Magn. Magn. Mater., **237**, 77–89 (2001)

[101] W. Lohstroh, R. J. Westerwaal, J. L. M. van Mechelen, C. Chacon, E. Johansson, B. Dam, and R. Griessen, *The structural and optical properties of $Mg_2NiH_x$ switchable mirrors upon hydrogen loading*, submitted to Phys. Rev. B

[102] W. Lohstroh, R. J. Westerwaal, B. Noheda, S. Enache, I. A. M. E. Giebels, B. Dam, and R. Griessen, *The nature of the black state of $Mg_2NiH_x$ switchable mirrors*, submitted to Phys. Rev. Lett.

[103] A. C. Lokhorst, M. C. R. Heijna, J. H. Rector, I. A. M. E. Giebels, N. J. Koeman, and B. Dam, *The properties of pulsed laser deposited $YH_2$ films for switchable devices*, J. Alloys Compd., **356-357**, 536–540 (2003)

[104] D. Lupu, R. Sârbu, and Biriş, *Semiconducting properties of $Mg_2NiH_4$*, Int. J. Hydrogen Energy, **12** (6), 425–426 (1987)

[105] A. Mandelis, *Diffusion waves and their uses*, Phys. Today, **53** (8), 29–34 (2000)

[106] J. C. McGuire and C. P. Kempter, *Preparation and properties of scandium dihydride*, J. Chem. Phys., **33**, 1584–1585 (1960)

[107] J. L. M. van Mechelen, B. Noheda, W. Lohstroh, R. J. Westerwaal, J. H. Rector, B. Dam, and R. Griessen, *Mg-Ni-H as selective coatings: Tunable reflectance by layered hydrogenation*, Appl. Phys. Lett., **84** (18), 3651–3653 (2004)

[108] V. M. M. Mercier and P. van der Sluis, *Toward solid-state switchable mirrors using a zirconium oxide proton conductor*, Solid State Ionics, **145**, 17–24 (2001)

[109] T. Miyake, F. Aryasetiawan, H. Kino, and K. Terakura, *GW quasiparticle band structure of $YH_3$*, Phys. Rev. B, **61** (24), 16491–16496 (2000)

[110] S. J. van der Molen, J. W. J. Kerssemakers, J. H. Rector, N. J. Koeman, B. Dam, and R. Griessen, *Hydriding kinetics of Pd capped $YH_x$ switchable mirrors*, J. Appl. Phys., **86** (11), 6107–6119 (1999)

[111] S. J. van der Molen, D. G. Nagengast, A. T. M. van Gogh, J. Kalkman, E. S. Kooij, J. H. Rector, and R. Griessen, *Insulating fcc-*$YH_{3-\delta}$ *stabilized by* $MgH_2$, Phys. Rev. B, **63**, 235116 (2001)

[112] S. J. van der Molen, M. S. Welling, and R. Griessen, *Correlated electromigration of H in the switchable mirror* $YH_{3-\delta}$, Phys. Rev. Lett., **85** (18), 3882–3885 (2000)

[113] G. K. Mor and L. K. Malhotra, *Hydriding characteristics of praseodymium thin films*, Thin Solid Films, **359**, 28–32 (2000)

[114] W. M. Mueller, J. P. Blackledge, and G. G. Libowitz, *Metal Hydrides* (Academic Press, New York, 1968)

[115] W. R. Myers, L-W. Wang, T. J. Richardson, and M. D. Rubin, *Calculation of thermodynamic, electronic, and optical properties of monoclinic* $Mg_2NiH_4$, J. Appl. Phys., **91** (8), 4879–4885 (2002)

[116] D. G. Nagengast, A. T. M. van Gogh, E. S. Kooij, B. Dam, and R. Griessen, *Contrast-enhancement of rare-earth switchable mirrors through microscopic shutter effect*, Appl. Phys. Lett., **75** (14), 2050–2052 (1999)

[117] D. G. Nagengast, J. Kerssemakers, A. T. M. van Gogh, B. Dam, and R. Griessen, *Epitaxial switchable Y-hydride mirrors*, Appl. Phys. Lett., **75**, 1724–1726 (1999)

[118] K. K. Ng, F. C. Zhang, V. I. Anisimov, and T. M. Rice, *Electronic structure of lanthanum hydrides with switchable optical properties*, Phys. Rev. Lett., **78** (7), 1311–1314 (1997)

[119] K. K. Ng, F. C. Zhang, V. I. Anisimov, and T. M. Rice, *Theory for metal hydrides with switchable optical properties*, Phys. Rev. B, **59** (8), 5398–5413 (1999)

[120] P. H. L. Notten, M. Kremers, and R. Griessen, *Optical switching of Y-hydride thin film electrodes*, J. Electrochem. Soc., **143** (10), 3348–3353 (1996)

[121] P. H. L. Notten, M. Ouwerkerk, H. van Hal, D. Beelen, W. Keur, J. Zhou, and H. Feil, *High energy density strategies: From materials research to battery integration*, J. Power Sources, **129**, 45–54 (2004)

[122] W. Oelerich, T. Klassen, and R. Bormann, *Metal oxides as catalysts for improved hydrogen sorption in nanocrystalline Mg-based materials*, J. Alloys Compd., **315**, 237–242 (2001)

[123] M. A. O'Leary, D. A. Boas, B. Chance, and A. G. Yodh, *Refraction of diffuse photon density waves*, Phys. Rev. Lett., **69** (18), 2658–2661 (1992)

[124] C. H. Olk, G. G. Tibbetts, D. Simon, and J. J. Moleski, *Combinatorial preparation and infrared screening of hydrogen sorbing metal alloys*, J. Appl. Phys., **94** (1), 720–725 (2003)

[125] M. Ouwerkerk, *Electrochemically induced optical switching of* $Sm_{0.3}Mg_{0.7}H_x$, Solid State Ionics, **115**, 431–437 (1998)

[126] M. Ouwerkerk, A.-M. Janner, P. van der Sluis, and V. M. M. Mercier, *Optical switching device*, United States patent application 20030227667

[127] T. P. L. Pedersen, C. Salinga, H. Weis, and M. Wuttig, *Mechanical stresses upon hydrogen induced optical switching in thin films*, J. Appl. Phys., **93** (10), 6034–6038 (2003)

[128] M. A. Pick, J. W. Davenport, M. Strongin, and G. J. Dienes, *Enhancement of hydrogen uptake rates for Nb and Ta by thin surface overlayers*, Phys. Rev. Lett., **43** (4), 286–289 (1979)

[129] A. Pundt, M. Getzlaff, M. Bode, R. Kirchheim, and R. Wiesendanger, *H-induced plastic deformation of Gd thin films studied by STM*, Phys. Rev. B, **61** (15), 9964–9967 (2000)

[130] J. J. Reilly and R. H. Wiswall, Jr., *The reaction of hydrogen with alloys of magnesium and nickel and the formation of* $Mg_2NiH_4$, Inorg. Chem., **7**, 2254–2256 (1968)

[131] A. Remhof, J. W. J. Kerssemakers, S. J. van der Molen, R. Griessen, and E. S. Kooij, *Hysteresis in* $YH_x$ *films observed with in situ measurements*, Phys. Rev. B, **65**, 054110–1–054110–8 (2002)

[132] A. Remhof, S. J. van der Molen, A. Antosik, A. Dobrowolska, N. J. Koeman, and R. Griessen, *Switchable mirrors for visualization and control of hydrogen diffusion in transition metals*, Phys. Rev. B, **66**, 020101(R) (2002)

[133] A. Remhof, G. Song, Ch. Sutter, A. Schreyer, R. Siebrecht, and H. Zabel, *Hydrogen and deuterium in epitaxial Y(0001) films: Structural properties and isotope exchange*, Phys. Rev. B, **59** (10), 6689–6699 (1999)

[134] A. Remhof, G. Song, K. Theis-Bröhl, and H. Zabel, *Reversible loading of epitaxial Y(00.1) films with hydrogen*, Phys. Rev. B, **56** (6), R2897–R2899 (1997)

[135] A. Remhof, R. J. Wijngaarden, and R. Griessen, *Refraction and reflection of diffusion fronts*, Phys. Rev. Lett., **90** (14), 145502 (2003)

[136] A. Remhof, R. J. Wijngaarden, and R. Griessen, *Refraction-like behaviour of hydrogen diffusion fronts*, J. Alloys Compd., **356-357**, 300–304 (2003)

[137] T. J. Richardson, R. D. Armitage, J. L. Slack, and M. D. Rubin, *Alternative materials for electrochromic mirror devices*, poster presentation at the Fourth International Meeting on Electrochromism (IME-4), August 21-23 2000, Uppsala, Sweden

[138] T. J. Richardson, J. L. Slack, R. D. Armitage, R. Kostecki, B. Farangis, and M. D. Rubin, *Switchable mirrors based on nickel-magnesium films*, Appl. Phys. Lett., **78** (20), 3047–3049 (2001)

[139] T. J. Richardson, J. L. Slack, B. Farangis, and M. D. Rubin, *Mixed metal films with switchable optical properties*, Appl. Phys. Lett., **80** (8), 1349–1351 (2002)

[140] M. Rode, A. Borgschulte, A. Jacob, C. Stellmach, U. Barkow, and J. Schoenes, *Evidence for ionic bonding in* $YH_{3-\delta}$, Phys. Rev. Lett., **87** (23), 235502 (2001)

[141] K. von Rottkay, M. Rubin, and P. A. Duine, *Refractive index changes of Pd-coated magnesium lanthanide switchable mirrors upon hydrogen insertion*, J. Appl. Phys., **85** (1), 408–413 (1999)

[142] N. M. Rowley and R. J. Mortimer, *New electrochromic materials*, Science Progress, **85**, 243–262 (2002)

[143] A. S. Roy, A. F. Th. Hoekstra, T. F. Rosenbaum, and R. Griessen, *Quantum fluctuations and the closing of the Coulomb gap in a correlated insulator*, Phys. Rev. Lett., **89** (27), 276402 (2002)

[144] J. Rydén, B. Hjörvarsson, T. Ericsson, E. Karlsson, A. Krozer, and B. Kasemo, *Unusual kinetics of hydride formation in Mg-Pd sandwiches, studied by hydrogen profiling and quartz crystal microbalance measurements*, J. Less-Common Met., **152**, 295–309 (1989)

[145] J. Schefer, P. Fischer, W. Hälg, F. Stucki, L. Schlapbach, J. J. Didisheim, K. Yvon, and A. F. Andresen, *New structure results for hydrides and deuterides of the hydrogen storage material* $Mg_2Ni$, J. Less-Common Met., **74**, 65–73 (1980)

[146] L. Schlapbach, *Surface properties and activation* (Springer, Berlin, 1992), vol. 67 of *Topics in Applied Physics – Hydrogen in Intermetallic Compounds II*, chap. 2

[147] L. Schlapbach and A. Züttel, *Hydrogen–storage materials for mobile applications*, Nature (London), **414**, 353–358 (2001)

[148] J. Schoenes, A. Borgschulte, A.-M. Carsteanu, H. Kierey, and M. Rode, *Structure and bonding in* $YH_x$ *as derived from elastic and inelastic light scattering*, J. Alloys Compd., **356-357**, 211–217 (2003)

[149] P. Selvam, B. Viswanathan, and V. Srinivasan, *X-ray photoelectron spectroscopic, electrical and magnetic studies on* $Mg_2NiH_4$, J. Electron Spectrosc. Relat. Phenom., **46**, 357–361 (1988)

[150] M. L. Shendeleva, *Instantaneous line heat source near a plane interface*, J. Appl. Phys., **95** (5), 2839–2845 (2004)

[151] J. Shinar, B. Dehner, R. G. Barnes, and B. J. Beaudry, *Anomalous resistivity peaks, localization transitions, and the electronic structure of substoichiometric lanthanum trihydrides*, Phys. Rev. Lett., **64** (5), 563–566 (1990)

[152] J. Shinar, B. Dehner, B. J. Beaudry, and D. T. Peterson, *Q-factor measurements of the bulk resistivity and nonmetal-metal transitions in* $LaH_x$ *and* $CeH_x$ $(x \geq 2.70)$, Phys. Rev. B, **37** (4), 2066–2073 (1988)

[153] P. van der Sluis, *Optical switches of gadolinium–magnesium multilayers*, Appl. Phys. Lett., **73** (13), 1826–1828 (1998)

[154] P. van der Sluis, *Chemochromic optical switches based on metal hydrides*, Electrochim. Acta, **44**, 3063–3066 (1999)

[155] P. van der Sluis and V. M. M. Mercier, *Solid state Gd-Mg electrochromic devices with* $ZrO_2H_x$ *electrolyte*, Electrochim. Acta, **46**, 2167–2171 (2001)

[156] P. van der Sluis, M. Ouwerkerk, and P. A. Duine, *Optical switches based on magnesium lanthanide alloy hydrides*, Appl. Phys. Lett., **70** (25), 3356–3358 (1997)

[157] R. D. Smith, P. Liu, S.-H. Lee, E. Tracy, and R. Pitts, *Interfacial stability of thin film fiber-optic hydrogen sensors*, Proceedings of the 2002 U.S. DOE Hydrogen Program Review, NREL/CP-610-32405 (2002)

[158] J. L. Soubeyroux, D. Fruchart, A. Mikou, M. Pezat, and B. Darriet, *Etude structurale du système* $Mg_2Ni$-$H_2$ *I – La solution solide* $Mg_2NiH_x$ *(*$x = 0.30$*)*, Mater. Res. Bull., **19**, 895–904 (1984)

[159] S. N. Sun, Y. Wang, and M. Y. Chou, *First-principle study of hydrogen ordering in* $\beta$-$YH_{2+x}$, Phys. Rev. B, **49** (10), 6481–6489 (1994)

[160] A. C. Switendick, *Electronic band structures of metal hydrides*, Solid State Commun., **8**, 1463–1467 (1970)

[161] A. C. Switendick, *Metal hydrides – structure and band structure*, Int. J. Quantum Chem., **5**, 459–470 (1971)

[162] T. J. Udovic, Q. Huang, R. W. Erwin, B. Hjörvarsson, and R. C. C. Ward, *Structural symmetry of* $YD_3$ *epitaxial thin films*, Phys. Rev. B, **61** (19), 12701–12704 (2000)

[163] T. J. Udovic, Q. Huang, and J. J. Rush, *Comment on "Theoretical prediction of the structure of insulating* $YH_3$*"*, Phys. Rev. Lett., **79** (15), 2920 (1997)

[164] P. Vajda, *Hydrogen in rare-earth metals, including* $RH_{2+x}$ *phases* (Elsevier Science, Amsterdam, 1995), vol. 20 of *Handbook on the Physics and Chemistry of Rare Earths*, chap. 137

[165] J. Völkl and G. Alefeld, *Diffusion of Hydrogen in Metals* (Springer-Verlag, Berlin, 1978), vol. 28 of *Topics in Applied Physics – Hydrogen in Metals I*, chap. 12

[166] X. W. Wang and C. Chen, *Nature of the insulating state in* $LaH_3$, Phys. Rev. B, **56** (12), 7049–7052(R) (1997)

[167] Y. Wang and M. Y. Chou, *Peierls distortion in hexagonal* $YH_3$, Phys. Rev. Lett., **71** (8), 1226–1229 (1993)

[168] Y. Wang and M. Y. Chou, *Structural and electronic properties of hexagonal yttrium trihydride*, Phys. Rev. B, **51** (12), 7500–7507 (1995)

[169] J. H. Weaver, R. Rosei, and D. T. Peterson, *Optical interband structure and the low energy plasmon in* $ScH_2$, Solid State Commun., **25**, 201–203 (1978)

[170] J. H. Weaver, R. Rosei, and D. T. Peterson, *Electronic stucture of metal hydrides. I. optical studies of* $ScH_2$, $YH_2$, *and* $LuH_2$, Phys. Rev. B, **19** (10), 4855–4866 (1979)

[171] R. J. Westerwaal, *Optimization of the Mg based switchable mirror*, Master's thesis, Vrije Universiteit Amsterdam (2002)

[172] R. J. Wijngaarden, J. N. Huiberts, D. Nagengast, J. H. Rector, R. Griessen, M. Hanfland, and F. Zontone, *Towards a metallic* $YH_3$ *phase at high pressure*, J. Alloys Compd., **308**, 44–48 (2000)

[173] A. R. Wildes, R. C. C. Ward, M. R. Wells, and B. Hjörvarsson, *The formation of epitaxial* $YH_2$ *in MBE grown yttrium thin films with a thin gold capping layer*, J. Alloys Compd., **242**, 49–57 (1996)

[174] V. Wittwer, M. Datz, J. Ell, A. Georg, W. Graf, and G. Walze, *Gasochromic windows*, Solar Energy Mater. Solar Cells (2004), in press

[175] W. Wolf and P. Herzig, *First-principles investigations for* $YH_3$ ($YD_3$)*: energetics, electric-field gradients, and optical properties*, Phys. Rev. B, **66**, 224112 (2002)

[176] W. Wolf and P. Herzig, *Energetics, electric-field gradients and optical properties of* $YH_3$ ($YD_3$) *by first-principle calculations*, J. Alloys Compd., **356-357**, 73–79 (2003)

[177] C. Wu, C. H. Crouch, L. Zhao, J. E. Carey, R. Younkin, J. A. Levinson, E. Mazur, R. M. Farell, P. Gothoskar, and A. Karger, *Near-unity below-band-gap absorption by microstructured silicon*, Appl. Phys. Lett., **78** (13), 1850–1852 (2001)

[178] Z. Wu, R. E. Cohen, D. J. Singh, R. Gupta, and M. Gupta, *Weighted density approximation description of insulating* $YH_3$ *and* $LaH_3$, Phys. Rev. B, **69**, 085104 (2004)

[179] O. J. Żogał, W. Wolf, P. Herzig, A. H. Vuorimäki, E. E. Ylinen, and P. Vajda, *Probing the* $YD_3$ *structure by* $^2H$ *NMR electric-field gradients: A comparison with first-principles calculations*, Phys. Rev. B, **64**, 214110 (2001)

[180] P. Zolliker, K. Yvon, J. D. Jorgensen, and F. J. Rotella, *Structural studies of the hydrogen storage material* $Mg_2NiH_4$*. 2. Monoclinic low-temperature structure*, Inorg. Chem., **25** (20), 3590–3593 (1986)